Aircraft Noise: Modelling & Measuring

Using aircraft noise measurements for noise model prediction improvement

M.A. Heilig

knowledge & development centre
Mainport Schiphol

TU Delft

Aircraft Noise: Modelling & Measuring

Using aircraft noise measurements for noise model prediction improvement

by

M.A. Heilig

to obtain the degree of Master of Science
at the Delft University of Technology,
to be defended publicly on Thursday July 23, 2020 at 15:00.

Student number:	3478679	
Project duration:	September 1, 2019 – July 31, 2020	
TU Delft supervisor:	Prof.dr.ir. M. Snellen	
LVNL supervisor:	Ir. F. Dijkstra	
AAS supervisor:	Ir. W. Dalmeijer	
Thesis committee:	Prof.dr.ir. M. Snellen	TU Delft
	Prof.dr. D.G. Simons	TU Delft
	Dr. I.C. Dedoussi	TU Delft
	Ir. J.A. Melkert	TU Delft

An electronic version of this thesis is available at `http://repository.tudelft.nl/`.

TU Delft

knowledge & development centre
Mainport Schiphol

Preface

Two years ago I started with my master in aerospace engineering with a specialisation in aircraft noise and climate effects. The reason I choose to focus on aircraft noise and climate effects in my master is that, in my own opinion, the future development of the aviation sector strongly depends on the sustainable growth of the sector. When I say sustainable, I mean it in the broadest sense of the word. This is why I wanted to focus on the attitude towards the aviation in communities around an airport as a result of aircraft noise exposure around the airport.

During the initial phase of my thesis research I was given the opportunity to determine the research question and subject. This freedom allowed me to set up a research design which I felt comfortable with and took joy in. I therefore would like to express my sincere gratitude towards my daily supervisor from the university, Mirjam Snellen, and my daily supervisor from LVNL, Ferdinand Dijkstra, for giving me the freedom to determine my own path. This freedom reminds me of a quote, which sums up the way I felt throughout my thesis.

"If you do what you love, you'll never work a day in your life."

This thesis is written for those who are interested in the discrepancies between aircraft noise calculations and aircraft noise measurements. This can either be for scientific purposes and the development of aircraft noise models or for legislative purposes and community management.

I would like to express my sincere gratitude towards all the people involved in this project. First of all I would like to thank my supervisor from the university, professor Mirjam Snellen, for the weekly update meetings and the constructive feedback she offered. My daily supervisor at LVNL, Ferdinand Dijkstra, helped me a lot with gaining the insight in the social and political significance of my work. He has a clear vision of the required developments for the aviation sector to achieve sustainable growth of the sector. These conversations gave me valuable insights in the aviation sector and provided the motivation to contribute to the sustainable growth of the sector. I hereby also express my gratitude towards Wouter Dalmeijer from Amsterdam Airport Schiphol (AAS) for the weekly work session at Schiphol and the access to the ANOMS application. Without access to the ANOMS application this research would not have been possible. I very much appreciate the constructive feedback of professor Dick Simons during the mid-term and the greenlight evaluation of my thesis research. Finally, I would like to thank my fellow graduate students at LVNL for their input and brainstorm sessions over a cup of coffee. I often found that taking a short coffee break together with my fellow students actually helped the process of ordering my thoughts and gaining valuable new insights.

M.A. Heilig
Haarlem, July 2020

Abstract

The number of aircraft movements at Schiphol airport has been increasing over the last few decades and is expected to keep growing. Together with the growth of the aircraft movements at the airport the nuisance experienced by residents near the airport also increases. As the aircraft noise nuisance increased the demand for modelling the aircraft noise exposure as a result of the increase in aircraft operations developed. There are still significant challenges associated with the aircraft noise calculations. Over the last few years the public demand to use aircraft noise measurements to validate and increase the accuracy of the aircraft noise calculations has grown.

The aircraft noise monitoring system around Schiphol airport (NOMOS) is compared to the aircraft noise monitoring system around Heathrow airport. The NOMOS system is currently only used for the provision of information to the public, whereas the noise monitoring system around Heathrow airport is also used for noise model calibration. Due to the large similarities between the two noise monitoring system it is determined that the NOMOS system can also be used for calibration of the aircraft noise model.

For this research the European Civil Aviation Conference (ECAC) Doc.29 aircraft noise modelling guidelines have been implemented in Python. Due to the unavailability of ECAC Doc.29 implementations no code-to-code comparison between the current implementation and other implementations of the same aircraft noise model guidelines was possible. The implementation of the ECAC Doc.29 guidelines used for this research has been verified against a reference case provided by ECAC.

Based on the baseline aircraft noise model performance with respect to aircraft noise measurements collected by NOMOS it has been determined that the Aircraft Noise and Performance (ANP) database is the main cause of the aircraft type dependent differences between the calculated and measured aircraft noise model. Therefore, the ANP database, consisting of aircraft performance data and Noise-Power-Distance (NPD) tables, has been calibrated by using ACMS logs provided by KLM. First, the calibration and validation of the aircraft performance has been performed. However, after the calibration of the aircraft performance a systematic difference remained between the calculated and measured aircraft noise level. This systematic difference was corrected for by calibration of the NPD tables.

The combined calibration of the aircraft performance and NPD tables is validated by using an independent set of aircraft operations. Based on the validation of the combined calibration it is found that no statistically significant differences are observed between performing only NPD table calibration and combined aircraft performance and NPD table calibration. It is however strongly recommended to always use the combined calibration of both the aircraft performance and the NPD tables. Only in this way the quality of all input parameters in the aircraft noise calculations can be ensured.

Contents

List of Figures

List of Tables

List of Acronyms

ACMS Aircraft Condition Monitoring System

ANOMS Airport Noise and Operations Management System

ANP Aircraft Noise and Performance

BAS Bewoners Aanspreekpunt Schiphol

BPF Blade Passing Frequency

DFPP Default Fixed Point Profile

ECAC European Civil Aviation Conference

FDR Flight Data Recorder

IATA International Air Transport Association

ICAO International Civil Aviation Organisation

IQR Interquartile Range

ISA International Standard Atmosphere

ISO International Organization for Standardization

KLM Koninklijke Luchtvaart Maatschappij

KNMI Koninklijk Nederlands Meteorologisch Instituut

MA Moving Average

MGLW Maximum Gross Landing Weight

NLR Nederlands Lucht- en Ruimtevaartcentrum

NMT NOMOS Measurement Tower

NOMOS Noise Monitoring System

NPD Noise Power Distance

NRM Nederlands Rekenmodel

OEW Operational Empty Weight

pdf Probability Density Function

rpm Revolutions Per Minute

SEL Sound Exposure Level

SPL Sound Pressure Level

TOW Take-Off Weight

WHO World Health Organisation

Nomenclature

α	Atmospheric attenuation	dB m^{-1}
β	Elevation angle	°
β_a	Attenuation decay constant	
Δh	Altitude change	m
ΔL	Noise level difference	dBA
ΔS	Lateral displacement	m
Δt	Time change	s
ΔV	Speed change	kts
δ	Pressure ratio	-
$\Delta_{A.n}$	A-weighting factor	dBA
Δ_{app}	Approach correction factor	dBA
Δ_{atm}	Atmospheric NPD correction factor	dBA
Δ_{ca}	Convective amplification correction	dB
Δ_{dep}	Departure correction factor	dBA
Δ_F	Finite segment correction	dB
Δ_g	Geometric spreading loss	dB
Δ_I	Engine installation correction	dB
δ_{RMS}	Root mean square error	dBA
Δ_{SOR}	Start of roll correction	dB
Δ_V	Duration correction	dB
ϵ	Bank angle	°
$\epsilon_{calculated}$	Calculation error	dBA
$\epsilon_{measured}$	Measurement error	dBA
ϵ_{other}	Contribution of other noise sources	dBA
γ	Flight path angle	°
γ_{air}	Specific heat ratio	-
Λ	Lateral attenuation correction	dB
λ	Flight segment length	m
λ	Longitude	°
λ	Wave length	m

λ_0	Reference longitude	[°
μ	Mean difference	-
ω	Radial frequency	rad s^{-1}
ϕ	Latitude	°
ϕ_0	Reference latitude	°
ψ	Incidence angle	°
ρ	Medium density	kg m^{-3}
σ	Standard deviation	-
σ_g	flow resistivity	kPa m s^{-2}
θ	Elevation angle	°
φ	Depression angle	°
A	Wave amplitude	Pa
a	Acceleration	m s^{-2}
B	Fan blades	-
c	Sound speed	m s^{-1}
D	Landing weight coefficient	-
d	Distance	m
d_1	Distance between the observer and the start-point of the flight segment	m
d_2	Distance between the observer and the end-point of the flight segment	m
d_λ	Scaled distance	m
d_p	Perpendicular distance between the observer and the flight segment	m
d_{ref}	Reference distance	m
d_s	Shortest distance between the flight segment and the observer	m
f	Wave frequency	Hz
f_0	Wave emission frequency	Hz
f_1	First harmonic frequency	Hz
f_{fuel}	Fuel flow	kg s^{-1}
f_k	k^{th} harmonic frequency	Hz
F_n	Net thrust	lb
f_s	Sampling frequency	Hz
g	Gravitational acceleration	m s^{-2}
h	Aircraft altitude	m
H_m	Microphone height	m
h_{rel}	Relative humidity	%

k	Wave number	rad m^{-1}
k_a	Attenuation wave number	rad m^{-1}
l	Lateral distance between the aircraft and the observer	m
$L_A(t)$	A-weighted sound level	dBA
$L_{calculated}$	Calculated noise level	dBA
L_{day}	Daytime A-weighted sound level	dBA
$L_{evening}$	Evening A-weighted sound level	dBA
$L_{measured}$	Measured noise level	dBA
L_{night}	Nighttime A-weighted sound level	dBA
$L_{x_{max}}$	Maximum x-weighted noise level	dBx
M	Mach number	-
N	Number of engines	-
$N1$	Fan rotational speed	rpm
P	Engine power	lb
p	p-value	-
p'	Pressure deviation from atmospheric pressure	Pa
P_1	Start-point engine power	lb
P_2	End-point engine power	lb
p_a	Atmospheric pressure	Pa
$p_{e,0}$	Reference effective pressure	Pa
p_e	Effective pressure	Pa
Q	Ground reflection coefficient	-
q	Distance between the closest point of approach and segment start-point	m
R	Aerodynamic coefficient	-
r	Distance between the source and observer	m
R^2	Coefficient of determination	-
r_1	Slant distance between the aircraft and the observer	m
r_2	Bottom reflected distance between the aircraft and the observer	m
R_{air}	Specific gas constant	$m^2\ s^{-2}\ °K^{-1}$
r_{ref}	Reference distance	m
r_{turn}	Turn radius	m
S_p	Closest point of approach	-
SEL_{seg}	Segment SEL Level	dBA
SS_{res}	Residual sum of squares	-

SS_{tot}	Total sum of squares	-
T	Engine thrust setting	lb
T	T-value	-
T	Wave period	s
t	Time	s
t_0	Aircraft noise event start time	s
t_1	Aircraft noise event end time	s
T_{air}	Air temperature	°K
T_{int}	Integration time	s
T_{max}	Maximum engine thrust	lb
t_{ref}	Reference time	s
T_{stat}	Static air temperature	°K
T_{tot}	Total air temperature	°K
V_1	Start-point speed	kts
V_2	End-point speed	kts
V_{app}	Final approach speed	kts
V_{CAS}	Calibrated airspeed	kts
V_g	Ground speed	kts
V_{ref}	Reference speed	kts
V_{seg}	Segment speed	kts
V_{TAS}	True airspeed	kts
V_w	Wind speed	kts
x	x-coordinate	m
y	y-coordinate	m

1 Introduction

In this chapter the background of aircraft noise exposure around Schiphol airport is outlined first. Secondly, the difficulties in the calculation of aircraft noise and the difficulties associated with the comparison of aircraft noise calculations and aircraft noise measurements are discussed. Thereafter the outline of this thesis report is presented. Finally, the research aim, the outline, and the design of the research is discussed

1.1. Background

As the global demand for passenger air transport has been increasing for the last decades and is expected to grow even more[4], the demand for movements around Amsterdam Airport Schiphol (IATA: AMS, ICAO: EHAM) (hereinafter referred to as Schiphol) has been growing similarly. The growth of Schiphol from 2005 till 2019, in terms of number of yearly aircraft movements, is depicted graphically in Figure 1.1[1]. The data presented in this figure supports the claim that the number of yearly movements at Schiphol has been increasing in the past 15 years. A small decrease in the number of aircraft movements is of aircraft movements is observed in 2009 as a consequence of global economic recession[56], but the aviation industry has since recovered.

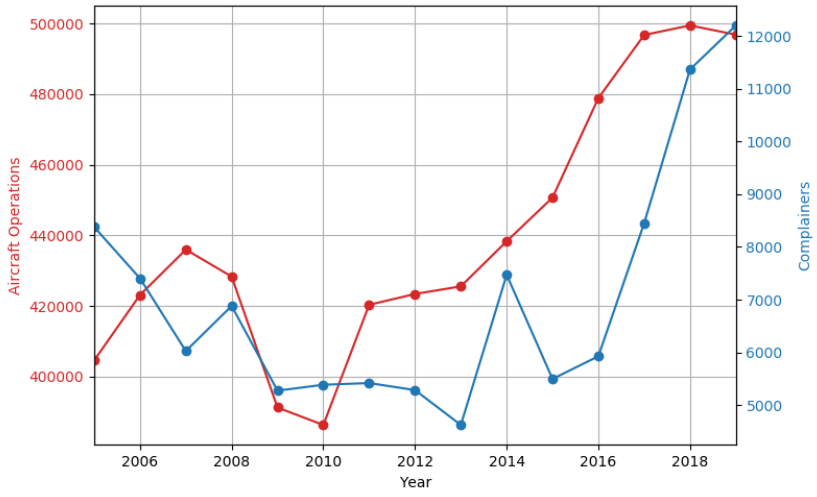

Figure 1.1: Number of yearly movements at Schiphol between 2005 and 2019 and the number of complaints received at BAS for the same time period.

One of the main effects of aircraft movements in the vicinity of populated areas is community exposure to noise as a consequence of human action, especially in a densely populated country such as the Netherlands[50]. Aircraft noise is ranked in third place when considering the source of noise nuisance in the Netherlands in 2016, right after road traffic and neighbourhood noise[49].

[1] Data retrieved from https://www.schiphol.nl/nl/schiphol-group/pagina/feiten-en-cijfers/, accessed on 01-10-2019

Even though significant noise reduction technologies at the source have been established over the last 60 years [35], ever more concerns are voiced by members of the public. 'Het NRC' reported that for residents near the airport more silent aircraft would not directly lead to a decrease in nuisance. There are other factors than sound, so called non-acoustical factors, that influence the human perception of aircraft noise[44]. The influence of non-acoustical factors is supported by the findings that the nuisance rating of the same level of aircraft noise has changed significantly between 1965 and 1990[23]. These findings are further supported by the observations in Figure 1.2, which indicates that the same noise exposure level around different airports at different moments in time results in a different level of nuisance.

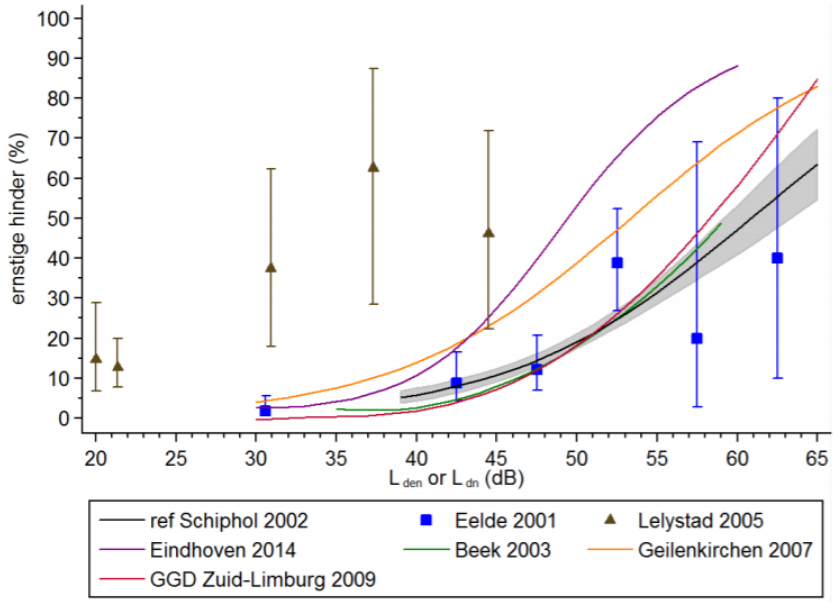

Figure 1.2: Relationships between aircraft noise exposure level and the level of nuisance in local communities. Taken from [50] p. 35.

The key to reducing nuisance would be to decrease the number of movements over the residential area[40]. The increase in members of the public voicing their concerns towards the 'Bewoners Aanspreekpunt Schiphol' (BAS) is presented in Figure 1.1[2]. Here it is observed that there is a positve correlation between the number of aircraft operations and the number of complaints at BAS. The effect of the economic recession of 2009 on the number of complaints at BAS is also clearly visible, indicating that the reduction of aircraft movements results in a reduction of complaints.

As the number of aircraft movements to and from Schiphol increase more questions are being raised by the general public and news papers about the way the nuisance due to aircraft noise around Schiphol is calculated. 'De Telegraaf' reported that the Dutch Aerospace Research Laboratory (NLR) found a discrepancy of one to two decibel between the theoretical calculations used by Schiphol and the measured sound exposure values [65]. After the 'belevingsvlucht', meant to demonstrate the effect of opening Lelystad Airport (IATA:LEY, ICAO: EHLE) for international commercial air traffic movements, a majority of the House of Representatives did no longer accept the systematic discrepancy between theoretical aircraft noise calculations and the measurements [66].

There is a clearly voiced desire coming from both the residents living around Schiphol and the political scene to incorporate actual aircraft noise measurements around Schiphol for the prediction of future aircraft noise exposure. The NLR stated that residents near the airport often prefer aircraft noise measurements over calculations, because of the higher perceived fidelity by the residents[12]. Even though the implementation of aircraft noise measurements for the improvement of aircraft noise calculations seems straight forward, there are some challenges associated with the implementation of aircraft noise measurements for the improvement of aircraft noise calculations. The research question to be answered in this thesis is:

> *How can aircraft noise measurements be implemented for the improvement of the quality of aircraft noise calculations?*

[2] Data retrieved from https://www.bezoekbas.nl/, accessed on 01-10-2019

1.2. Current Challenges

Multiple studies have found that significant differences are present between the calculated and measured levels of aircraft noise [3, 24] as can be seen in Figure 1.3. It is observed from this figure that there is a systematic tendency of the aircraft noise calculations to underestimate the noise level produced by the aircraft for each of the measurement location sites. Furthermore, it was also found that the difference between the calculated and measured aircraft noise level is strongly dependent on the category or type of aircraft[24].

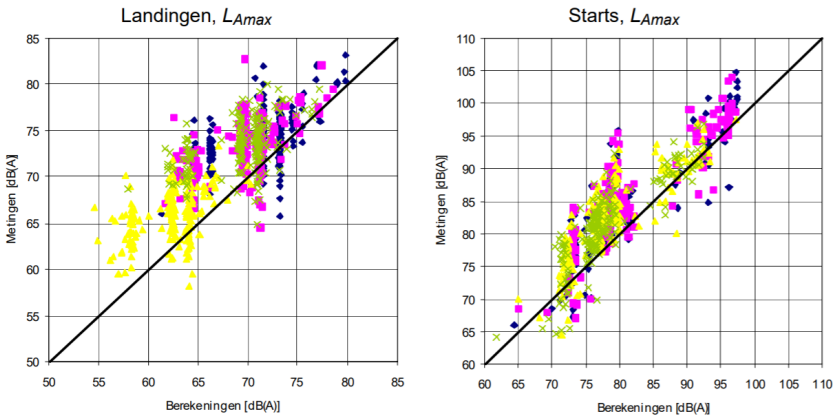

Figure 1.3: Correlation between calculated (x-axis) and measured (y-axis) aircraft noise for landing (left) and departing (right) aircraft. The different markers indicate a different measurement location site. Taken from [24] p. 49.

There are several challenges associated with the comparison between measured and modelled aircraft noise levels. These challenges are both associated with the reliability of aircraft noise measurements, the assumptions and limitations of aircraft noise models, and the availability of high accuracy input data[19]. Another challenge in the prediction of the aircraft noise is the limited amount of data obtainable from radar observations. Furthermore, there is no standard method for the comparison of predicted and measured aircraft noise levels, meaning that comparison to other studies is difficult.

Measurement Reliability

Aircraft noise measurements are carried out in circumstances which cannot always be controlled, as these aircraft noise measurements are performed in the field. These measurements are often performed in residential areas, where the background environmental noise strongly influences the noise level at the microphone location. Furthermore, the reliability of the aircraft noise measurements is affected by the meteorological conditions during the noise event[57].

Aircraft Tracks

The aircraft position over time is one of the main input parameters for the prediction of the aircraft noise level. The uncertainty in the aircraft position reported by the primary surveillance radar can be off by as much as twice the wing span of the aircraft[38]. The way to mitigate the uncertainty in the input flight track would be to make use of the aircraft Flight Data Recorder (FDR)[19]. However, most aircraft operators are reluctant to share this data as the data in the FDR might be commercially sensitive.

Limited Data

The working principles of the flight crew and the airline and aircraft type specific operation practices result in a spread in the measured aircraft noise level[20, 63]. The parameters associated with the airline and aircraft type specific operation practices, such as flap setting and moment of gear deployment, are not available from radar data. These parameters can only be obtained from the FDR, which is not freely obtainable.

1.3. Thesis Outline

First the basics of acoustics which are required for the understanding of the physical principles associated with propagation of a sound wave through the atmosphere are discussed in chapter 2. The outline of the research and the outline of the result analysis are presented in chapter 5. A description of the noise measurement system currently in place around Schiphol airport is presented in chapter 3. This chapter contains both

a comparison between the aircraft noise measurement system used for information purposes (Schiphol) and for model calibration purposes (Heathrow) and a detailed description of the data recorded by the noise monitoring system around Schiphol. The aircraft noise prediction model used for this research is the ECAC Doc.29 aircraft noise model. The implementation and verification of the ECAC Doc.29 aircraft noise model guidelines is outlined in chapter 4. The results of the comparison between the calculated and measured aircraft noise level are presented in chapter 6. As a first step the analysis of the aircraft noise model performance with the default aircraft noise model performance is determined. The baseline aircraft noise model performance is subsequently used to determine statistically significant effects of the different aircraft flyover event characteristics, such as meteorological conditions, distance between the aircraft and the microphone, and the specific aircraft type, on the observed differences between the calculated and measured aircraft noise level. Secondly, the effect of the possible improvements through calibration of the Aircraft Noise and Performance (ANP) database for the aircraft noise calculations are discussed. The effect of the calibration of the ANP database on the aircraft noise calculations is subsequently validated using an independent dataset. Finally, the conclusions and recommendations based on the findings from this research are presented in chapter 7.

1.4. Research Outline & Design

The aim of this research is to identify and implement possible improvements for the ECAC Doc.29 aircraft noise model. It has been found from literature that large discrepancies are observed between the calculated and measured aircraft noise level. As a result of the differences between the calculated and measured aircraft noise levels public trust in the quality of the aircraft noise models has been affected. The public trust in the correctness of the aircraft noise measurements is higher than the public trust in the correctness of the aircraft noise model, which is why there is a clear desire to validate the aircraft noise model by using aircraft noise measurements[12]. Therefore, the aim of this thesis is:

Identify and implement improvements for the ECAC Doc.29 aircraft noise model
by
Comparing the calculated noise level to aircraft noise measurements taken by the NOMOS system around Schiphol airport.

The aircraft noise model used for this research is the ECAC Doc.29 aircraft noise model. This model has been selected as there is a shift towards a harmonised method for aircraft noise calculations around European airports. However, implementations of the ECAC Doc.29 aircraft noise model are not freely available online. Therefore for this research the guidelines presented in the ECAC Doc.29 guidance documents[7, 8] have been implemented in Python3.7[53]. In this implementation of the ECAC Doc.29 guidelines the Numpy[41], Pandas[39], and Matplotlib[26] packages are used.

As mentioned previously one of the challenges in current aircraft noise calculations is the ability of code-to-code comparison of aircraft noise model implementations. This issue has to a certain extend been resolved by the European Civil Aviation Conference (ECAC) by the provision of a verification guide for the ECAC Doc.29 aircraft noise model. The implementation of the ECAC Doc.29 aircraft noise model used for this research is also verified using the noise model verification guide. However, no data is currently available on the performance of other implementations of the ECAC Doc.29 aircraft noise model, meaning that the implementation used for this research can only be verified against the reference performance provided in the verification guide. No statement can be made about the performance of the aircraft noise model implemented for this research with respect to other ECAC Doc.29 noise model implementations developed by other researchers.

The verified implementation of the ECAC Doc.29 aircraft noise model is firstly used to determine a baseline performance of the aircraft noise model by comparing the default aircraft noise model results to the aircraft noise measurements. Together with the noise model output the following input parameters for the noise calculations and the associated aircraft noise measurements are recorded:

- Meteorological conditions during the aircraft noise measurement:
  - Wind speed,
  - Occurrence of precipitation,
  - Ambient air temperature,
  - Relative humidity, and
  - Ambient air pressure.
- Geometrical characteristics of the aircraft flyover at the moment of maximum L_A:

  - Slant distance between the aircraft and the microphone, and
  - Altitude of the aircraft.
- Aircraft specific characteristics:
  - Type of aircraft (ICAO type code), and
  - Type of operation.

The correlations between the input parameters and the difference between the calculated and measured aircraft noise level are subsequently used to identify areas of improvement for the reduction of the calculation error in the ECAC Doc.29 aircraft noise model. In this way aircraft noise measurement are used to identify the possible improvements for aircraft noise calculations.

Once the improvements in the aircraft noise calculations have been implemented and verified, these improvements are validated. Validation of the aircraft noise model improvements using aircraft noise measurement feedback are validated both in the temporal and spatial domain. Validation of the aircraft noise model improvements in the temporal domain is performed by considering aircraft operations from a different time frame than the aircraft operations used for the improvements of the aircraft noise model. The validation of the aircraft noise model improvement in the spatial domain is performed by randomly selecting measurement locations which are used for the calibration of the noise model and measurement locations which are used for the validation of the calibration. If improvements in the aircraft noise model are observed for both the calibration and validation datasets, both in the temporal and spatial domain, the improvements of the aircraft noise model are considered to be valid.

2

Basics of Acoustics

In this chapter the basic physical characteristics of sound are discussed. First the definitions of sound and noise are determined, which are the definitions to be used throughout this thesis. Secondly, the commonly used way for the quantification of sound levels, both for a single noise event and long-term noise, are discussed. Thereafter the effects occurring between the source of the sound or noise and the location of the observer are presented. Finally, the frequency dependent weighting of the sound level to correct for the sensitivity of the human ear is elaborated upon.

2.1. Definition

The difference between sound and noise is not always clear, but the definition for the purpose of this thesis is given first. Secondly, the characteristics of sound waves and the corresponding physical quantities are discussed.

2.1.1. Sound and Noise

Noise is usually defined as sound that is unwanted by the observer of the sound. Even though the term unwanted can be considered as subjective, for example one person might deem a certain sound unwanted and another person does not share in this opinion, all sound generated by an aircraft is commonly thought of as unwanted sound. Therefore, the terms aircraft sound and aircraft noise are used interchangeably.

2.1.2. Sound Waves

Sound is a pressure disturbance from the governing atmospheric pressure which is propagating through the atmosphere in the form of an acoustic wave. Even though sound waves are capable of propagating through other mediums than the atmosphere, these are not considered in this evaluation of aircraft sound. An acoustic wave is a longitudinal wave, which means that the displacement of the particles is in the direction of propagation of the wave, as is shown in Figure 2.1. This propagating wave causes local increases in pressure (compression areas) and local decreases in pressure (rarefaction areas), which propagate in the direction of the propagation of the wave.

The source on the left of Figure 2.1 is radiating at a single frequency. If the sound source is also a point source, the pressure deviation from the atmospheric pressure (p' [Pa]) is given by the equation below.

$$p'(r,t) = \frac{A}{r}\cos\left(\omega(t-\frac{r}{c})\right) \tag{2.1}$$

The p' notation is used, because the sound pressure is generally much smaller than the governing atmospheric pressure. The sound pressure originating from a point source radiating at a single radial frequency (ω [rad/s]) is given by Equation 2.1, where A is the amplitude of the pressure disturbance 1m from the source, r is the distance from the source in meters, t is the time in seconds, and c is the speed of sound in the current medium in meters per second. For any sinusoidal wave, the following characteristics can be easily derived:

- Wave length (λ [m]),
- Wave frequency (f [Hz]) or period (T [s]), and

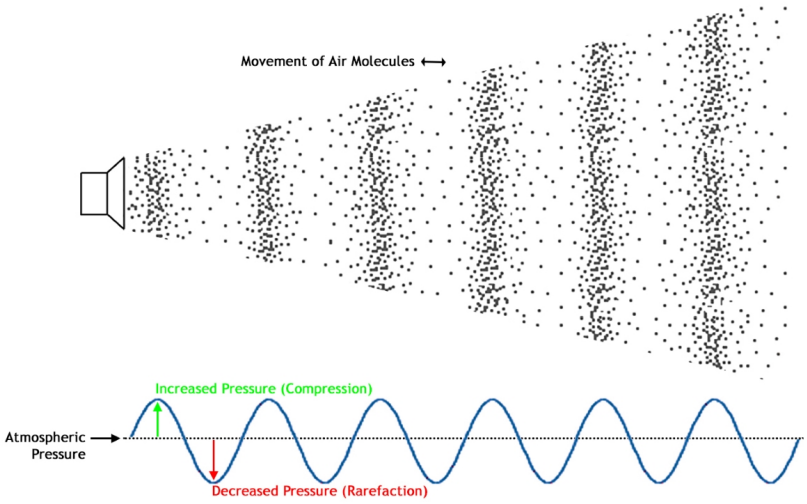

Figure 2.1: Visualisation of movement of air molecules in an acoustic wave

- Propagation speed (c [m/s]).

The characteristics mentioned above are related to one another by the equation below, which indicates that the wave length is inversely proportional to the frequency of the wave.

$$\lambda = c\ T = \frac{c}{f} \tag{2.2}$$

The remaining wave characteristic is the propagation speed, which in the case for wave propagation through air is determined by the ratio of the specific heat at constant pressure and constant volume (γ [-]), which is 1.4 for air, the specific gas constant (R_{air} [$m^2 s^{-2} K^{-1}$]), which is 2807.05 for air, and the ambient air temperature (T_{air} [°K]). The speed of sound in air is given by the equation below.

$$c = \sqrt{\gamma_{air} R_{air} T_{air}} \tag{2.3}$$

2.2. Quantification

To be able to calculate and measure the sound level of an event of interest it is necessary to have a conventional way of quantifying the sound characteristics of the event. The characteristics of the single aircraft noise event metrics can be integrated over time, which results in the long term noise metrics.

2.2.1. Decibel Scale

The amount of energy that is contained in a sound wave is commonly expressed in decibel (dB), because of the range of audible effective pressure levels of the average person. At a frequency of 1000 Hz the threshold of hearing for an average person is 2 10^{-5} Pa whereas the threshold of pain is 200 Pa[31]. Because of this large range of audible pressure levels the sound level is commonly expressed as Sound Pressure Level (SPL) as defined by the equation below.

$$SPL = 10 \log_{10} \left(\frac{p_e^2}{p_{e,0}^2} \right) \tag{2.4}$$

Aircraft noise metrics can be divided in single event noise metrics and long term noise metrics. Single event noise metrics, as the name already implies, are used to describe the characteristics of an individual noise event such a an aircraft fly-over event. On the other hand, long term noise metrics are used to provide a measure of the average (e.g. daily, monthly or yearly) noise exposure with varying intensity. Aircraft fly-overs are a good example of noise exposure with varying intensity over time as these show large peaks in the sound level.

Decibel Addition
Due to the nature of the decibel scale addition of two decibel values might at first seem counterintuitive. The decibel scale is a logarithmic scale with base 10, which means that a $60dB$ event is actually equal to 10 times a $50dB$ event. Several examples of decibel addition are:

$$50\text{ dB} + 50\text{ dB} = 10\log_{10}\left(10^{\frac{50}{10}} + 10^{\frac{50}{10}}\right) \approx 53.0\text{ dB}$$
$$60\text{ dB} + 50\text{ dB} = 10\log_{10}\left(10^{\frac{60}{10}} + 10^{\frac{50}{10}}\right) \approx 60.4\text{ dB}$$
$$70\text{ dB} + 50\text{ dB} = 10\log_{10}\left(10^{\frac{70}{10}} + 10^{\frac{50}{10}}\right) \approx 70.0\text{ dB}$$

From the examples above it can be seen that a doubling in sound level causes an increase of $3.0dB$. Furthermore, the effect of the less dominant signal quickly diminishes if the difference in sound level is more than $10dB$.

2.2.2. Single Event Noise Metrics

Multiple metrics can be used to describe different characteristics of an individual noise event. The two metrics used throughout this research are the maximum sound level (L_{Amax} [dBA]) during an observation and the Sound Exposure Level (SEL [dBA])[32].

$$L_{Amax} = max(L_x(t)) \quad t_0 \leq t \leq t_1 \quad [dB] \tag{2.5}$$

$$SEL = 10\log_{10}\left(\int_{t_0}^{t_1} 10^{\frac{L_A(t)}{10}}\, dt\right) \quad t_0 \leq t \leq t_1 \quad [dBA] \tag{2.6}$$

In Equation 2.5 the A subscript indicates the weighting applied to the sound level, as is described in the next paragraph. For the SEL the signal is typically weighted using the A frequency weighting. For the L_{Amax} the time interval is the entire range between the time of the start of the measurement (t_0 [s]) and the time of the end of the measurement (t_1 [s]). For the SEL the time interval can be selected such that the sound level at both t_0 and t_1 is $10dBA$ lower than the L_{Amax} of that interval in the case of an aircraft flyover event. This interval corresponds to the shaded area in Figure 2.2, where a generic sound signal is presented. The SEL corresponding to this noise event is calculated to be $93.1dBA$.

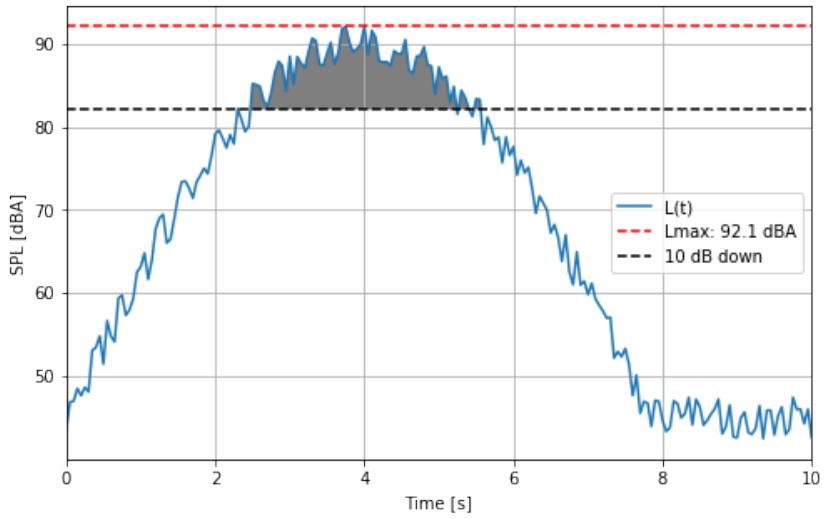

Figure 2.2: Example sound level over time for a typical aircraft flyover.

2.2.3. Long Term Noise Metrics

An indicator of long term noise exposure for aircraft noise throughout Europe is the so called Day-Evening-Night average sound level (L_{DEN} [dBA])[16]. This level assigns a weight to an aircraft noise event based on

the moment of occurrence of the noise event during the day. The definition of the L_{DEN} as set in the directive of the European Parliament is given by Equation 2.7, where L_{day}, $L_{evening}$ and L_{night} are the day, evening and night A-weighted equivalent sound level determined for all the day, evening and night periods of a year respectively in accordance with ISO 1996-2: 1987[27].

$$L_{DEN} = 10\log_{10}\left(12\ 10^{\frac{L_{day}}{10}} + 4\ 10^{\frac{L_{evening}+5}{10}} + 8\ 10^{\frac{L_{night}+10}{10}}\right) - 10\log_{10}(24) \tag{2.7}$$

2.3. Effects

It makes intuitive sense that the sound emitted by the source, the aircraft, and the sound at the observer are different. This is due to several effects that take place when a sound signal moves from the source to the observer. Throughout this section an example calculation of an aircraft flyover event is considered.

Aircraft Flyover Sound Propagation

For this example an aircraft flying at an altitude of $457.2m$ (1,500 ft) at a speed of $100m\ s^{-1}$ (194.4 kts) is considered. Furthermore, the aircraft flyover event is considered at a projected along track distance (L [m]) of at most 2,000 m from the microphone location. The microphone is mounted at an elevation (H_m [m]) of $2.0m$. The geometry of the aircraft flyover example is presented in the figure below.

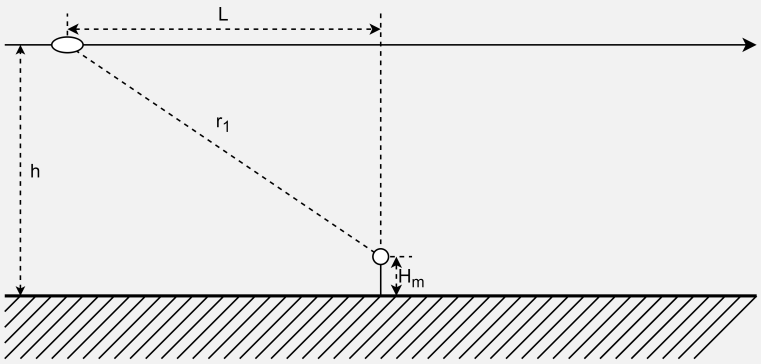

Figure 2.3: Geometry of the aircraft flyover example

As a result of the speed of $100m\ s^{-1}$ of the aircraft, the projected along track distance between the aircraft and the microphone is given by:

$$L = 2000 - 100\ t$$

The corresponding slant distance between the aircraft and the microphone (r_1 [m]) is given by:

$$r_1 = \sqrt{(h - H_m)^2 + L^2}$$

The slant distance between the aircraft and the microphone is dependent on the height of the aircraft with respect to the ground (h [m]), the microphone height (H_m [m]) and the projected along track distance between the aircraft and the microphone. The slant distance is subsequently used to determine the sound pressure at the microphone, which is given by:

$$p(r,t) = Re\left[\frac{S}{r}\ e^{i\ (k\ r - \omega\ t)}\right]$$

The sound pressure at the location of the observer depends on the source strength (S [Pa]), the distance between the aircraft and microphone (r [m]), the wave number (k [rad m^{-1}]), and the radial frequency of the wave (ω [rad s^{-1}]). The wave number and radial frequency are respectively given by:

$$k = \frac{2\ \pi}{\lambda}$$

$$\omega = 2\ \pi\ f$$

For this example a single frequency wave is considered to be emitted from the aircraft at a frequency of $1000 Hz$ with a source strength of $100 Pa$.

2.3.1. Geometrical Spreading

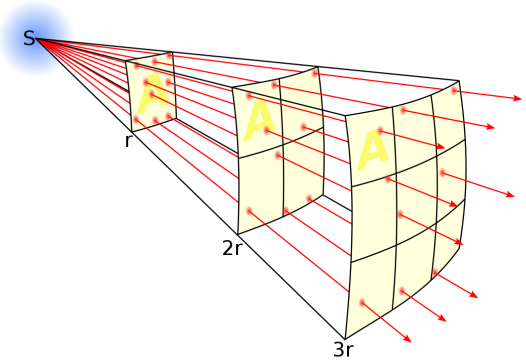

Figure 2.4: Effect of distance on the total wave front area.

Figure 2.4 shows that the area of the wave front grows quadratically with respect to the distance from the source. The resulting relationship is commonly known as the 'inverse square law'. The loss in sound level (Δ_g [dB]) as a result of geometrical spreading is given by the equation below, where r [m] is the distance and the reference distance (r_{ref} [m]) is the distance at which the sound level is known.

$$\Delta_g = 10 \log_{10}\left(\left(\frac{r}{r_{ref}}\right)^2\right) = 20 \log_{10}\left(\frac{r}{r_{ref}}\right) \tag{2.8}$$

The geometrical spreading as indicated by the equation above only holds for a source which is considered to be a point source. If the distance between the different noise sources of the aircraft, e.g. both engines, flaps, and landing gear, is small with respect to the distance between the aircraft and the observer, the aircraft can be modelled as a single point source. Furthermore, the sources have to be incoherent, meaning that no destructive interference occurs.

If the distance between the source and the observer is doubled, the ratio between the distance between the source and the observer and the reference distance is also doubled. This subsequently leads to an increase in geometrical spreading according to $\Delta_g = 20 \log_{10}(2) \approx 6.0$ dB. Therefore, a doubling in the distance between the point source and the observer yields a $6.0 dB$ increase in the loss due to geometrical spreading.

Aircraft Flyover Sound Propagation
The slant distance between the aircraft and the microphone is presented in the figure below on the left. The corresponding free field sound pressure signal at the microphone location is presented in the figure below on the right.

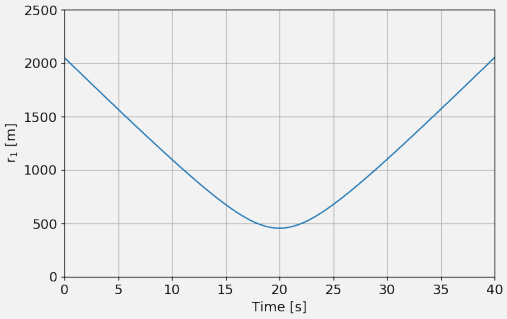

Figure 2.5: Slant distance between the aircraft and microphone.

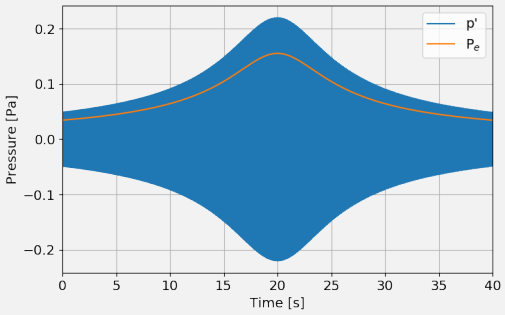

Figure 2.6: Free field pressure level at the microphone (blue) and the corresponding mean effective pressure (orange).

As mentioned previously, the SPL at the microphone is given by:

$$SPL = 10 \log_{10} \left(\frac{p_e^2}{p_{e,0}^2} \right)$$

The SPL corresponding to the pressure level in Figure 2.6 as a function of time is presented in Figure 2.7. The SPL as a function of the slant distance between the aircraft and the microphone is presented in Figure 2.8. The effect of geometric spreading is clearly visible in this figure, where a SPL of $75.41dB$ is observed for a distance of $600m$ between the aircraft and the microphone and a SPL of $69.39dB$ is observed for a distance of $1200m$ between the aircraft and the microphone. A doubling in the distance between the aircraft and the microphone results in a $6.02dB$ loss in the SPL of the sound signal.

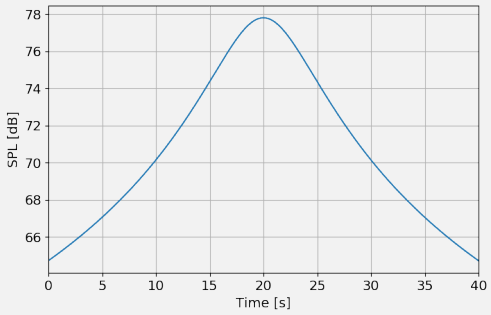

Figure 2.7: SPL at the microphone as a function of time.

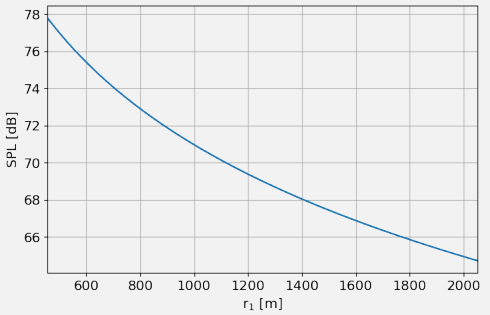

Figure 2.8: SPL at the microphone as a function of distance between the aircraft and the microphone.

2.3.2. Doppler Effect

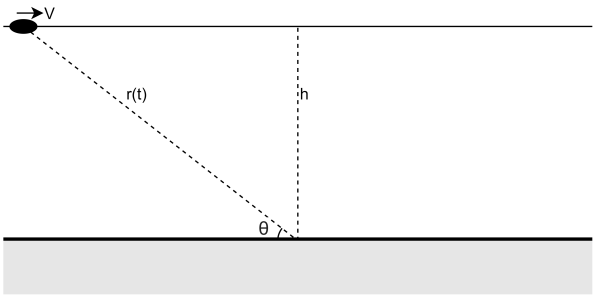

Figure 2.9: Typical aircraft flyover representation. Based on [58] Figure 1.21: Aircraft flyover flight path (upper figure).

Figure 2.9 shows a typical flight path of an aircraft over a sound receiver, where the distance to the receiver (r [m]) and the corresponding longitudinal elevation angle (θ [°]) are varying during the flyover event. When a sound source is in motion with respect to the observer a shift in the frequency of the signal is observed, which is commonly known as the Doppler effect. The Doppler effect is the apparent change in the frequency of a sound wave caused by relative motion between the source and the observer. The relation between the emitted frequency at the source (f_0 [Hz]) and the frequency at the observer (f [Hz]) is given by the equation below.

$$\frac{f}{f_0} = \frac{1}{1 - M\cos(\theta)} \tag{2.9}$$

In the equation above, the Mach number (M [-]) is the ratio between the source velocity through the medium and the propagation speed of the wave in the same medium. A typical Doppler shift for an aircraft flyover event is shown in Figure 2.10. It can be seen that as the aircraft approaches the observer, for t<20, an apparent increase in frequency is observed. When the aircraft has passed and is now moving away from the observer a decrease in frequency is observed. Both observations are in line with the expectations from Equation 2.9. The maximum Doppler shift is observed when the longitudinal elevation angle approaches 0 or 180 degrees, which means that the frequency shift approaches $\frac{1}{1-M}$ and $\frac{1}{1+M}$ respectively.

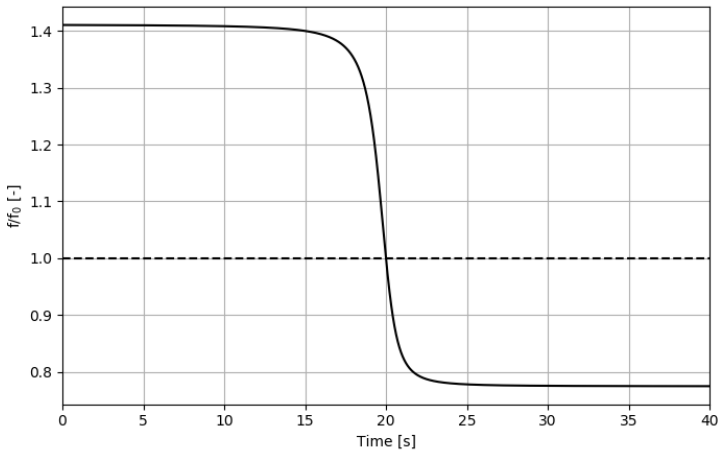

Figure 2.10: Typical Doppler shift during an aircraft flyover event. M = 0.29, h = 100m and $0 \leq \theta \leq 180$.

A second effect of the motion of the source with respect to the observer is that the strength of the source is modified by convective amplification[18]. The correction corresponding to convective amplification (Δ_{ca} [dB]) is given by the equation below. It is observed from the convective amplification presented in Figure 2.11 that the sound level increases as the aircraft moves towards the location of the observer and the sound level decreases as the aircraft moves away from the observer location. This is in line with the expected behaviour from the convective amplification presented in the equation below.

$$\Delta_{ca} = 10\log_{10}\left(\frac{1}{(1 - M\cos(\theta))^4}\right) \tag{2.10}$$

Aircraft Flyover Sound Propagation
The Doppler effect is implicitly included in the complex representation of a sound pressure at the microphone location. This can be better visualised when a lower frequency wave is considered, as is presented in the figure below for a wave with a frequency of $1Hz$. For t<20s, when the aircraft is moving towards the microphone, an increase in the frequency of the sound wave recorded by the microphone is observed. For t>20s, when the aircraft is moving away from the microphone, a decrease in frequency of the sound wave recorded by the microphone is observed.

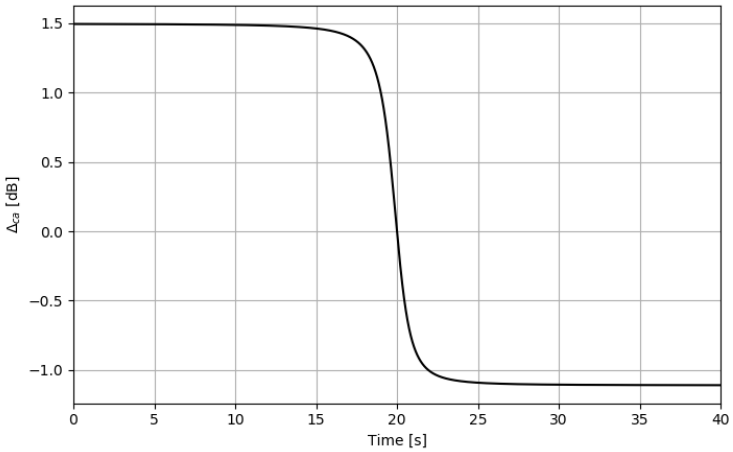

Figure 2.11: Typical convective amplification during an aircraft flyover event. M = 0.29, h = 100m and $0 \leq \theta \leq 180$.

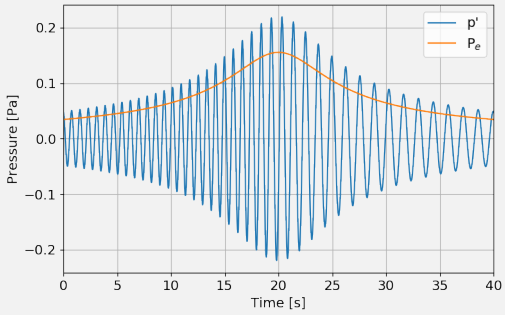

Figure 2.12: Pressure level at the microphone location for the free field considering a sound wave emitted by the aircraft with a frequency of 1Hz.

The spectrogram of the 1,000Hz sound wave is presented in the figure below. This spectrogram clearly contains the Doppler effect, resulting in an increase in the observed frequency when the aircraft is moving towards the microphone and a decrease when the aircraft is moving away from the microphone. These observations are in line with the observations in the figure above and the expectations of the Doppler effect.

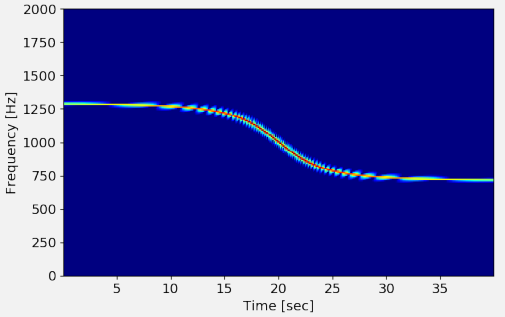

Figure 2.13: Spectrogram of the 1,000Hz sound wave signal recorded by the microphone.

2.3.3. Lloyd's Mirror Effect

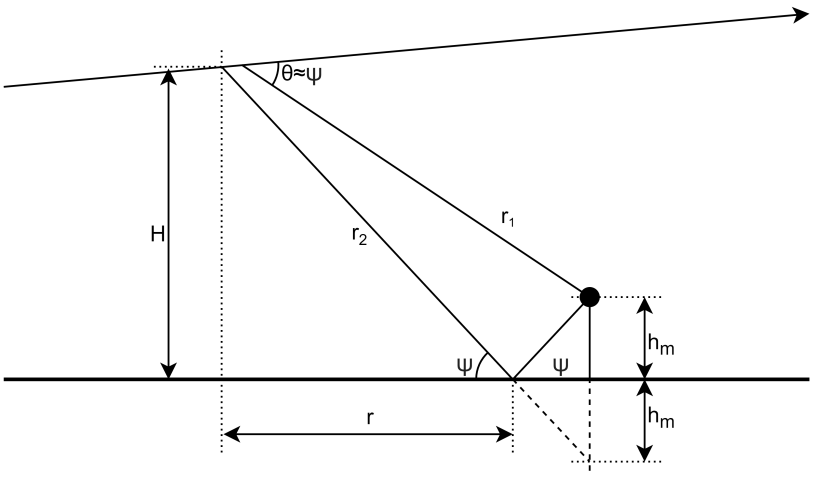

Figure 2.14: Geometry corresponding to the Lloyd's mirror effect

In general a microphone is not located in free-space, meaning that there are reflective surfaces which cause reflections of the sound wave. Figure 2.14 shows the effect of such a reflective surface. The signals arriving at the microphone are both the sound waves travelling along the direct path (r_1 [m]) and the ground surface reflected path (r_2 [m]). This effect has initially been observed by using light instead of sound waves[37] and is called the Lloyd's mirror effect.

The interference between the direct path signal and the ground surface reflected path can cause both an increase in the sound level, constructive interference, or a decrease in sound level, destructive interference. The type of interference depends on the path length difference between the direct and ground surface reflected path, the wavelength of the sound signal and phase shift of the sound wave at the reflective surface. Even though Figure 2.14 focuses on the effect of a ground surface, the same principle applies to other types of reflective surfaces, such as walls or roofs.

Aircraft Flyover Sound Propagation

It is observed from Figure 2.14 that not only the direct sound signal from the aircraft, but also a ground reflected sound signal arrives at the microphone. The type of interference of the two signals, either constructive or destructive, depends on the phase difference of the direct and the ground reflected signal at the microphone location. The pressure at the microphone location as a result of the ground reflected path is given by the equation below.

$$p(r,t) = Re\left[Q\,\frac{S}{r}\,e^{i\,(k\,r-\omega\,t)}\right]$$

It should be noted that the distance between the aircraft and the microphone location for the ground reflected signal is not the same as the distance between the aircraft and the microphone location for the direct sound signal. The distance between the microphone location and the aircraft for the ground reflected sound wave is given by the equation below.

$$r_2 = \sqrt{(h+H_m)^2 + L^2}$$

When a sound signal is reflected by a surface, both a phase change and a change in magnitude occur. Both the change of phase and magnitude depend on the flow resistivity (σ [kPa m s^{-2}]) of the reflective surface and the angle of incidence of the sound wave. The reflection coefficient (Q [-]) is given by the equation below.

$$Q = |Q|\;e^{i\,\beta} = \frac{\frac{Z_n}{\rho_\infty\,c}\sin(\psi) - 1}{\frac{Z_n}{\rho_\infty\,c}\sin(\psi) + 1}$$

Where

$$\frac{Z_n}{\rho_\infty c} = 1 + 9.08 \left(\frac{\sigma}{f}\right)^{0.75} + i\ 11.9 \left(\frac{\sigma}{f}\right)^{0.73}$$

The sound pressure as a result of both the ground reflected sound signal and the direct sound signal is obtained by the summation of the two signals. The total sound pressure at the microphone location as a result of the two sound signals is given by the equation below.

$$p(r,t) = Re\left[\frac{S}{r_1}\, e^{i\,(k\,r_1 - \omega\,t)} + Q\,\frac{S}{r_2}\, e^{i\,(k\,r_2 - \omega\,t)}\right]$$

The frequency and along track distance dependent ground reflection effect for the example aircraft flyover event over a grass ground surface (σ = 250$kPa\ m\ s^{-2}$) is presented in the figure below. Here it is observed that the maximum increase in SPL is 6.0dB, which corresponds to a doubling of the pressure.

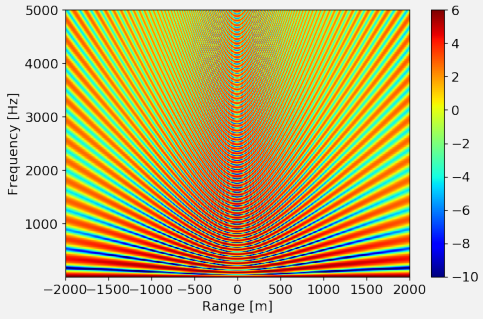

Figure 2.15: Frequency and lateral distance dependent ground reflection correction over a grass surface for a microphone at an elevation of 2m.

2.3.4. Atmospheric Absorption

It is well known that as the distance between the source and the observer increases the sound level at the observer decreases. Besides the geometrical spreading of the sound energy another effect that causes a decrease in the sound energy is the irreversible conversion of sound energy to heat[36]. The atmospheric characteristics that influence the atmospheric absorption of sound energy are[55]:

- The frequency of the sound wave,
- The ambient air temperature,
- The ambient air pressure, and
- The ambient relative humidity.

Atmospheric absorption losses of sound propagating through the atmosphere are caused by classical absorption, which can be divided in viscous losses, heat conduction losses, diffusion losses and radiation losses, and molecular relaxation of polyatomic gases in the atmosphere. The two most common polyatomic gases in the atmosphere are nitrogen (N_2) and oxygen (O_2), which combined account for 99.04% of the dry air by volume[68]. The effect of other polyatomic gases, such as carbon dioxide (CO_2) and nitric oxide (NO) are neglected because of their low occurrence in the atmosphere.

Figure 2.16 shows the atmospheric absorption coefficient as a function of frequency calculated in accordance with ISO 9613-1[28] for atmospheric conditions as mentioned in the description. From this figure it is concluded that the dominant cause of sound absorption for frequencies below 1kHz is the relaxation of nitrogen molecules. For frequencies between 1kHz and 85kHz the dominant cause of sound absorption is the relaxation of oxygen molecules. At frequencies above 85kHz classical absorption becomes the most dominant cause, but this is well beyond the range of human audibility.

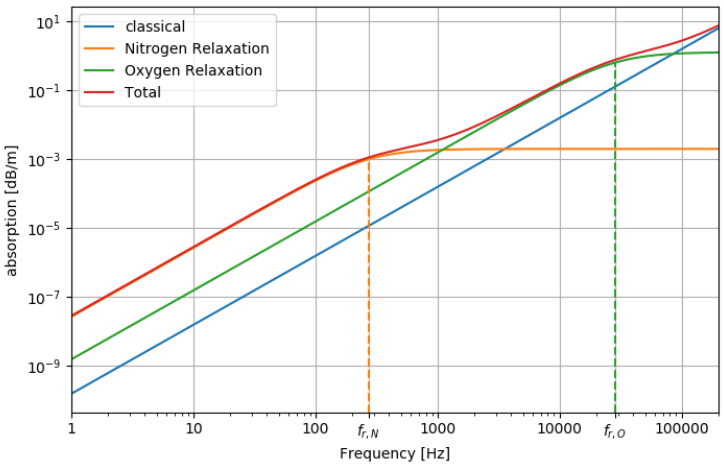

Figure 2.16: Atmospheric absorption of sound as a function of frequency. Calculated for a temperature of 10, a relative humidity of 80% and a atmospheric pressure of 101.325 kPa.

Aircraft Flyover Event

The effect of atmospheric absorption of the sound signal strongly depends on the frequency of the sound wave, as is also observed in Figure 2.16. The effect of atmospheric absorption on sound signals received at the microphone location originating from the aircraft at a frequency of $10Hz$, $100Hz$, $1{,}000Hz$, and $10{,}000Hz$ are considered. These signals are presented in the figures below, where standard atmospheric conditions are used for the determination of the sound attenuation. The standard atmospheric conditions are:

- Ambient air temperature (T_{air}): $15.0°C$,
- Atmospheric pressure (p_a): $101325Pa$, and
- Relative humidity (h_{rel}): 80.0%.

The atmospheric absorption of the sound signal can be approximated as an exponential decay function. This results in the complex wave number given by the equation below.

$$k_a = k + i\,\beta_a$$

Where

$$\beta_a = \frac{\alpha}{20\log_{10}(e)}$$

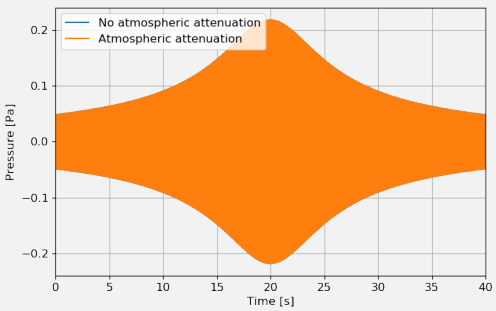

Figure 2.17: Effect of atmospheric attenuation at $10Hz$.

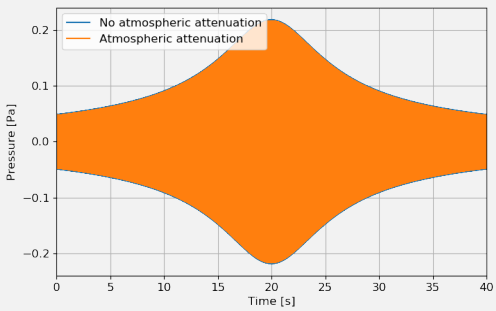

Figure 2.18: Effect of atmospheric attenuation at $100Hz$.

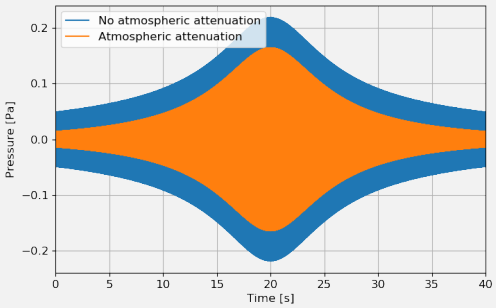

Figure 2.19: Effect of atmospheric attenuation at 1,000Hz.

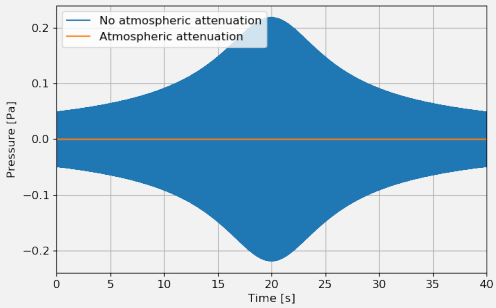

Figure 2.20: Effect of atmospheric attenuation at 10,000Hz.

From the figures above it is observed that at a sound wave frequency of 10Hz and 100Hz the atmospheric attenuation barely affects the sound wave. However, at higher frequencies the effect of atmospheric attenuation grows rapidly. This is in line with the expected behaviour of the atmospheric attenuation presented in Figure 2.16.

2.4. Frequency Weighting

The sensitivity of the human ear is dependent on the frequency of the sound[17]. In order to account for this sensitivity, frequency dependent sound weighting is introduced. The most common frequency weighting methods, A, B, C, and D weighting, are shown in Figure 2.21. Of these four different frequency weighting factors, the A weighting factor is the one most commonly used in aviation.

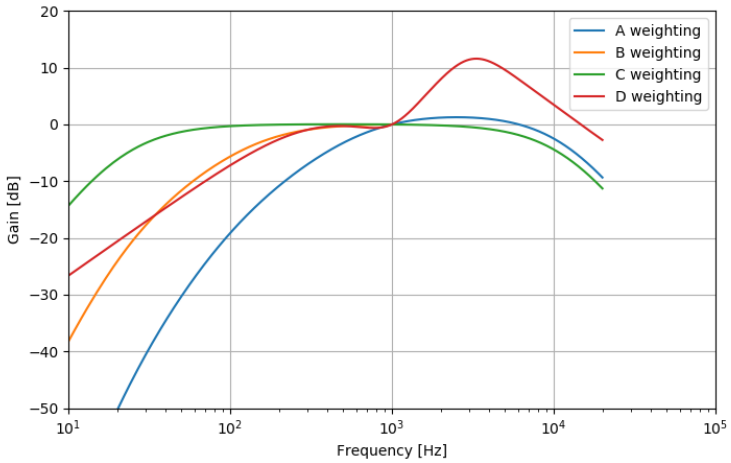

Figure 2.21: Different frequency weighting factors

The effect of applying the A-weighting is that more weight is given to sound signals with a frequency between 1.0 and 6.1 kHz. This effect is illustrated by Figure 2.22, where three different signals with comparable overall sound pressure levels (OSPL) are shown. Signal 1 has most of its power at the lower frequency range whereas signal 2 has most of its power at the higher frequency range, to which the human ear is more sensitive. Signal 3 is somewhat between signal 1 and signal 2, which has approximately equal energy over all frequencies. The resulting OSPL from the unweighted and A-weighted signals are presented in Table 2.1.

Even though the OSPL values of the unweighted signal are rather close together, with a maximum difference of 0.2 dB, the resulting A-weighted OSPL (OASPL) of the different signals can differ by almost 25 dBA. This example clearly illustrates the effect of A-weighting based sound level corrections. Therefore, there is no single correction factor to transform the OSPL of a signal to the OASPL if the spectral information of the signal is not provided.

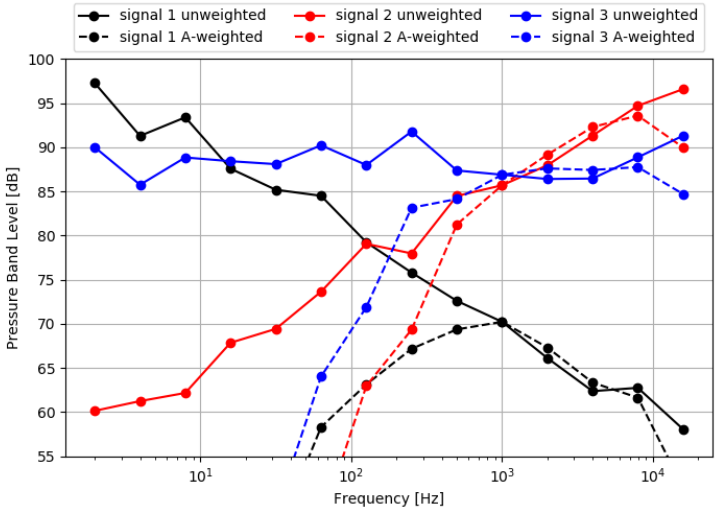

Figure 2.22: A-weighting frequency example

Table 2.1: Resulting OSPL from the A-weighting frequency example

Weighting	Unit	Signal 1	Signal 2	Signal 3
Unweighted	[dB]	100.1	100.1	100.3
A-weighted	[dBA]	75.6	98	94.8

3

Noise Measurements

This chapter discusses the way in which aircraft noise measurement are performed around Schiphol airport. First the requirements for a measurement to be valid for research are discussed. Secondly, the noise monitoring system currently in place around Schiphol is detailed. Finally, an overview of the data collected by the noise monitoring system around Schiphol is given.

3.1. Requirements

As discussed previously there are challenges associated with performing aircraft noise measurements in the field. Aircraft noise measurements are like any other measurement in the real world subject to measurement uncertainty, which can significantly affect the validity of the measurement[67]. In order to determine the validity of an aircraft noise measurement, requirements have to be posed on several aspects. The aspects of an aircraft noise measurement discussed in ISO standard 20906[29] are atmospheric conditions and the location of the measurement device. After the requirements presented in ISO standard 20906 are discussed, the requirements to diminish the effects of background noise and lateral attenuation are presented.

3.1.1. Atmospheric Conditions

Atmospheric conditions have a significant impact on the propagation of sound through the atmosphere[36]. The main atmospheric properties affecting the propagation of sound are wind, precipitation, temperature, relative humidity and atmospheric pressure. The propagation of sound does not only depend on the atmospheric conditions, but also the frequency corresponding to the sound.

The requirements on atmospheric conditions for aircraft noise measurements are provided in ISO standard 20906 [29]. The ISO standard recommends noise measurements to be excluded when one of the following conditions applies:

- Any occurrence of precipitation, and
- Wind speed above $10 m\ s^{-1}$.

When the meteorological data at Schiphol for the whole of 2018 is considered, application of the ISO standard requirements results in the measurements being rejected for 20% of the time. The aim of measurement rejection is to reduce measurement uncertainty corresponding to reduced measurement variation. Reduced measurement variation lowers the measured standard deviation[52].

3.1.2. Location

ISO standard 20906 does not only pose requirements on the atmospheric conditions, but also on the features of the noise monitor location. The aim of this ISO standard is to guarantee that the measurement site is free of any obstructions to the field of view within a range of 10dB(A) below the L_{Amax}, which is equivalent to an elevation angle of 20° from the ground to the aircraft[29].

Another requirement on the measurement site is that the elevation of the microphone above ground is at least $6m$ in order to minimise the effect of ground reflection on the measurements. In order to reduce the amount of reflections it is also required that there are no reflective surfaces within a distance of $10m$ of the measurement device[29].

3.1.3. Threshold

Aircraft noise measurements generally do not take place in a controlled laboratory environment, which means that other noise sources are likely to be present during the noise measurement. The background noise affects the measured value of the SEL and L_{Amax}. The effect of the background noise on the measured SEL and L_{Amax} is diminished if the L_{Amax} of the noise event strongly exceeds the background noise level.

In order to diminish the effects of background noise on the aircraft noise measurement it is suggested to only include measurements where the L_{Amax} exceeds the threshold level by at least 10dB(A)[10]. If this condition is not complied with, the aircraft noise measurement is rejected.

3.1.4. Lateral Attenuation

Posing a requirement on the elevation angle reduces the effect of over ground attenuation. The over ground attenuation highly depends on the surface reflectivity around the measurement device. To minimise the lateral attenuation effects it is suggested that only aircraft noise measurements with an elevation angle (β [°]) larger than 60° should be considered[10]. The elevation angle of the aircraft flyover event is defined as the angle between the ground and the line of sight between the ground and the aircraft, as can be seen in Figure 3.1.

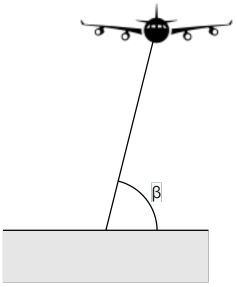

Figure 3.1: Elevation angle of an aircraft flyover event.

3.1.5. Requirement Combination

A decision tree showing if a certain aircraft noise measurement can be considered as usable is shown in Figure 3.2. An aircraft noise measurement is only considered usable if all three of the requirements presented above are met.

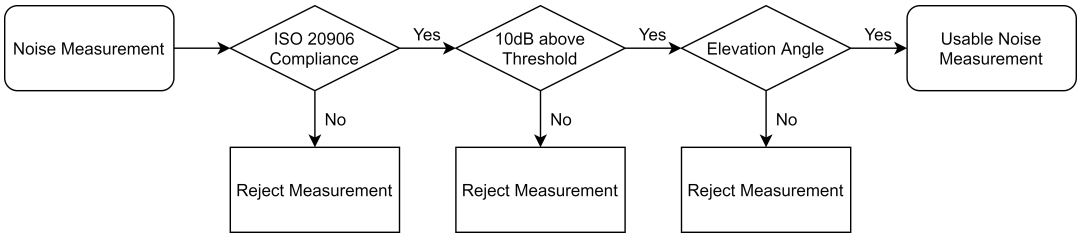

Figure 3.2: Decision tree to determine the usability of an aircraft noise measurement. Based on [10] p. 4 Figure 2: Noise measurement data processing.

3.2. Current Noise Monitoring Systems

This section focuses on the different noise monitoring systems currently in place around several airports, both in The Netherlands and other countries. A noise monitoring system can be used for different purposes. The three main purposes of an aircraft noise monitoring system are[50]:

- Public information
- Enforcement
- Model calibration

The only noise monitoring system that serves a different purpose than public information is the system in place around Heathrow airport as can be seen in Table 3.1. However, if no large differences are observed between the current noise monitoring systems around Schiphol airport and Heathrow airport, the noise monitoring system around Schiphol airport can also be used for enforcement and model calibration purposes. Therefore, the noise monitoring systems currently in place at Schiphol and Heathrow are described in more detail below.

Table 3.1: Characteristics of different noise monitoring systems located at different airports.

Airport	Country	Devices	Purpose
Schiphol	The Netherlands	41	Public information
Eindhoven	The Netherlands	9	Public information
Vancouver	Canada	20	Public information
Heathrow	United Kingdom	50	Public information, enforcement and model calibration
Frankfurt	Germany	29	Public information
Sydney	Australia	12	Public information

3.2.1. Schiphol

The current system for measuring aircraft noise around Schiphol is the NOise MOnitoring System (NOMOS), which has been active since 1993. The system has been installed and is maintained by Brüel & Kjær[1]. NOMOS currently consists of a total of 41 active single microphone measurement devices placed in the area around Schiphol, two of which are used to detect and monitor low frequency noise. The data coming from NOMOS is stored and processed by Royal Schiphol Group. The locations of the currently active NOMOS measurement posts are presented in Figure 3.3.

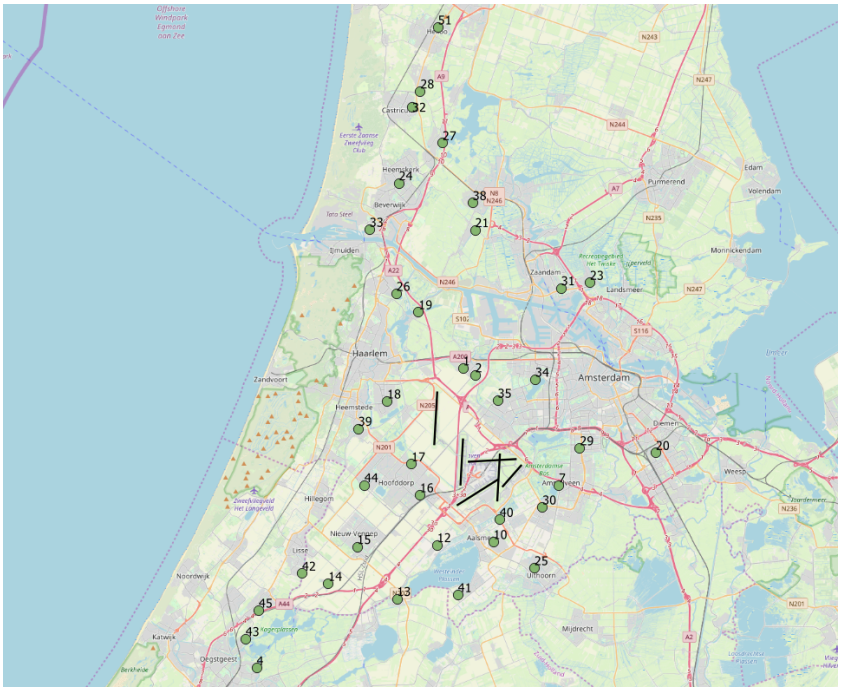

Figure 3.3: Locations of the NOMOS measurement devices around Schiphol.

All NOMOS measurement devices are equipped with class 1 rated microphones[61], which means that for an angle of elevation larger than 60° the uncertainty of the microphone is 0.7dB(A) for the frequencies of

[1]https://www.bksv.com/en

interest. This accuracy applies regardless of the location of the microphone[62]. However, the main purpose of NOMOS is providing information to local residents and is neither used nor designed for scientific purposes, which means that not all NOMOS measurement locations are in line with the ISO 20906 standard.

The number of NOMOS measurement posts has changed over time, meaning that measurement devices have been added to or removed from the total system. Therefore, differences in the exact type of hardware occurs for different measurement post locations but the general performance of the measurement devices in terms of measurement accuracy is similar. Yet another difference between NOMOS measurement posts is the type of ground surface; some devices are installed above the ground and other devices are installed on rooftops, causing a difference in ground reflection characteristics.

3.2.2. Heathrow

The noise monitoring system around Heathrow is an integrated part of the Airport Noise and Operations Management System (ANOMS)[2]. This system integrates the aircraft tracks provided by the British Air Navigation Service Provider and the noise measurements around the airport. ANOMS consists of a total of 50 mobile and fixed measurement post locations. The mobile measurement posts can be deployed at locations that are of interest at that moment, whereas the fixed measurement post locations around Heathrow are shown in Figure 3.4[3].

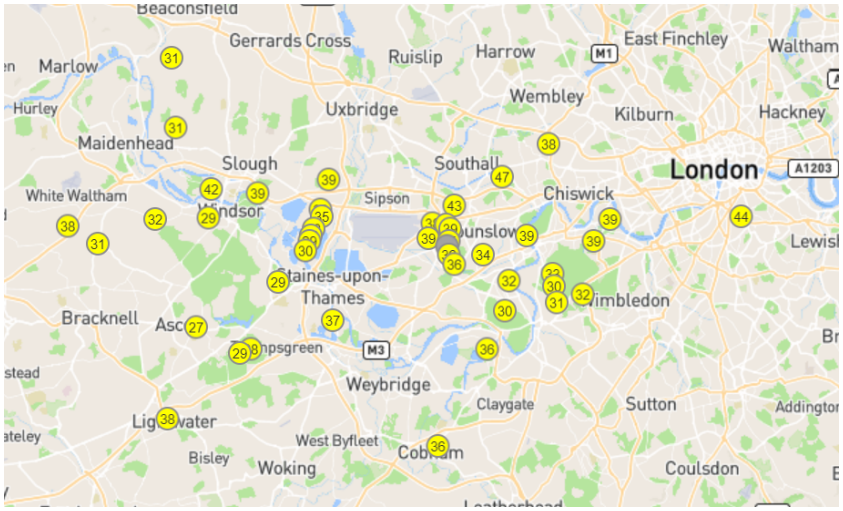

Figure 3.4: Locations of the ANOMS measurement devices around Heathrow.

Both the NOMOS system at Schiphol and the ANOMS system at Heathrow have been installed and are maintained by Brüel & Kjær. Furthermore, the ANOMS system consists of the same class 1 microphones as the NOMOS system. Due to the large similarities between the NOMOS and ANOMS system it is determined that the NOMOS system can also be used for noise model calibration.

3.3. Measurement Data

The data collected by NOMOS can be accessed through the ANOMS 9 application of Brüel & Kjær. NOMOS collects both noise measurement data, which is described first, and radar data, which is described thereafter.

3.3.1. Noise Metrics

For each measurement performed by the NOMOS system the SEL and L_{Amax} values are presented to the user with an accuracy of $0.1 dBA$. Besides these noise metrics the noise level in dBA per second can also be extracted by the user. The noise level per second for an example measurement taken at measurement post 13 is shown in Figure 3.5. The SEL and L_{Amax} values presented in ANOMS for this specific aircraft noise event and the values obtained from the dBA time series in Figure 3.5 are presented in Table 3.2.

In Table 3.2 it is observed that the values presented in ANOMS and the values resulting from the time series are similar. Due to ease of accessibility the choice is made to only use the values directly presented by

[2]https://www.heathrow.com/company/local-community/noise, accessed on 19-05-2020
[3]https://webtrak.emsbk.com/lhr4, accessed on 19-05-2020

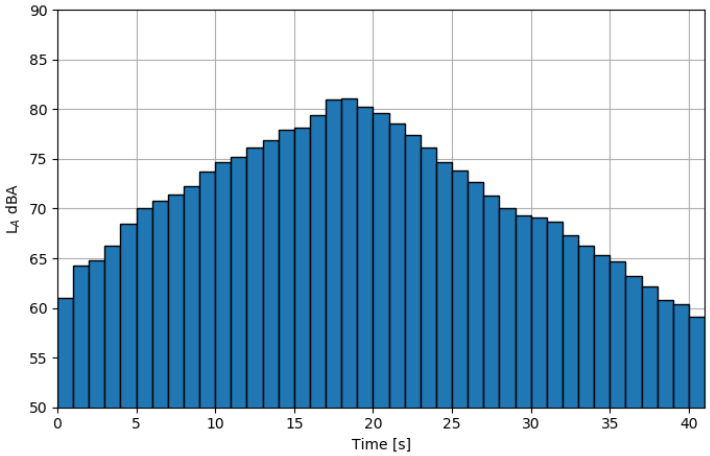

Figure 3.5: Example of time series aircraft noise level at measurement post 13.

ANOMS for the research.

Table 3.2: Noise metrics resulting from ANOMS and the time series.

Metric	ANOMS	Time Series
LAmax	81.0	81.1
SEL	90.9	90.88

Another way in which the sound information of the aircraft flyover event is stored is in mp3 files. These mp3 files are stored in the ANOMS database and can be accessed individually up to 3 months after the measurement has taken place. The pressure obtained from an example mp3 file is presented in Figure 3.6. Not only the measured pressure deviation is presented in this figure, but also the effective pressure (p_e [Pa]) level is included. The effective pressure is given by the equation below. It should be noted that the integration time (T_{int} [s]) is taken such that a sufficiently long part of the pressure signal is considered.

$$p_e = \sqrt{\frac{1}{T_{int}} \int_0^{T_{int}} \left(p'(t)\right)^2 dt} \tag{3.1}$$

The effective pressure can subsequently be used to determine the unweighted overall sound pressure level (OSPL). The unweighted OSPL, together with the A-weighted OSPL from the time series available in ANOMS, and the A-weighted OSPL determined using the mp3 data, is presented in Figure 3.7. From the comparison between the A-weighted OSPL retrieved from ANOMS and the A-weighted OSPL from the mp3 file in the figure below it is concluded that large discrepancies exist. This is a consequence of the fact that the mp3 files stored by ANOMS are resampled at a sampling frequency of $8kHz$. Therefore the mp3 files cannot be used for the determination of the L_{Amax} or SEL associated with an aircraft noise event.

3.3.2. Radar Data

The NOMOS system uses the Schiphol radar for the detection of aircraft noise events [61]. Therefore all noise measurements related to aircraft movements are directly linked to the operation and track. The operational data in ANOMS contains the type of operation; Arrival (A), Departure (D), or Overflight (O). The operational data is also linked to the ICAO type code of the aircraft and the aircraft registration.

The update frequency of the Schiphol radar is 0.25 Hz, meaning that the aircraft position is updated every 4 seconds. The radar data for each individual flight contains:

- **Horizontal position**: Latitude and longitude of the aircraft in decimal degrees.
- **Vertical position**: Altitude of the aircraft in feet.
- **Velocity**: The ground speed in knots derived from the difference in position between two observations.

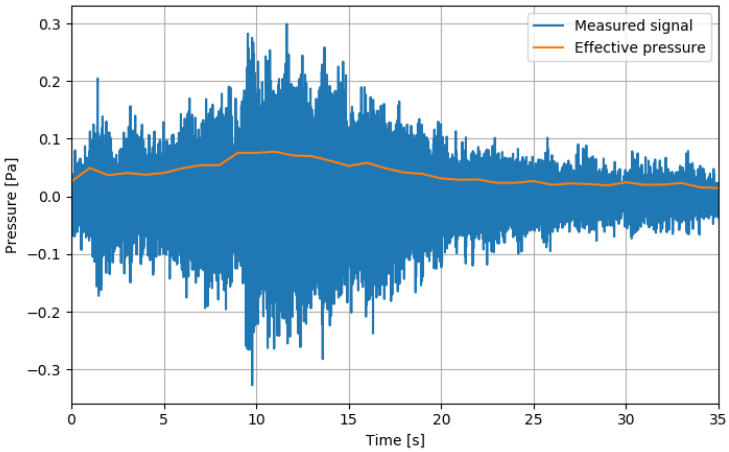

Figure 3.6: Pressure signal obtained from the example mp3 file.

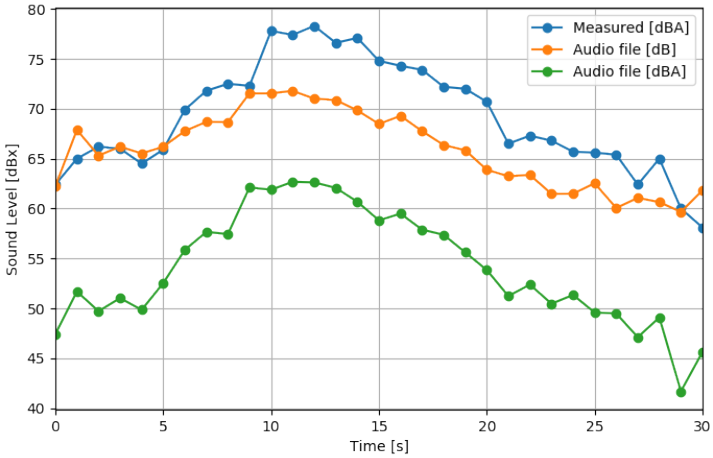

Figure 3.7: Comparison between the A-weighted OSPL retrieved from ANOMS (blue), the unweighted OSPL obtained from the mp3 file (orange), and the A-weighted OSPL obtained from the mp3 file (green).

- **Track time**: The date and time corresponding to the radar observation.

This radar data allows for a complete visualisation of the flight track of the aircraft. A more elaborate example of the data from the Schiphol radar is given in the next chapter.

4

Noise Calculations

There are two models which are used in the Netherlands for the modelling of aircraft noise. The first model is the Dutch 'Nederlands Rekenmodel' (NRM)[25] and the second model is the European Civil Aviation Conference (ECAC) Doc.29 aircraft noise model[7–9]. For Schiphol the transition has been made from the NRM towards ECAC Doc.29, which would result in uniformity in the noise calculations for all European airports[2]. Therefore, it is decided for this research to focus on the implementation of ECAC Doc.29 instead of the NRM. Furthermore, the segmentation based aircraft noise models, including the ECAC Doc.29 aircraft noise model and NRM, are currently considered to be the best practise models[43].

First the expressions of the noise metrics associated with an individual flight path segment are presented. Secondly the input parameters for the aircraft noise model are described. Thereafter the conversion of the input parameters to a noise level is presented. Finally, the verification of the implementation for this research based on the reference cases presented by ECAC is discussed. It should be noted that the aircraft noise calculation method discussed in this chapter focuses on the determination of the aircraft noise exposure for a single aircraft noise event rather than long-term aircraft noise exposure.

4.1. Segment Level Expressions

The segment level sound metric values are calculated by applying corrections to the infinite flight path values as provided in the Aircraft Noise Performance (ANP) data[1]. The segment contributions towards the maximum exposure level and the SEL are given by Equation 4.1.

$$\begin{aligned} L_{max_{seg}} &= L_{max}(P,d) + \Delta_I(\varphi) - \Lambda(\beta,l) \\ SEL_{seg} &= SEL_{\infty}(P,d) + \Delta_V + \Delta_I(\varphi) - \Lambda(\beta,l) + \Delta_F \end{aligned} \tag{4.1}$$

The correction terms in the equation above correct for the following effects[8]:

- Δ_V *Duration Correction*: The ANP data is normalised for a reference speed. This factor accounts for deviation from the reference speed and hence the exposure time deviation. The duration correction is only applicable to the SEL calculation.
- $\Delta_I(\varphi)$ *Engine Installation Correction*: Due to the installation location of the engines (e.g. on the fuselage or wing) shielding, refraction and reflection of sound occurs. These effects cause a variation in lateral directivity. The engine installation correction is applicable to both the maximum level and SEL calculations.
- $\Lambda(\beta,l)$ *Lateral Attenuation Correction*: At low angles to the ground there is an interaction between direct and reflected sound waves. This effect furthermore also accounts for non-uniformities in the the atmosphere mainly caused by the proximity to the ground.
- Δ_F *Finite Segment Correction*: The ANP data, as mentioned previously, is applicable for flight path segments of infinite length. However, the modelled segment has a finite length, which means that the SEL of the segment is always lower than the SEL of the infinite flight path. The finite segment correction is therefore only applicable to the SEL.

[1] Data retrieved from https://www.aircraftnoisemodel.org/, accessed on 11-09-2019

The maximum level of a sequence of segments is simply the largest value of the maximum level of each of the individual segments. For the SEL the combination of a sequence of segments is slightly more complicated as it is the decibel sum of each of the individual segment contributions to the SEL (SEL_{seg} [dBA]). The calculation of the SEL as a result of the contribution of each individual segment is presented in the equation below.

$$SEL = 10 \log_{10} \left(\sum 10^{\frac{SEL_{seg}}{10}} \right) \tag{4.2}$$

4.2. Input Parameters

The input parameters of the noise prediction model can be divided in track specific parameters, which are assumed to be constant throughout the track of the aircraft, and segment specific parameters. Track specific parameters are the aircraft type and the aircraft weight, which is assumed to remain constant throughout the track. The segment specific parameters, which have to be specified at the beginning and end of each individual segment are:

- **The position of the aircraft**: Usually specified by radar in terms of longitude, latitude in degrees and altitude in feet.
- **Ground speed**: Usually specified by radar in knots.
- **Bank angle**: Generally not directly available, but has to be estimated based on radar data and aircraft performance.
- **Thrust setting**: Generally not directly available, but has to be estimated based on radar data and aircraft performance.

4.2.1. Aircraft Position

As already mentioned the aircraft position from radar data is generally specified in a longitude (λ [°]), latitude (ϕ [°]) in degrees and altitude (h [ft]). In order for the radar data to be used as input to the model, the longitude and latitude have to be converted to an x-,y-coordinate system with the units meters associated to it. In order to do make the conversion from the longitude and latitude system to an x-,y-coordinate system, a reference point for the local flat earth approximation has to be specified. For the sake of uniformity, the same reference point is used as the reference point used by LVNL for the flat earth approximation; the location of the air traffic control tower at Schiphol. The wgs84 coordinates of the air traffic control tower at Schiphol are specified in Table 4.1.

Table 4.1: Schiphol tower reference coordinates in degrees.

Longitude	λ_0	52.307514
Latitude	ϕ_0	4.762456

The conversion from the longitude and latitude system to the x-,y-coordinate system is provided by the equations below. The correction factor in the first equation using the cosine of the latitude accounts for the fact that the meridians are getting closer together when the distance from the equator increases. This effect does not occur in the y-direction and therefore does not have to be corrected for.

$$x = 60 \ (\lambda - \lambda_0) \ 1852 \cos\left(\phi_0\right) \tag{4.3}$$

$$y = 60 \ \left(\phi - \phi_0\right) \ 60 \ 1852 \tag{4.4}$$

An example of an unprocessed radar track as provided by the ANOMS system is shown in Figure 4.1. After the processing as explained by the equations above, the resulting track that can be used as input for the model is shown in Figure 4.2. It should also be noted that the altitude is transformed from feet to meters using a simple unit conversion factor.

4.2.2. Ground Speed

The ground speed of the aircraft can be directly obtained from the ANOMS system. The ground speed provided by the ANOMS system is presented in the unit of knots, which means that it has to be converted to meters per second using a simple unit conversion. The ground speed profile corresponding to the radar tracks

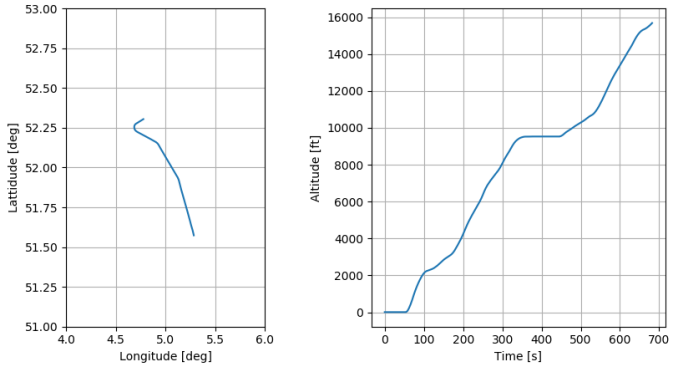

Figure 4.1: Unprocessed example radar track with ground track (longitude and latitude) on the left and vertical profile (altitude and time) on the right.

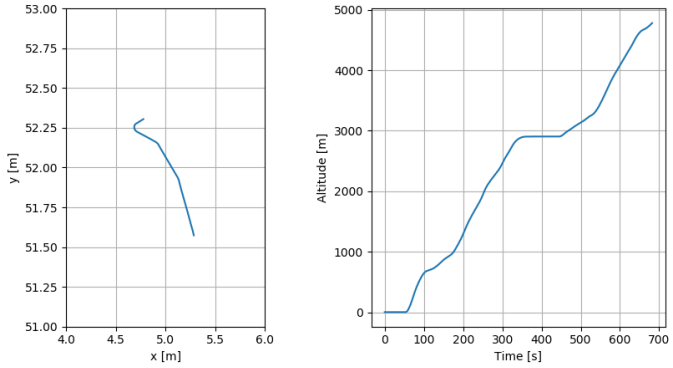

Figure 4.2: Processed example radar track with ground track (x and y) on the left and vertical profile (altitude and time) on the right.

presented in Figure 4.1 can be found in Figure 4.3. The ground speed profile can be used for subsequent calculations, such as bank angle and thrust estimation.

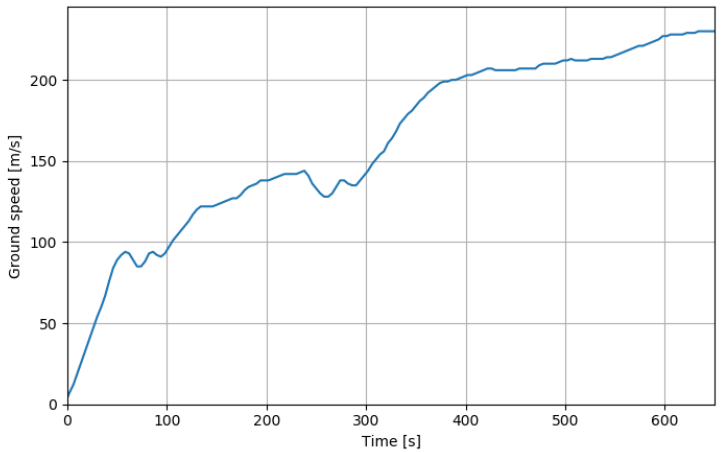

Figure 4.3: Example of ground speed profile obtained from the ANOMS system.

4.2.3. Bank Angle

The bank angle (ε [°]) is one of the required input parameters that cannot be directly obtained from the radar data in the ANOMS system. However, an estimation of the bank angle can be made by using the equation presented below. The bank angle can be estimated by using the ground speed of the aircraft (V_g [kts]), the turn radius in feet (r [ft]) and gravitational acceleration in feet per second squared (g [ft s^{-2}]). The estimation of the aircraft bank angle is given by the equation below.

$$\varepsilon = \tan^{-1}\left(\frac{2.85\ V_g^2}{r\ g}\right) \tag{4.5}$$

For the sake of simplicity and ease of the calculation, only the horizontal element of the turn is considered. The increase in altitude during a turn is considered to be negligible [8]. The turn radius at a given point is estimated by fitting a circle through the x- and y-coordinate of the point under consideration, the previous point and the next point[47]. An illustration of how the process of estimating the turn radius is done can be found in Figure 4.4. The resulting bank angle estimated using the radar track presented in Figure 4.2 is shown in Figure 4.5.

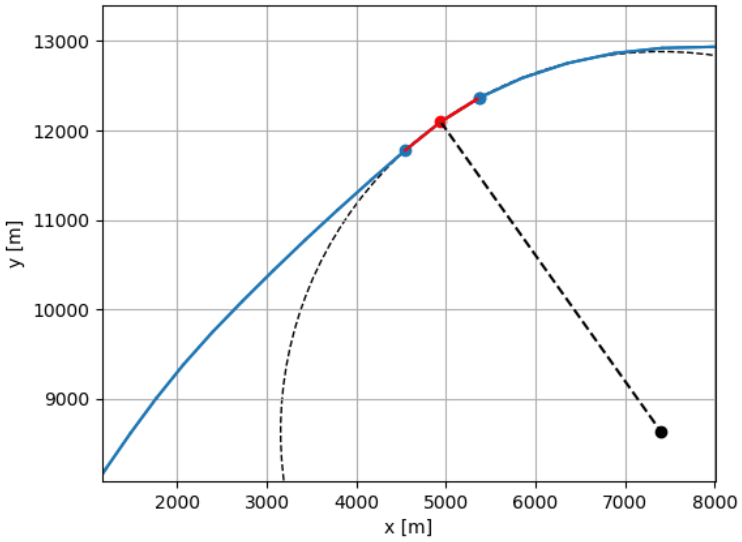

Figure 4.4: Example of turn radius estimation based on three radar points. The blue dots indicate the previous and next track point and the red dot indicates the point under consideration. The black dot indicates the estimated point around which the turn is performed and the black dotted line connecting this point to the red dot is the turn radius.

From Figure 4.5 it can be observed that the estimated bank angle resulting from the radar data, the blue line in this figure, is rather fluctuating. This fluctuating behaviour of the resulting signal is a consequence of the limited accuracy of the data provided by the radar, both in terms of the aircraft position and the velocity. These fluctuations in the signal can be suppressed by using a moving average filter, which is essentially a low-pass filter and eliminates high frequency noise from the signal. The elimination of high frequency fluctuations in the estimated bank angle seems sensible, as an aircraft is rather inert against fast fluctuations. The elimination of high frequency noise in the signal can be clearly observed from the moving average in Figure 4.5. It is furthermore observed that the application of the moving average filter also lowers the peak values observed in the bank angle. Smoothing of the bank angle reduces the effect of outliers as a consequence of radar data inaccuracy, which means that a more reliable resulting bank angle is obtained[47]. Finally, it should be noted that a bank angle of 25° is common when the aircraft is placed in a holding pattern, but it is uncommon to reach a bank angle of 25° during a departure. Therefore, the damping effect the moving average filter has on the bank angle estimation is considered to be accurate.

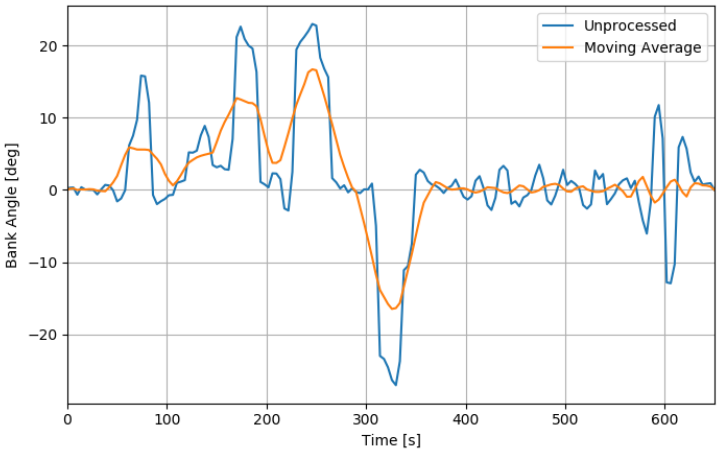

Figure 4.5: Example of resulting bank angle approximation using radar track.

Moving Average Filter

A moving average (MA) filter is used to provide smoothing of the data. A symmetric MA filter averages the data of the (M-1)/2 data point before the point of interest, at the point of interest and the (M-1)/2 data points after the point of interest. This means that the unsmoothed data is smoothed using a total of M data points for each individual data point. The averaging is therefore performed using M values. The averaging is therefore performed using M values. A symmetric MA filter with an M of 5 at data point 80 would result in[59]:

$$y[80] = \frac{x[78] + x[79] + x[80] + x[81] + x[82]}{5}$$

In the general form the MA filter is given by the equation below, where x is the input signal and y is the output signal of the MA filter.

$$y[i] = \frac{1}{M} \sum_{j=-\frac{M-1}{2}}^{\frac{M-1}{2}} x[i+j]$$

Like any filter the MA filter can be transformed from the time domain to the frequency domain. The frequency domain response of the MA filter is given by the equation below, which is visualised in Figure 4.6, where the x-axis represents the ratio between the frequency (f [Hz]) and the sampling frequency (f_s [Hz]).

$$H[f] = \frac{\sin\left(\pi\, M\, \frac{f}{f_s}\right)}{M \sin\left(\pi\, \frac{f}{f_s}\right)}$$

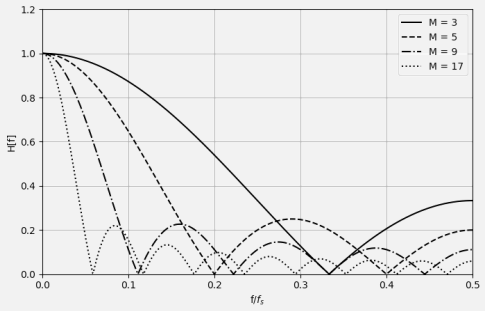

Figure 4.6: Frequency response of the MA filter for different values of M.

4.2.4. Thrust

The two parameters directly used to estimate the noise produced by an aircraft during a noise event is the distance between the aircraft and the observer and the aircraft thrust setting. Therefore, a reliable method for the estimation of the thrust setting is crucial to accurate aircraft noise calculations. However, the thrust setting cannot be obtained directly from radar data, which means that it has to be estimated based on the available data. Different methods exist for estimating the thrust delivered by the engines:

- Radar based
- N1 estimation based
- Performance based

Radar Based Thrust Estimation Method

As the name implies, the radar based thrust estimation mainly uses the data directly available from the radar tracks and is given by:

$$\frac{F_n}{\delta} = E + F\ V_{CAS} + G_A\ h + G_B\ h^2 + H\ T_{air} \tag{4.6}$$

Only the atmospheric properties, ambient air temperature and pressure, have to be estimated. This is done by using the International Standard Atmosphere (ISA) in combination with the meteorological conditions at sea level. The ambient air temperature (T_{air} [$^\circ C$]) is directly used in the thrust estimation and the pressure is used both for the ratio between the local air pressure and the mean sea level air pressure (δ [-]) and the conversion of true airspeed (V_{TAS} [kts]) to calibrated airspeed (V_{CAS} [kts]). Furthermore the radar based thrust estimation method depends on the altitude of the aircraft (h [ft]). The coefficients needed for the thrust estimation (E [lb], F [lb kts^{-1}], G_A [lb ft^{-1}], G_B [lb ft^{-2}] and H [lb $^\circ$C^{-1}]) are obtained for the specific aircraft and operation type from the ANP database. The relation between the true airspeed and the calibrated airspeed is given by the equation below.

$$V_{CAS} = V_{TAS}\ \sqrt{\delta\ \frac{288.15}{T + 273.15}} \tag{4.7}$$

The V_{CAS} and V_{TAS} profile of the aircraft over time is presented in Figure 4.7. It is observed that the difference between the V_{CAS} and V_{TAS} increases over time, which is a result of the increasing altitude of the aircraft and the decrease is ambient atmospheric pressure (P_a [Pa]) associated with it. The effect of the aircraft altitude on the ratio between the V_{CAS} and V_{TAS} is presented in Figure 4.8. The ratio between the V_{CAS} and V_{TAS} presented in this figure supports the observation that the difference between both airspeeds increases as the aircraft altitude increases. It is also observed that the difference between the two airspeeds is less than 10% at aircraft altitudes below 2,000m. This means that the two airspeeds can be used interchangeably in the aircraft thrust estimation, especially when there is no available data on the atmospheric conditions at the aircraft.

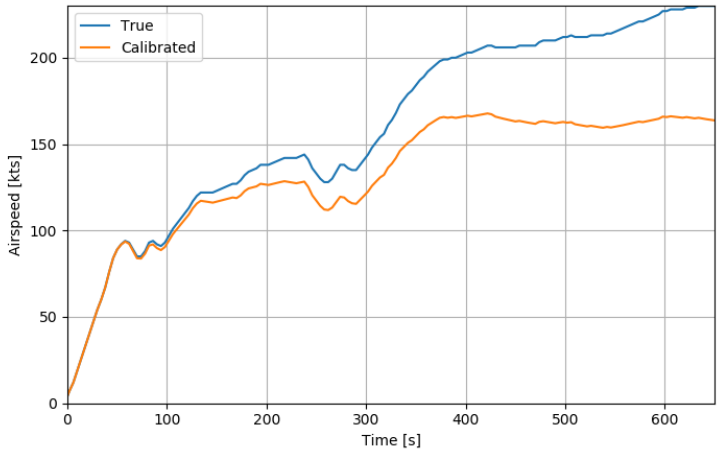

Figure 4.7: Example of resulting calibrated airspeed in relation to the true airspeed.

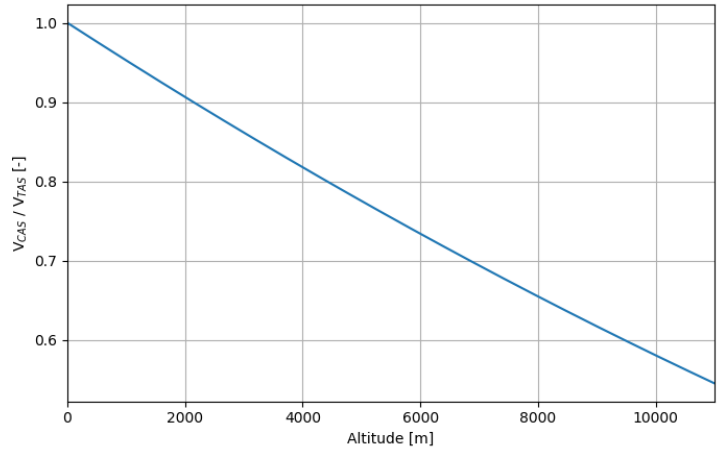

Figure 4.8: Effect of the aircraft altitude on the ratio of the V_{CAS} and V_{TAS}.

N1 Based Thrust Estimation Method

The radar based thrust estimation can be extended to also include the fan rotational speed as input parameter as given by the equation below[8].

$$\frac{F_n}{\delta} = E + F\ V_{CAS} + G_A\ h + G_B\ h^2 + H\ T + K_3 \left(\frac{N1}{\sqrt{\theta_{air}}}\right) + K_4 \left(\frac{N1}{\sqrt{\theta_{air}}}\right)^2 \tag{4.8}$$

It should be noted that the coefficients in this equation (E, F, G_A, G_B, and H) are different from the coefficients in Equation 4.6 and that the additional coefficients (K_3 [lb rpm^{-1}] & K_4 [lb rpm^{-2}]) are taken from the ANP database. A second note is that the fan rotational speed (N1 [rpm]) is not available from the radar data. The N1 during an aircraft flyover can be estimated by analysing the noise measurement of that flyover event[48]. Furthermore, the ratio between the ambient air temperature at the aircraft altitude and the standard reference air temperature (θ_{air} [-]) is given by the equation below.

$$\theta_{air} = \frac{T_{air} + 273.15}{288.15} \tag{4.9}$$

N1 Estimation

The fan rotational speed can be estimated from spectral analysis of the aircraft noise measured during an aircraft flyover event. The blade passing frequency (BPF) of the fan is determined by the number of fan blades (B [-]) and the fan rotational speed according to:

$$BPF = f_1 = \frac{B\,N1}{60}$$

Usually the higher harmonics of the BPF are also observed in the spectral analysis, occurring at $f_k = k\,f_1$. The BPF and the corresponding higher harmonics can be seen in the figure below. The vertical black line indicates the moment at which the aircraft is at its closest point of approach to the observer. The Doppler shift is also clearly visible in the dashed black lines.

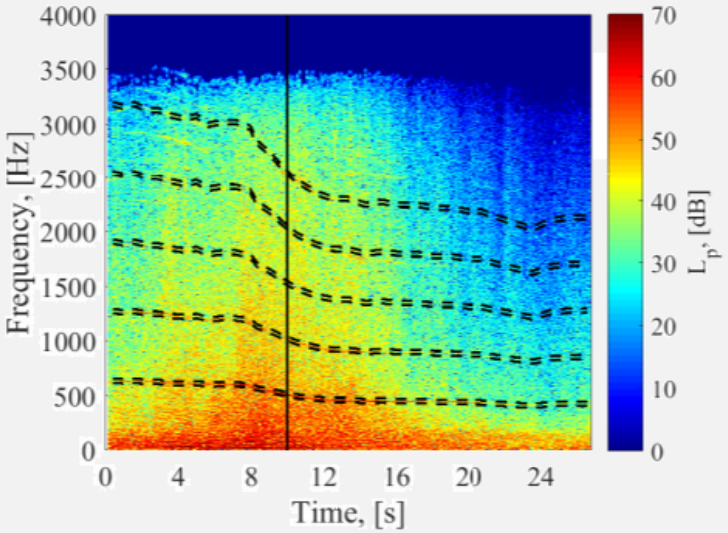

Figure 4.9: BPF and higher harmonics estimation. Taken from [48] pg. 4 Figure 1.

Performance Based Thrust Estimation Method

The performance based thrust estimation requires an estimation of the aircraft weight (W [lb]), the drag over lift ratio corresponding to the aircraft configuration (R [-]) and the acceleration or deceleration along the flight path (a [m s^{-2}]). Other parameters affecting the thrust estimation are the flight path angle (γ [°]) and the bank angle (ε [°]).

$$\frac{F_n}{\delta} = W\,\frac{R\,\frac{\cos(\gamma)}{\cos(\varepsilon)} + \sin(\gamma) + \frac{a}{g}}{N\,\delta} \tag{4.10}$$

The recommended method for estimating the aircraft weight for the thrust estimation depends on the type of operation, i.e. arrival or departure. For arriving aircraft the current weight throughout the entire approach is assumed to be 90% of the Maximum Gross Landing Weight (MGLW) as specified in the ANP database. The procedure for estimating the weight of a departing aircraft is slightly more elaborate as the distance between the airport of departure and the destination plays a significant role in the amount of fuel required for the trip. The stage length, which is used to estimate the Take-Off Weight (TOW) of an aircraft, is based on the great circle distance between the origin and destination airport. The stage lengths used in the ANP database are presented in Table 4.2. The subsequent translation from the stage length to the estimated aircraft weight for the B772 aircraft is also presented in this table.

The aerodynamic coefficient is specified for a specific phase of flight, depending on the aircraft configuration. As the aircraft configuration cannot be identified from radar data, the configuration has to be estimated based on the available parameters. The main parameters used for the specification of the aircraft configuration are the calibrated airspeed and the altitude. As an example the aerodynamic coefficient corresponding to a default procedural approach for a Boeing 737-700 is provided in Table 4.3. The values presented in this

Table 4.2: Stage length in relation to trip length and the associated representative range and aircraft take off weight for the B772 aircraft.

Stage Length	Trip Length [nm]	Representative Range [nm]	Weight [lb]
1	0-500	350	429900
2	500-1000	850	442400
3	1000-1500	1350	456100
4	1500-2500	2200	483100
5	2500-3500	3200	516400
6	3500-4500	4200	551700
7	4500-5500	5200	589400
8	5500-6500	6200	629500
9	6500 +	-	656000

table are taken from the ANP database. The case may occur that the combination of air speed and altitude in the radar data is not compatible with the values supplied by the ANP database. In that case the aircraft configuration is estimated using the calibrated airspeed alone, as this is considered to be the most driving factor for the aircraft configuration. The aerodynamic coefficient estimated for the flight track in the current example can be seen in Figure 4.10. The jumps from one level of aerodynamic coefficient to another, rather than a smooth transition, is because of the jump in flap settings based on the calibrated airspeed and altitude, which are more realistic than a smooth transition.

Table 4.3: Aerodynamic coefficients corresponding to a default procedural approach for a Boeing 737-700

Stage	V_{CAS} [kts]	Alt [ft]	Flap_ID	R [-]
0	250+	6000+	T_ZERO	0.0552
1	250-171	6000-3000	T_ZERO	0.0552
2	171-140	3000-1500	T_5	0.0749
3	140-133	1500-1000	A_15	0.1048
4	133-0	1000-0	A_40	0.1434

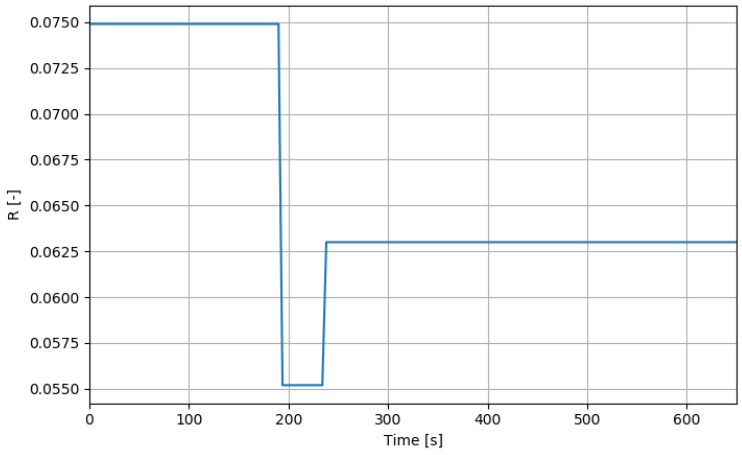

Figure 4.10: Example of resulting aerodynamic coefficient approximation using radar track.

The remaining parameters to be specified are the flight path angle and the acceleration along the flight path. The flight path angle is estimated by comparing the vertical displacement (Δh [m]) to the vertical displacement (ΔS [m]) along the flight segment under consideration by using the equation below.

$$\gamma = \tan^{-1}\left(\frac{\Delta h}{\Delta S}\right) \tag{4.11}$$

The flight path angle for the example flight as given in Figure 4.1 is shown in Figure 4.11. The positive flight path angle indicates that the aircraft is climbing, which is in line with the altitude profile as presented in Figure 4.1. The acceleration or deceleration of the aircraft is obtained by differentiation of the aircraft speed from the radar data with respect to time as is given by the equation below, where the acceleration is determined by using the speed difference between two radar observations (ΔV [kts]) and the time between two radar observations (Δt [s]).

$$a = \frac{\Delta V}{\Delta t} \tag{4.12}$$

For the equation above the acceleration of the aircraft is not directly available from radar data, but obtained by differentiation of the aircraft speed. The acceleration profile resulting from the example radar track is given in Figure 4.12. In the acceleration profile the take-off and two additional acceleration segments can be clearly identified.

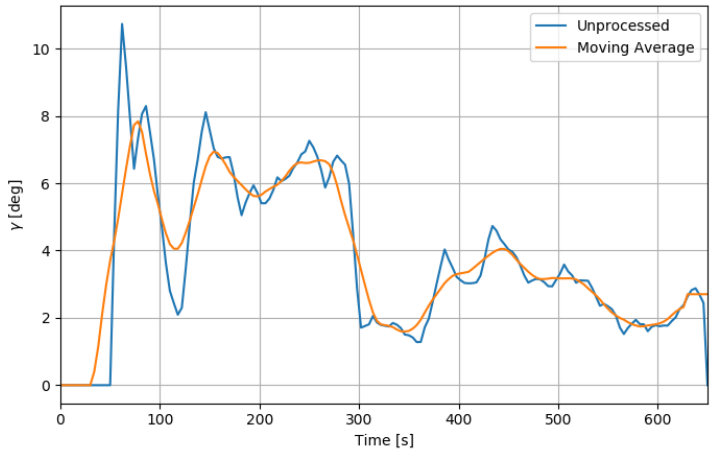

Figure 4.11: Example of resulting flight path angle approximation using radar track.

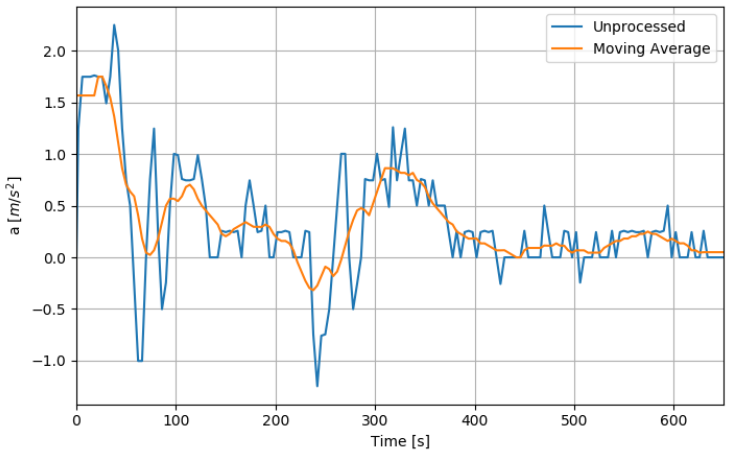

Figure 4.12: Example of resulting acceleration approximation using radar track.

Now that all parameters required for the performance based thrust estimation, Equation 4.10, are provided the thrust estimation is performed. The thrust can be broken down into three components:

- An aerodynamic component ($F_{n,aero}$ [lb]):

$$F_{n,aero} = W \frac{R}{\cos(\gamma)}$$

- A potential energy component ($F_{n,pot}$ [lb]):

$$F_{n,pot} = W \sin(\gamma)$$

- A kinetic energy component ($F_{n,kin}$ [lb]):

$$F_{n,kin} = W \frac{a}{g}$$

The total estimated thrust is the sum of the three individual thrust components. An important condition which has to be imposed on the the total estimated thrust is that it cannot be negative, which should make sense. If the total estimated thrust falls below zero, the estimated thrust is forced to be zero. The thrust component and the resulting total thrust estimations are shown in Figure 4.13. Even though the contribution of the kinetic energy component falls below zero, which indicates deceleration instead of acceleration, the total thrust estimation never falls below zero. This means that the requirement of the total thrust level to be positive is not activated.

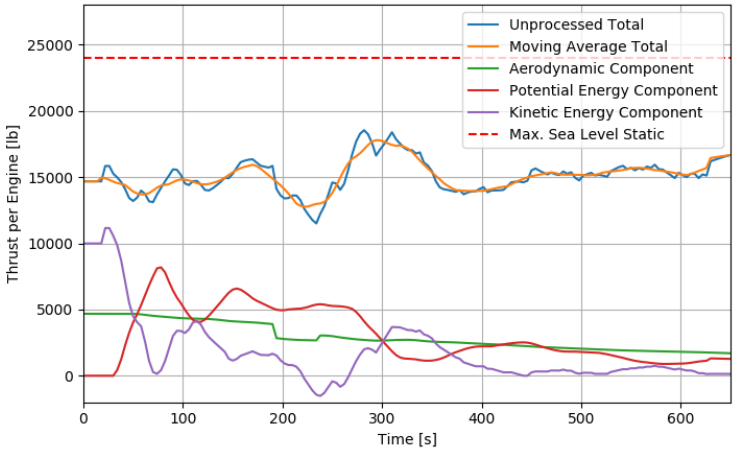

Figure 4.13: Example of resulting total thrust approximation using radar track.

Thrust Estimation Method Selection

Three different thrust estimation methods have been outlined here, but only one thrust estimation method can be implemented for the baseline aircraft model performance. It has been found that the implementation of the aircraft performance based thrust estimation method yields the best results when considering individual aircraft noise events[34]. Therefore, the aircraft performance based thrust estimation method is implemented for the determination of the baseline aircraft noise model performance.

Even though the radar based and N1 based thrust estimation methods are not implemented in the baseline aircraft noise model performance, these are not discarded. For the calibration of the input parameters in the aircraft noise model in section 6.2 the performance of both thrust setting estimation methods is also evaluated.

4.3. Doc.29 Model Implementation

This section outlines the implementation of the noise modelling guidelines of the Doc.29 aircraft noise model. First, the geometry associated with the aircraft noise calculations are discussed. Secondly, the way in which the data from the NPD tables is obtained is outlined. Finally, the corrections which have to be used to account for noise propagation effects, such as shielding effects, are discussed.

4.3.1. Geometric

Each segment of the full flight path is defined by the following begin-point (S_1) and end-point (S_2) characteristics:

- **Horizontal Position**: x- and y-coordinate of the begin- and end-point with respect to the selected reference point.
- **Vertical Position**: z-coordinate of the begin- and end-point with respect to mean sea level reference altitude. It is noted that the geometry of the area under investigation can be such that there are local difference between terrain altitude and mean sea level, which has to be set by the user.
- **Velocity**: The ground speed is defined at the begin- and end-point of the segment.
- **Thrust**: The engine thrust setting is defined at the begin- and end-point of the segment.

Based on the begin- and end-point of the flight segment and the location of the observer (O), the following geometric parameters are identified in Figure 4.14:

- S_p: The closest point of approach between the observer and the (extended) flight segment path.
- d_1, d_2: The distance between the observer and the start- and end-point of the flight segment.
- d_p: The perpendicular distance between the observer and the (extended) flight segment path.
- d_s: The shortest distance between the flight segment path and the observer.
- λ: The length of the flight segment path.
- q: The distance between the closest point of approach of the (extended) flight segment path and the start-point of the flight segment path. This is negative if S_p is located behind S_1.

The values of d_s and q depend on the location of the observer with respect to the flight segment. The observer can either be behind the whole flight segment, between the start- and end-point of the flight segment or in front of the whole flight segment. From Figure 4.14 the following values of d_s and q can be observed for the difference cases:

- **Observer behind the whole flight path segment**: d_s is equal to d_1 and the value of q is negative (Figure 4.14a).
- **Observer between start- and end-point of the flight path segment**: d_s is equal to d_p and the value of q is positive, but smaller than λ (Figure 4.14b).
- **Observer in front of the whole flight path segment**: d_s is equal to d_2 and the value of q is positive and larger than λ (Figure 4.14c).

The distance used for the determination of the L_{Amax} is d_s. The distance used for the determination of the SEL depends on whether the segment under consideration is an airborne or ground segment. The distance used for the determination of SEL in an airborne segment is d_p and d_s in a ground segment.

If the aircraft is seen from the front, as illustrated in Figure 4.15, several geometrical angles can be identified. In this figure the elevation angle (β [°]) is determined based on the lateral distance between the aircraft and the observer (l [m]) and the height of the aircraft (h [m]). Therefore, the elevation angle of the aircraft is given by the equation below.

$$\beta = \tan^{-1}\left(\frac{h}{l}\right) \tag{4.13}$$

The elevation angle ranges between 0° and 90°. The depression angle (φ [°]) is obtained by adding the bank angle (ε [°]) of the aircraft to the elevation angle as indicated by the equation below. The sign of the equation depends on the location of the observer with respect to the aircraft. The sign is positive if the observer is at the starboard side and negative if the observer is on the porch side of the aircraft.

$$\varphi = \beta \pm \varepsilon \tag{4.14}$$

Now that the distance has been determined, the next step for the determination of the noise level is to define the engine power setting (P [lb]) associated with the observer location. If the observer is behind or in front of the whole flight path segment, the engine power setting at the observer is P_1 or P_2 respectively. P_1 and P_2 are the engine power setting associated with the start- and end-point of the flight segment. If the observer is between the start- and end-point of the flight segment the engine power setting associated with the observer location is defined by Equation 4.15.

$$P = \sqrt{P_1^2 + \frac{q}{\lambda} \cdot \left(P_2^2 - P_1^2\right)} \tag{4.15}$$

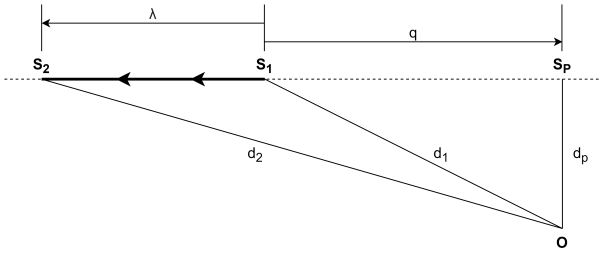

(a) Observer location behind the whole flight path segment.

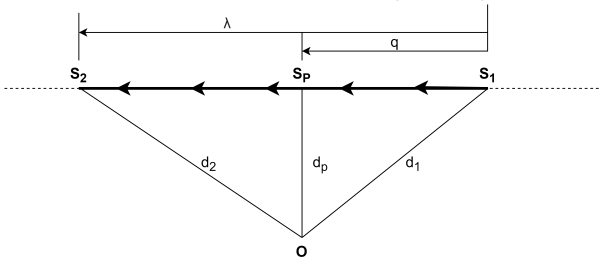

(b) Observer location between the start- and end-point of the flight path segment.

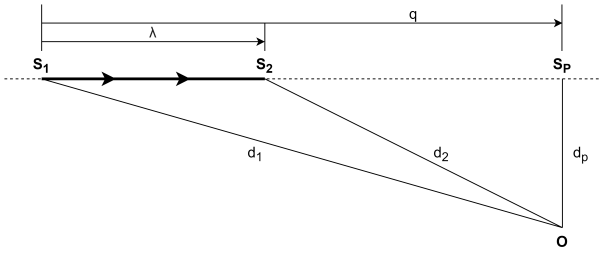

(c) Observer location in front of the whole flight path segment.

Figure 4.14: Horizontal view of the geometric parameters of the flight path segment under consideration with respect to the location of the observer. Based on [8] Figure 4-2a - 42-c.

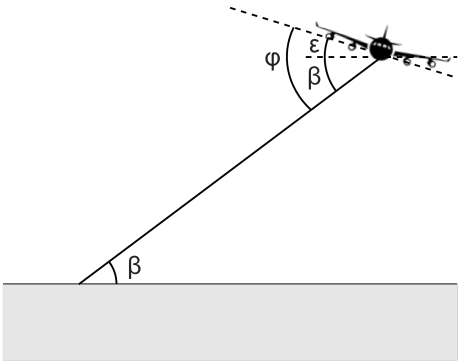

Figure 4.15: Schematic front view of an aircraft position. The dashed line indicates the plane in which the wings are located. Based on [8] Figure 4-3.

4.3.2. NPD Tables

As the name already implies, the Noise Power Distance (NPD) tables allow for the determination of the noise level based on the distance between the aircraft and the observer and the power associated with the segment at the observer. An example NPD table is shown graphically in Figure 4.16, where each line corresponds to a specific engine power setting.

The reference NPD tables as provided in the ANP database cannot always directly be applied to the aircraft type under consideration. The NPD table correction factors associated with atmospheric attenuation, aircraft substitution and NPD table interpolation and extrapolation are outlined below.

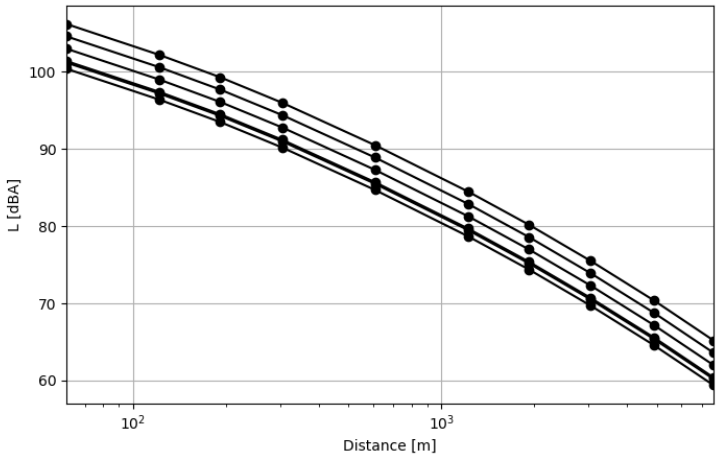

Figure 4.16: Example NPD curves.

Atmospheric Attenuation

As a sound wave propagates through the atmosphere a portion of the energy of the sound wave is absorbed by the atmosphere. Even though the NPD tables already contain the effect of distance between the source and the observer on the noise level, this is based on reference atmospheric conditions. If the atmospheric conditions differ from the reference atmospheric conditions a correction has to be applied to the NPD tables.

As mentioned previously the rate of atmospheric absorption of a sound wave is strongly dependent on the frequency of the sound wave. This means that some spectral information for the aircraft type under consideration has to be available. This spectral information is contained in the spectral classes part of the ANP database. The spectral data of a departing B772 aircraft is presented in Figure 4.17.

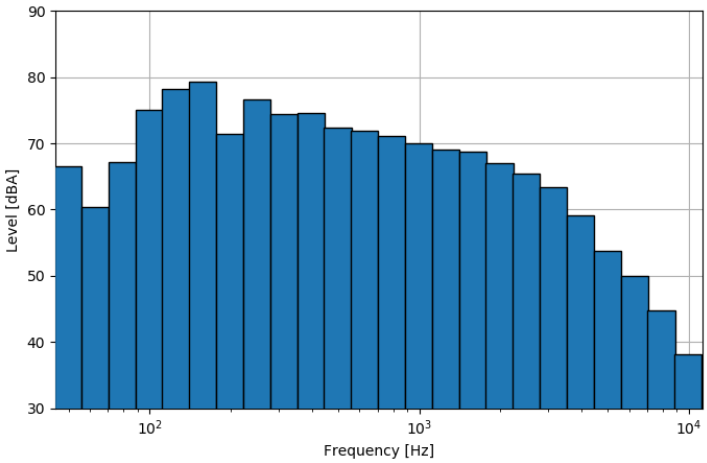

Figure 4.17: 1/3-Octave band spectrum for the a departing B772 aircraft.

The spectrum in the figure above is normalised by using the SAE-AIR-1845 correction for atmospheric absorption using the standard atmosphere with default atmospheric attenuation coefficients ($\alpha_{n,def}$ [dB m^{-1}]) at a reference distance (d_{ref} [m]) of 305m. The unattenuated spectrum (L_n [dBA]) is obtained by correcting the default spectrum ($L_{n,def}$ [dBA]) for the atmospheric attenuation in the standard atmosphere. The unattenuated spectrum is given by the equation below, where the subscript n identifies the 1/3-octave band under consideration. The 1/3-octave bands for which the spectral level is available in the ANP database is the 17$^{\text{th}}$ till the 40$^{\text{th}}$.

$$L_n\left(d_{ref}\right) = L_{n,def}\left(d_{ref}\right) + \alpha_{n,def}\ d_{ref} \tag{4.16}$$

The spectrum corrected for atmospheric attenuation using actual atmospheric conditions is given by the equation below. Here it is once again demonstrated that the atmospheric attenuation coefficient for a certain 1/3-octave band (α_n [dB m^{-1}]) is dependent on the ambient air temperature (T_{air} [°C], ambient air pressure (p_a [Pa]), relative humidity (h_{rel} [%]), and the distance associated with the NPD table entry (d_i [m]).

$$L_{n,atm}\left(T_{air}, p_a, h_{rel}, d_i\right) = L_n\left(d_{ref}\right) - 20\log\left(\frac{d_i}{d_{ref}}\right) - \alpha_n\left(T_{air}, p_a, h_{rel}\right)\ d_i \tag{4.17}$$

The difference between the atmospheric attenuation corrected spectrum and the default spectrum is used to determine the atmospheric attenuation NPD correction factor (Δ_{atm} [dBA]). The atmospheric attenuation NPD correction factor is given by the equation below. It should be noted that the 1/3-octave band center frequency A-weighting ($\Delta_{A,n}$ [dBA]) is included to correct for the A-weighting in the SEL and L_{Amax}.

$$\Delta_{atm}\left(T_{air}, p_a, h_{rel}, d_i\right) = 10\log\left(\sum_{n=17}^{40} 10^{\frac{L_{n,atm}\left(T_{air}, p_a, h_{rel}, d_i\right) - \Delta_{A,n}}{10}}\right) - 10\log\left(\sum_{n=17}^{40} 10^{\frac{L_{n,def}\left(d_i\right) - \Delta_{A,n}}{10}}\right) \tag{4.18}$$

Aircraft Substitutions

Not all aircraft types are included in the ANP database, which means that for several aircraft a substitution has to be made. The recommended substitutions and the corresponding correction factors are determined based on the ICAO type code of the aircraft under consideration. The ICAO aircraft type code based ANP substitution table contains an approach correction factor (Δ_{app} [dBA]) and an departure correction factor (Δ_{dep} [dBA]). The ICAO aircraft type code based ANP substitution table for the Boeing 777 series aircraft and the corresponding NPD table correction factors are presented in Table 4.4.

Table 4.4: ICAO type code based ANP substitution for the Boeing 777 series aircraft.

Airframe Manufacturer	ICAO code	ANP proxy	Δ_{dep} [dBA]	Δ_{app} [dBA]
The Boeing Company	B772	777200	2.4	1.3
The Boeing Company	B773	777300	0.5	0.7
The Boeing Company	B77L	7773ER	-0.2	-0.2
The Boeing Company	B77W	7773ER	0.0	0.0

Interpolation and Extrapolation

As both the distance between the aircraft and the observer and the power setting associated with the observer location are continuous, it is highly unlikely that these exactly correspond to one of the NPD table entries. If the distance and power setting to be looked up are between the minimum and maximum values contained in the NPD, a linear interpolation is performed with respect to the power setting and a logarithmic interpolation is performed with respect to the distance according to the equation below. If the segment power setting or the distance is beyond the range as provided in the NPD table a linear extrapolation is performed for the power setting and a logarithmic extrapolation for the distance. The logarithmic interpolation and extrapolation of the sound level with respect to the distance between the aircraft and observer is in line with the expected behaviour from geometrical spreading.

$$L(d,P) = L(d_i,P_i) + \frac{L(d_{i+1},P_i) - L(d_i,P_i)}{\log_{10}(d_{i+1}) + \log_{10}(d_i)}\left(\log_{10}(d) - \log_{10}(d_i)\right) + \frac{L(d_i,P_{i+1}) - L(d_i,P_i)}{P_{i+1} - P_i}\left(P - P_i\right) \tag{4.19}$$

4.3.3. Corrections

As mentioned previously there are several factors which have to be compensated for through correction terms. These factors are used to correct for the event duration, the location of the aircraft engines, lateral attenuation and the finite length of the flight path segment.

Duration Correction

The aircraft generally flies at a speed which is different from the reference speed (V_{ref} [kts]) of the ANP database, which is $160 kts$. This means that, all other parameters being equal, the maximum sound level remains the same but the SEL is affected. The duration of the noise event associated with a specific flight path segment is inversely proportional to the speed of the aircraft during that segment (V_{seg} [kts]). Therefore, the duration correction is given by the equation below.

$$\Delta_V = 10 \log_{10} \left(\frac{V_{ref}}{V_{seg}} \right) \tag{4.20}$$

If the location of the observer is either in front or behind the whole flight path segment under consideration, the segment velocity is the velocity corresponding to the nearest segment point. However, if the observer location is between the start- and endpoint of the flight path segment, the segment velocity is given by the equation below, which depends on the start- and end-point velocity of the segment (V_1 [kts] and V_2 [kts] respectively), the flight segment length (λ [m]) and the position of the observer along the flight segment (q [m]). For a visualisation of the last two parameters the reader is referred back to Figure 4.14.

$$V_{seg} = \sqrt{V_1^2 + \frac{q}{\lambda} \left(V_2^2 - V_1^2 \right)} \tag{4.21}$$

Figure 4.18 shows the effect of the segment velocity on the duration correction for a reference velocity of 160 kts, which is the reference velocity used for the NPD database. For typical low altitude flight speeds between 100 and 220 kts, the duration correction ranges between +2.0 and -1.4 dBA.

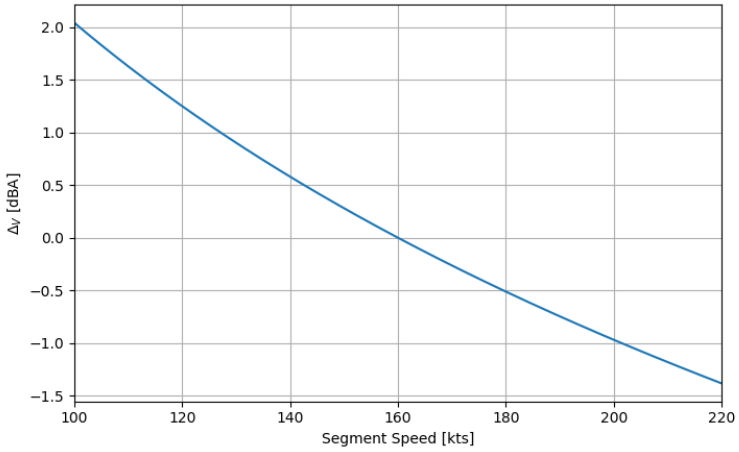

Figure 4.18: Effect of segment speed on duration correction.

Engine Installation

The noise radiation pattern of the aircraft is strongly affected by the location of the engines. The engine installation effect is approximated by the equation below, where the values of a, b, and c depend on the engine installation location. The engine location dependent coefficients are presented in Table 4.5.

$$\Delta_I(\varphi) = 10 \log_{10} \left(\frac{\left(a \cos^2(\varphi) + \sin^2(\varphi) \right)^b}{c \sin^2(2\varphi) + \cos^2(2\varphi)} \right) \tag{4.22}$$

A visualisation of the engine installation correction is shown in Figure 4.19. It should be noted that the engine installation correction is not applicable to propeller aircraft. The second observation is that the effect of the engine installation is stronger for fuselage mounted engines than wing mounted engines. This makes intuitive sense as the shielding by the fuselage is stronger when the engines are located closer to the fuselage.

Table 4.5: Engine installation correction coefficients depending on the engine location

Engine Location	a	b	c
Wing	0.0039	0.062	0.8786
Fuselage	0.1225	0.329	1.0

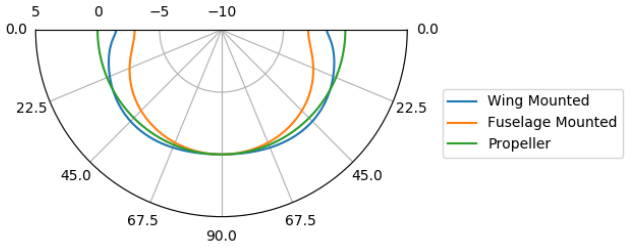

Figure 4.19: Engine installation correction as a function of depression angle (φ [°]) for each engine installation location.

Lateral Attenuation

The measured sound level at an observer located to the side of the flight path segment is generally lower than the sound level at the same distance, but directly below the flight path. For this reason the sound level at an observer at a lateral distance away from the flight path segment differs from the value as tabulated in the NPD database. The excess lateral attenuation is approximated by the equation below. The excess lateral attenuation correction as presented below accounts for ground effects, atmospheric refraction, and aircraft shielding[33].

$$\Lambda\left(\beta, l\right) = \Gamma\left(l\right) \cdot \Lambda(\beta) \tag{4.23}$$

Where

$$\begin{array}{ll} \Gamma\left(l\right) = 1.098\ \left(1 - e^{-0.00274\ l}\right) & 0m \leq l \leq 914m \\ \Gamma\left(l\right) = 1 & l > 914m \end{array} \tag{4.24}$$

$$\begin{array}{ll} \Lambda\left(\beta\right) = 1.137 - 0.0229\ \beta + 9.72\ e^{-0.142\ \beta} & 0° \leq \beta < 50° \\ \Lambda\left(\beta\right) = 0 & 50° \leq \beta \leq 90° \end{array} \tag{4.25}$$

Figure 4.20 shows excess lateral attenuation as a function of the combination of lateral distance and the elevation angle. It is observed that the maximum level of excess lateral attenuation for a certain elevation angle is achieved at a lateral distance of 914 m. This is in line with the expected behaviour of the equations above.

The model for the lateral attenuation of aircraft noise described by the equations above is developed by the Society of Automotive Engineers (SAE)[60]. This lateral attenuation model is not only used for the Doc.29 model, but is commonly used in aircraft noise models. Other aircraft noise models, including the Dutch NRM model[25] and the British Aircraft Noise Contour (ANCON) model[42], use the same SAE standard for the prediction of excess lateral attenuation. The SAE model for lateral attenuation is considered to be the best practise model that has found wide implementation[5].

Finite Segment Correction

The SEL values tabulated in the NPD database are related to a flight path segment of infinite length. In practise however the flight path segment always has a finite length, which means that the sound energy at the observer is only a fraction of the infinite flight path segment length value. This correction is given the equation below.

$$\Delta_F = 10 \log_{10}\left(\frac{1}{\pi}\left(\frac{\alpha_2}{1+\alpha_2^2} + \tan^{-1}\left(\alpha_2\right) - \frac{\alpha_1}{1+\alpha_1^2} - \tan^{-1}\left(\alpha_1\right)\right)\right) \tag{4.26}$$

Where

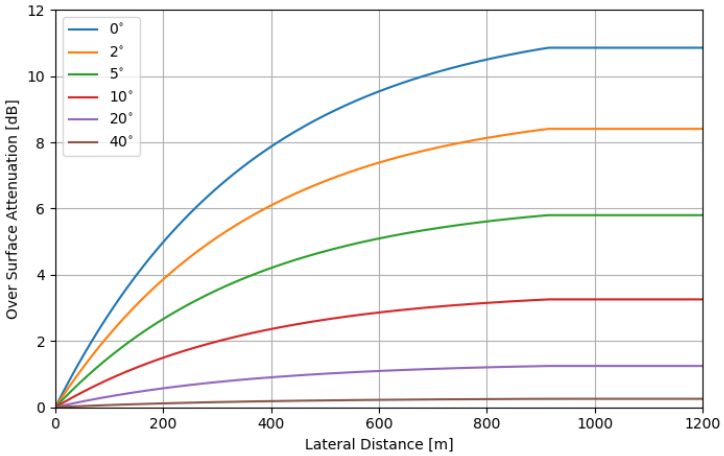

Figure 4.20: Lateral attenuation as a function of lateral distance and elevation angle

$$\alpha_1 = -\frac{q}{d_\lambda} \tag{4.27}$$

$$\alpha_2 = -\frac{q-\lambda}{d_\lambda} \tag{4.28}$$

Where the scaled distance (d_λ [m]) is given by the equations below. The reference velocity (V_{ref} [kts]) and reference time (t_{ref} [s]) are $160kts$ and $1s$ respectively. It is recommended to impose a lower bound of -150 dB on the finite segment correction[8]. It should be noted that the distance used for the NPD table interpolation or extrapolation in the case of the finite segment correction is the slant distance between the observer and the extended flight path segment (d_p [m]) for both the SEL and the L_{Amax}.

$$d_\lambda = \frac{2}{\pi}\, V_{ref}\, t_{ref}\, 10^{\frac{SEL(P,d_p)-L_{Amax}(P,d_p)}{10}} \tag{4.29}$$

4.4. Model Verification

The guidelines for the model verification [9] prescribe the recommended method for verification of an aircraft noise prediction model based on ECAC Doc.29 aircraft noise model guidelines[7, 8]. The model verification guide contains all relevant computations of the parameters of interest for a set of four different routes performed by three different aircraft. The routes contained in this guide are:

- Straight Arrival (AS),
- Curved Arrival (AC),
- Straight Departure (DS), and
- Curved Departure (DC).

These routes and the modelled runway location are presented graphically in Figure 4.21. All routes are assessed for the three different aircraft types; wing-mounted jet engines (JETW), fuselage-mounted jet engines (JETF), and propeller engines (PROP). The SEL values calculated by the model are compared to those provided by ECAC [2]. The performance indicator used for verification suggested is the root-mean-square of the difference between the modelled and reference SEL values. This root-mean square error (δ_{RMS} [dBA]) is given by the equation below.

$$\delta_{RMS} = \sqrt{\frac{\sum_{i=1}^{n}\left(SEL_{mod,i} - SEL_{ref,i}\right)^2}{n}}. \tag{4.30}$$

[2] Data retrieved from https://www.ecac-ceac.org/ecac-docs/, accessed on 12-07-2019

In the equation above the parameter n indicates the number of reference SEL values available in the verification data. The goal for the model developer is to reduce the root-mean-square of the difference between the modelled and reference SEL values to a value of the order of 0.01 dB or less. The model is said to be verified if this required root-mean-square is lower than the threshold value. The results for the noise model verification are presented in Table 4.6. Based on the root-mean square error values presented in this table for the different types of operation the current implementation of the ECAC Doc.29 guidelines is considered to be verified.

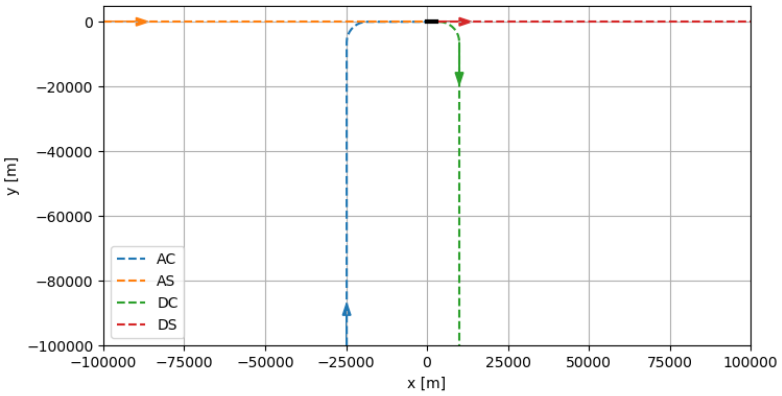

Figure 4.21: Routes used for aircraft noise model verification. Taken from [9] p. 5 Figure 3-1: Reference case routes. The black line segment indicates the runway location.

Table 4.6: Resulting root-mean-square ($\delta_{RMS}[dB]$) of noise model verification.

	JETW	JETF	PROP
AS	$4.29\ 10^{-4}$	$4.34\ 10^{-4}$	$4.67\ 10^{-4}$
AC	$6.06\ 10^{-4}$	$6.34\ 10^{-4}$	$6.84\ 10^{-4}$
DS	$3.71\ 10^{-4}$	$3.70\ 10^{-4}$	$5.62\ 10^{-4}$
DC	$4.19\ 10^{-4}$	$4.10\ 10^{-4}$	$5.60\ 10^{-4}$

5
Methodology

In this chapter the methodology of the research is presented. First, the data sources which were used to obtain the data required for this research are outlined. Thereafter the methodology for the analysis of the results of the aircraft noise model is presented.

5.1. Data Collection

Multiple types of data are used for this research. The different data types which are used for this research are:

- Aircraft Noise and Performance (ANP) database,
- Meteorological data,
- Noise measurement data,
- Aircraft track data, and
- Aircraft Condition and Monitoring System (ACMS) data.

The ANP database is an online data resource which is essential to execute aircraft noise calculations in line with the ECAC Doc.29 guidelines. After signing up at the website[1] the ANP database can be obtained freely. This website allows both for online visualisation of the tables of the ANP database and downloads in .csv format. For this research the newest version of the ANP (V2.2, released on 22-02-2018) is used as it also contains the ANP data for the B38M aircraft and an updated version of the aircraft substitution table. It is worth noting that even though the ANP database is managed by Eurocontrol, the data provided by the manufacturers is not validated. Validation of the ANP database is the responsibility of the user of the database.

The meteorological data in the Netherlands is collected and stored by the Koninklijk Nederlands Meteorologisch Instituut (KNMI). The hourly average meteorological conditions at Schiphol are freely obtained from the KNMI website[2]. The meteorological data contains, among other parameters, the wind speed and direction, atmospheric pressure, local air temperature, and relative humidity. The meteorological conditions are subsequently used to determine the atmospheric sound absorption rate and the usability of the aircraft noise measurement. It should be noted that only the meteorological conditions at ground level are recorded by the KNMI, meaning that no meteorological data is available for different altitudes.

The noise measurement data of the aircraft noise measurement system currently in place around Schiphol (NOMOS) is collected and stored by Brüel & Kjær[3]. The real time noise measurements performed by the NOMOS system and visualisations of aircraft flyover event parameters are presented on a website[4]. However, for this research the parameters of individual aircraft noise events are of interest which are not available from the website. The database of the NOMOS measurements can only be accessed through the ANOMS 9 application, which requires login credentials to access the NOMOS data. For this research login credentials to the ANOMS 9 application has been provided by Royal Schiphol Group. Furthermore, the ANOMS 9 application allows for retrieval of the aircraft parameters, such as aircraft type and registration number, and the associated radar tracks.

[1] https://www.aircraftnoisemodel.org/
[2] https://www.knmi.nl/nederland-nu/klimatologie/uurgegevens
[3] https://www.bksv.com/en
[4] https://noiselab.casper.aero/ams/

ACMS logs are collected and stored by the operator of the aircraft and are therefore not freely available. For this research the required ACMS logs were anonymised and provided by Royal Dutch Airlines (KLM). The ACMS logs contain, among other aircraft parameters, the aircraft weight, fuel flow to the engines, true airspeed, aircraft position, and the flap setting.

5.2. Result Analysis

The main parameter of interest resulting from the aircraft noise measurement and calculation for an individual aircraft flyover event is the SEL. The comparison of the measured noise level ($SEL_{measured}$ [dBA]) and calculated noise level ($SEL_{calculated}$ [dBA]) for an individual aircraft flyover event is given by the equation below[34].

$$SEL_{calculated} - SEL_{measured} = \Delta L = \pm\epsilon_{calculated} \pm \epsilon_{measured} - \epsilon_{other} \tag{5.1}$$

Differences observed between aircraft noise calculations and aircraft noise measurements (ΔL [dBA]) for the same event can originate from more than one error source. The three potential sources of discrepancies between aircraft noise calculations and measurements are:

- Errors in the aircraft noise calculations ($\epsilon_{calculated}$)
- Errors in the aircraft noise measurements ($\epsilon_{measured}$)
- Error due to other noise sources (ϵ_{other})

The signs in the equation above indicate the possible signs for the different sources of error. Both the calculated and measured error can either be positive, which leads to an overestimation of the aircraft noise, or negative, which leads to an underestimation of the aircraft noise. The contribution of other noise sources always mean that the resulting measured noise level is higher than the calculated noise level for the same noise event.

5.2.1. Error Mitigation Strategies

The difference between the calculated and measured values of aircraft noise are considered to be unwanted. Where possible, mitigation strategies are devised to reduce each of the individual components of the errors.

Other Noise Sources

The mitigation of the effect that other sources have on the measured noise level cannot be achieved with the current NOMOS measurement devices, as a result of the current design of the NOMOS system. Two possible mitigation strategies for the effect of other noise sources are:

1. Only analysing aircraft noise events from periods during which the effect of other noise sources is expected to be sufficiently low. An example of this would be by analysing only the nighttime operations.

2. Only analysing aircraft noise events at measurement post locations near the airport. Near the airport the aircraft fly lower, which means that generally more sound is produced by the aircraft. If the sound level of the aircraft sufficiently exceeds the sound level from other sources the contribution of other sources can be neglected.

In order to reduce the effect of background noise during the aircraft noise measurements only nighttime (23:00-07:00) aircraft noise measurements are used. It is expected that the background noise level during the nighttime is lower compared to the daytime as a result of lower human activity. This strategy has a mitigating effect on the background noise level.

Measurement Error

Within the normal operating range a class-I noise measurement system is allowed to have a standard deviation of 0.7 dBA [29]. This uncertainty can only be mitigated by implementing more a more accurate aircraft noise measurement system. Unfortunately, due to the great cost associated with the action of replacing the entire aircraft noise measurement system around Schiphol this is not a viable option.

As mentioned previously the presence of the ground causes sound signal reflections, which in turn cause either constructive or destructive sound signal interference at the microphone location. This effect has a frequency dependent behaviour and is referred to as the Lloyd's Mirror effect. The presence of reflective

surfaces near the measurement post location was assessed for each location individually. These surfaces are also not allowed to block the line of sight between the measurement device and the aircraft location.

Setting the threshold at which the measurement system starts to record the noise event is a trade-off between measuring too much sound, including environmental noise, and excluding too much sound from the aircraft. As mentioned previously the maximum SPL of the aircraft noise event should exceed the level at which the measurement device is triggered by at least $10dB$ to get a reliable noise measurement. If this $10dB$ exceedance of the threshold value is not met, too much of the noise generated by the aircraft is discarded. The NOMOS system uses a threshold of $60dBA$, meaning that aircraft noise events with a measured maximum L_{Amax} lower than $70dBA$ are not included in the comparison.

5.2.2. Performance Metrics

The two metrics used for the determination of the performance of the aircraft noise calculation method are the mean difference (μ) and the standard deviation (σ) of the difference between the calculated and measured aircraft noise level. The mean difference between the calculated and measured value of a parameter provides an indication of the systematic error in the estimation method. The standard deviation of the differences between the calculated and measured values provides an indication of the precision of the estimation method. These performance metrics are used to provide an indication of the performance of the aircraft noise calculations, the aircraft weight estimation, and the thrust setting estimation.

Statistical Moments

If the dataset approximates the probability density function (pdf), the n-th moment of this pdf is given by[22]:

$$\mu_n = \int_{-\infty}^{\infty} (x-c)^n \, f(x) \, dx$$

For the determination of the moment of a certain pdf the value of c is usually taken to be zero. Some commonly used moments are:

- **The first raw moment**: Also known as the mean, which is the expected value of the random variable X.
$$\mu = E[X]$$
- **The second central moment**: Also known as the variance, which is the first moment of the random variable X centered around the mean. The standard deviation is the positive root of the variance.
$$\sigma \equiv \left(E\left[\left(X - \mu \right)^2 \right] \right)^{\frac{1}{2}}$$

5.2.3. Noise Model Improvements

To determine the effect of alterations of the aircraft noise model, a baseline model performance is determined. This baseline model performance serves as a benchmark to which the result of any change in the aircraft noise model is compared.

The key to increasing the correctness of the aircraft noise model is to be capable to demonstrate the validity of the model. The calibration and validation steps associated with the aircraft noise model consist of two distinct elements; the calibration and validation of the aircraft noise model and the calibration and validation of the input parameters.

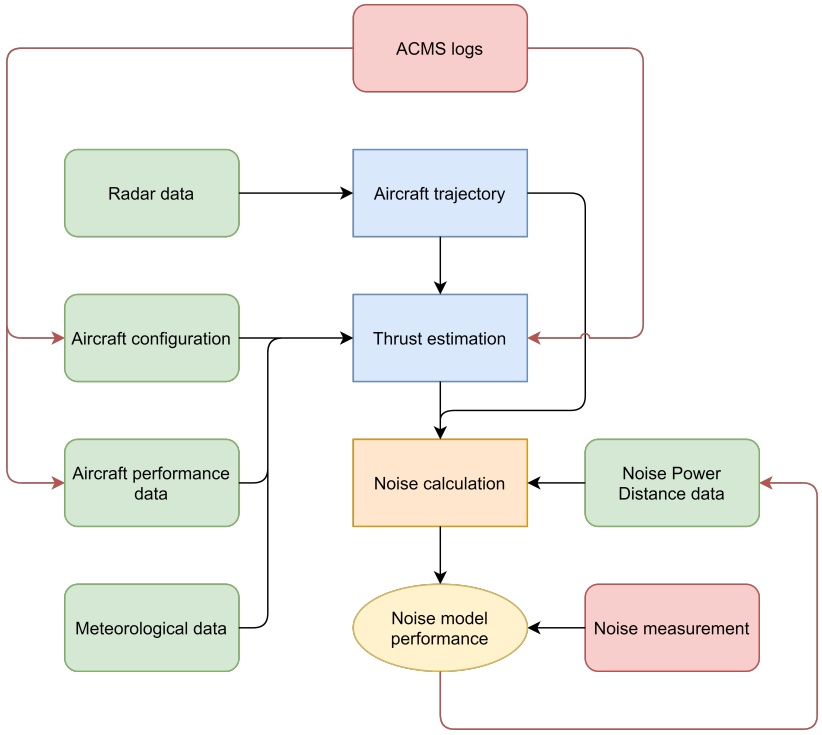

Figure 5.1: Calibration and validation strategy of individual elements of the aircraft noise prediction model. The black lines indicate the flow of calculations through the aircraft noise model. The red lines indicate the aircraft noise model calibration. Based on [14] Figure 1: Validation Model.

Model Uncertainties

The quality of the model output is mainly determined by the quality of the quality of the model itself. It is observed from Figure 5.1 that the aircraft noise calculations also require an estimation model for the thrust setting and the aircraft trajectory. The aircraft trajectory model cannot be calibrated or validated by the ACMS logs provided by KLM as these are anonymised, which means that they cannot be correlated to radar tracks from ANOMS9. The thrust setting estimation method however is compared to the data in the ACMS logs to determine the best performing method for thrust estimation.

The outcome of the noise calculations model is compared to noise measurements performed by the NOMOS measurement system. Observed differences between the calculated and measured aircraft noise can be attributed to different causes. However, because the contribution of other noise sources and the measurement error mitigated or the measurements have been rejected if the event is considered to be not attributable to an aircraft flyover event, the remaining element in the difference between the calculated and measured noise level is caused by calculation errors. Two potential approaches for mitigating the differences between the calculated and measured aircraft noise level are[51]:

1. Suggest aircraft noise model improvements, and
2. NPD data calibration.

As mentioned previously all relevant parameters of the aircraft noise event are recorded. The first aim is to uncover a correlation between the difference between the calculated and measured aircraft noise level and the different aircraft flyover event parameters. A statistical significant correlation is used as an indication that the parameter has an effect on the difference between the aircraft noise calculations and measurements. The NPD data is considered as one of the input parameters for the aircraft noise calculations and is therefore discussed below.

Input Uncertainties

The quality of a calculation based on input parameters can at best be as reliable as the quality of the input parameters. This means that when a great uncertainty is present in the input parameters, a similar uncertainty is to be expected from the resulting calculations[1]. The errors in the input for the modelling of aircraft noise

are considered to be additive [14]. The input parameters for the aircraft noise calculations, the green boxes in Figure 5.1, are:

- Aircraft configuration parameters,
- Aircraft trajectory,
- Aircraft performance database,
- Meteorological conditions, and
- NPD data.

Both the aircraft configuration and aircraft performance database are compared directly to data provided in the ACMS logs of that specific flight. The validation of the aircraft configuration and aircraft performance database is of great importance as these are used as subsequent input parameters for the thrust estimation. Once the input parameters for the thrust estimation and the thrust estimation method have been validated the NPD tables are calibrated and validated.

If a systematic error is observed in the model output, a calibration is performed to account for the systematic error[12]. Calibration of the NPD data aims at reducing the calculation error component by calculating correction factors for each individual NPD table entry based on the observed calculation error. This calibration allows for validation of the NPD data based on aircraft noise measurements. There are two conditions which should be kept in mind while performing the calibration of the NPD data[30]. These two conditions state that:

1. The noise level shall decrease with increasing distance, and
2. The noise level shall increase with increasing power setting.

Both conditions seem sensible, but each of them should be checked after performing the calibration. If one of the conditions is not satisfied after the calibration, the entry itself and the surrounding entries are re-evaluated. In this process priority is given based on the number of calibration events associated with the conflicting entries and the average elevation angle associated with the aircraft noise events[30].

The effect of aircraft performance and NPD tables is validated by checking the performance both in the temporal and spatial domain. For the validation of the effect of the NPD table calibration in the time domain is performed by the use of an independent set of aircraft operations. For the validation of the effect of NPD table calibration in the spatial domain is performed by dividing the NOMOS Measurement Towers (NMTs) in groups with similar aircraft characteristics. The NMTs with the similar aircraft characteristics are subdivided in calibration and validation groups at random where 75% of the NMTs are used for calibration and 25% of the NMTs are used for validation.

5.2.4. Aircraft Performance Calibration

Aircraft performance calibration and validation is essential for the accuracy of the calculated aircraft noise level produced during an aircraft flyover event[14]. The three main elements of the aircraft performance database which are used for the thrust estimation are:

- Aircraft Weight (W [lb])
- Flap setting ([°])
- Aerodynamic coefficient (R [-])

The current method for aircraft weight estimation for departing aircraft in the Doc.29 model is based on the length of the trip between the origin airport and the airport of destination. The current method for aircraft weight estimation for approaching aircraft in the Doc.29 model is 90% of the Maximum Landing Weight (MLW)[8].

However, another method for the estimation of the aircraft landing weight is based on the final approach speed. The final approach speed is based on a weight dependent reference approach speed (V_{ref} [kts])[15]. This reference approach speed is generally attained between 1,000ft and 70ft above the altitude of the runway threshold[54]. The aircraft landing weight can be estimated by the approach true airspeed (V_{app} [kts]) and an aircraft type dependent weight estimation coefficient (D [kts $\cdot$ lb$^{-\frac{1}{2}}$]) using the equation below[13].

$$W = \left(\frac{V_{app}}{D}\right)^2 \tag{5.2}$$

A similar approach can be taken for the weight estimation of departing aircraft based on radar observations. The aircraft weight at departure is estimated using the departure true airspeed (V_{dep} [kts]) and another aircraft type dependent weight estimation coefficient (C [kts $\cdot$ lb$^{-\frac{1}{2}}$]) using an equation similar to Equation 5.2. The estimation of the aircraft weight at take off is given by the equation below[13].

$$W = \left(\frac{V_{dep}}{C}\right)^2 \tag{5.3}$$

The aircraft configuration in terms of flap setting and gear deployment affects the drag produced by the aircraft. The current flap scheduling is based on the aircraft altitude above the runway threshold. However, another method for the estimation of the points of configuration change of the aircraft based on radar data is the use of the calibrated airspeed[6]. The results in terms of mean calibrated airspeed (μ [kts]) and the associated standard deviation (σ [kts]) of the airspeed based flap angle estimation method for the Boeing 757 aircraft are presented in Table 5.1.

Table 5.1: Speed based flap scheduling for the Boeing 757 aircraft. Taken from [6] p. 3.

Flap Angle [°]	μ [kts]	σ [kts]
5	193	10
15	180	12
20	170	9
25	151	7
30	139	20

The aerodynamic coefficient is effectively the drag to lift ratio of the aircraft associated with a specific configuration. Calibration of the drag to lift ratio based on the data available in the FDR allows for an accurate estimation of the aircraft thrust setting over time[46]. The result of radar based thrust estimation compared to the data available in the FDR is shown in Figure 5.2. It is noted that the radar based thrust estimation on average tends to approximate the actual thrust setting rather well, but the radar based method also tends to overshoot and undershoot the fluctuations in the thrust estimation. These over- and undershoots of the estimated thrust level do not pose a significant problem in the estimation of the aerodynamic coefficient, as the aerodynamic coefficient is based on the average drag associated with a particular aircraft configuration.

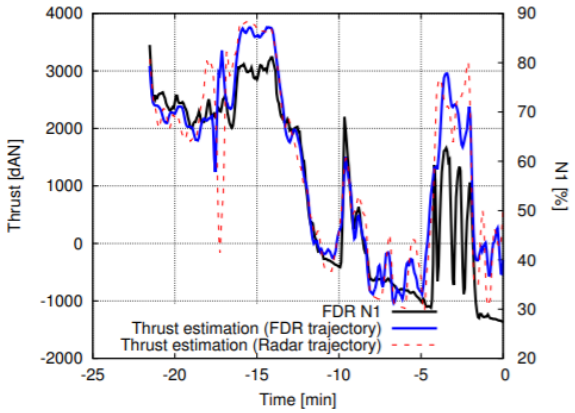

Figure 5.2: Comparison between radar based thrust estimation and FDR data. Taken from [46] Figure 2: Thrust and fuel flow estimation for the example flight.

6

Results

In this chapter the results of the aircraft noise model are presented. The first step in the analysis of the results obtained from the aircraft noise model and measurements comparison is the determination of the baseline aircraft noise model performance. The baseline aircraft noise model performance is used to determine possible areas of improvement for the aircraft noise model. Secondly, the possible aircraft noise model improvements are discussed and implemented. Finally, the improvements of the aircraft noise model are validated both in the temporal and spatial domain.

6.1. Baseline Model

The initial results comparing the calculated and measured aircraft noise level of aircraft noise events during the night of 2018 are shown in Figure 6.1. For this selected period of time a total amount of 42,225 aircraft noise measurements have been registered. A reduction in the mean difference and the standard deviation of the residuals means that the predictive capabilities of the aircraft noise model increase.

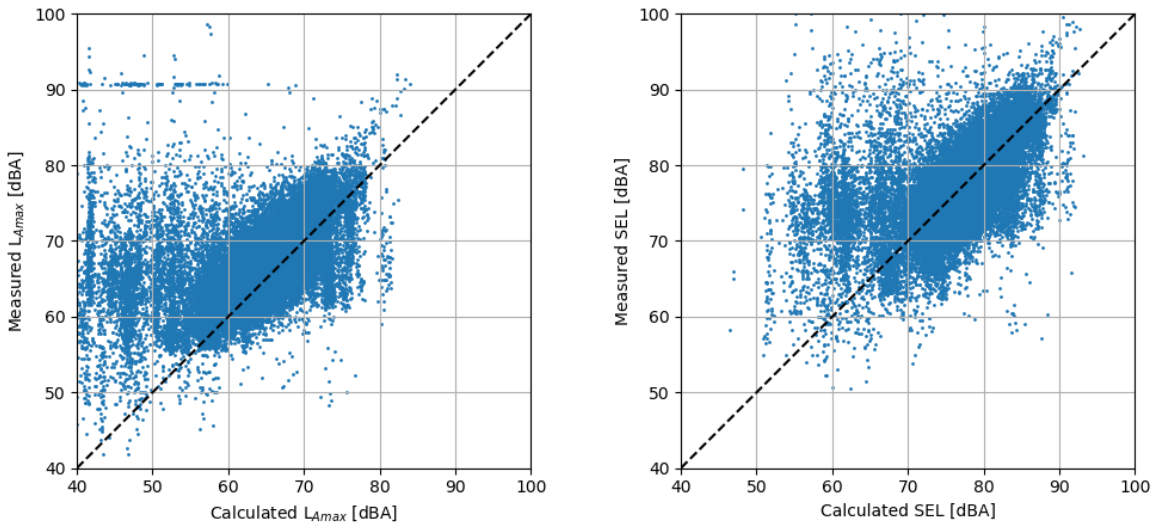

(a) L_{Amax}

(b) SEL

Figure 6.1: Comparison between calculated and measured aircraft noise level. Note that no requirements have yet been imposed on the aircraft noise measurements.

For the comparison between the calculated and measured aircraft noise level in the figure above no requirements have been imposed on the aircraft noise measurements. First the effect of posing requirements on the aircraft noise measurements is presented to obtain the valid measurements. Once the valid measure-

ments have been obtained these are, together with the calculated noise levels, used to determine possible improvements for the aircraft noise model.

6.1.1. Measurement Requirements

It is expected that the measurement requirements as presented previously in Figure 3.2 influence the mean difference and the standard deviation of the difference between the calculated and measured aircraft noise level. The three requirements which have to be met for an aircraft noise measurement to be accepted are restated below:

- ISO 20906 weather requirements (Figure 6.2),
- 10 dBA above threshold (Figure 6.3), and
- Elevation angle (Figure 6.4).

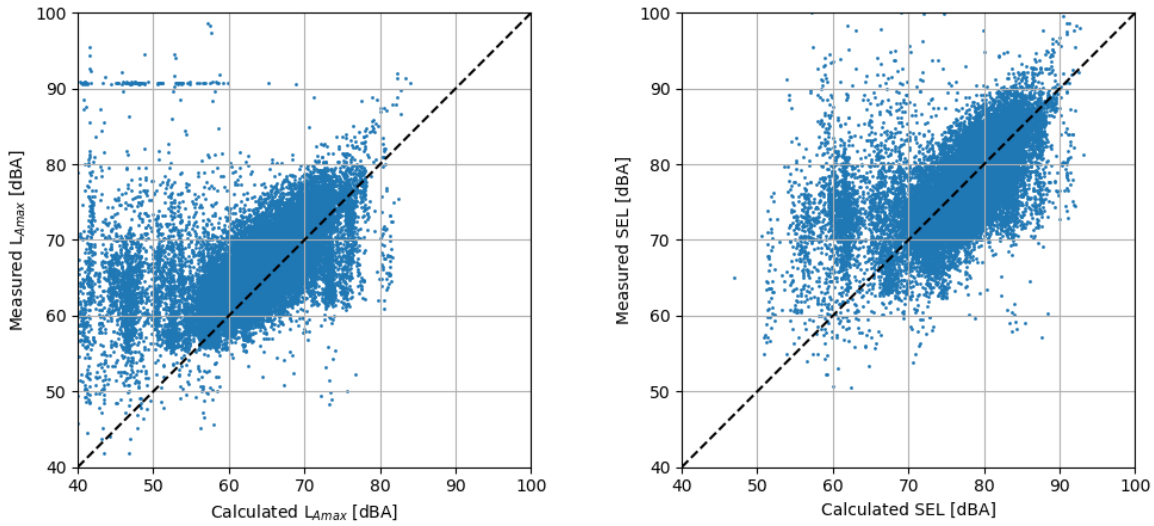

(a) L_{Amax} (b) SEL

Figure 6.2: Comparison between calculated and measured aircraft noise level. Only the ISO 20906 weather condition requirements have been imposed on the aircraft noise measurements.

In Figure 6.2 the aircraft noise measurements that are in compliance with the weather conditions as specified in ISO 20906 and the corresponding calculated aircraft noise levels are presented. It is noted that imposing the weather condition requirements on the aircraft noise measurements slightly improves the mean difference and standard deviation of the level differences for both the SEL and L_{Amax} as is tabulated in Table 6.1.

The threshold used at the NOMOS measurement devices can be varied over time. However, the threshold of microphone during the aircraft noise event is not made available, which means that no threshold level can be determined for the aircraft noise measurement. Therefore, it was determined to use the highest possible threshold of the NOMOS system of $60dBA$ as general microphone threshold for this research. As a result of one fixed microphone threshold level there is a clear cut-off line present in Figure 6.3, where the $10dBA$ above threshold requirement has been imposed on the measured data in combination with the ISO 20906 weather condition requirements. It should be noted that imposing the threshold requirement not only discards the low level invalid measurements, but also the low level valid measurements. In the measured maximum noise level no distinction is made between different noise sources, which means that the high noise level can be caused by another noise source than the aircraft. This effect is compensated for by imposing the minimum elevation angle requirement as can be seen in Figure 6.4. The minimum elevation angle requirement ensures that there is an aircraft in the vicinity of the noise measurement device during the measurement period.

After applying all three measurement requirements, the total amount of usable aircraft noise measurements has decreased by 89.5%, meaning that only 10.5% of the aircraft noise measurement during the nighttime period of 2018 can be used for further analysis. However, it should be noted that the mean difference

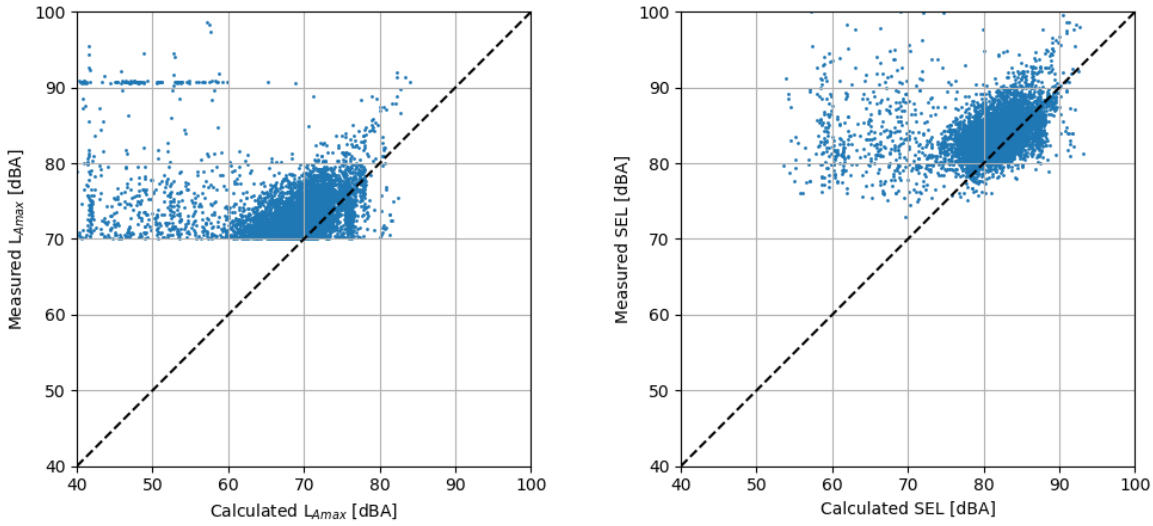

(a) L_{Amax} (b) SEL

Figure 6.3: Comparison between calculated and measured aircraft noise level. Both the ISO 20906 weather condition requirements and the threshold requirement have been imposed on the aircraft noise measurements.

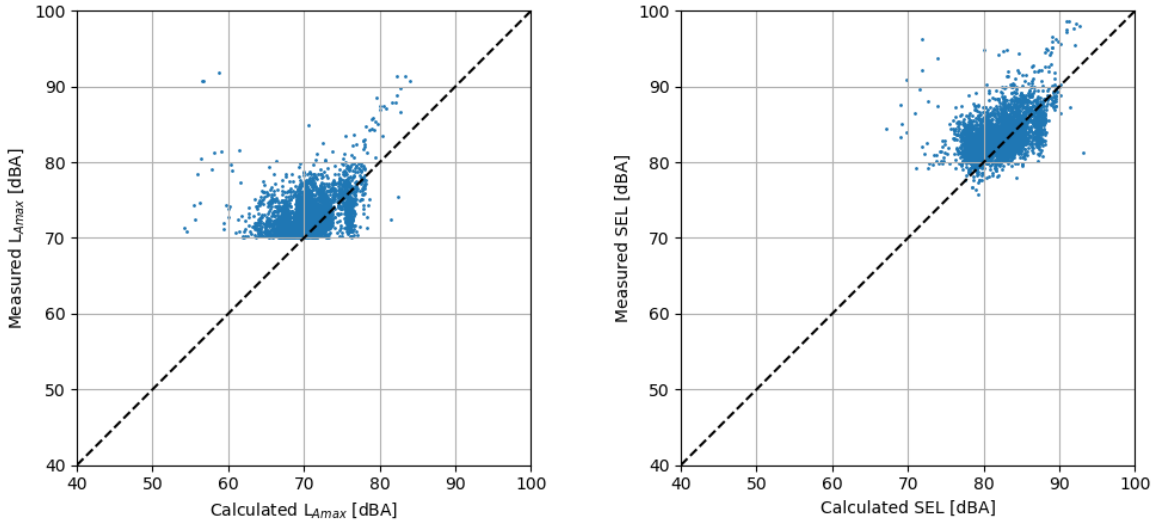

(a) L_{Amax} (b) SEL

Figure 6.4: Comparison between calculated and measured aircraft noise level. The ISO 20906 weather condition requirements, the threshold requirement and the minimum elevation angle requirement have been imposed on the aircraft noise measurements.

and the standard deviation of the differences between the calculated and measured aircraft noise level both strongly decrease by applying the requirements on the measurements.

6.1.2. Model Improvements

In order to determine the possible areas of model improvements the parameters influencing the aircraft noise calculations are organised in three groups. The three groups under consideration are:

- Meteorological effects,
- Geometric effects, and
- Operational effects.

Table 6.1: Effect of aircraft noise measurement requirements on the comparison between calculated and measured aircraft noise level

Requirements	Lamax		SEL	
	μ [dBA]	σ [dBA]	μ [dBA]	σ [dBA]
None	-3.40	6.98	-0.78	6.40
ISO 20906	-2.94	6.60	-0.48	6.21
Threshold	-5.53	8.83	-4.08	8.63
Elevation angle	-2.74	2.95	-1.74	2.88

For each of the groups their corresponding parameters are compared to the difference between the calculated and measured aircraft noise level (ΔL [dBA]). The difference between the calculated and measured aircraft noise level is given by the equation below, where the calculated ($L_{calculated}$ [dBA]) and measured ($L_{measured}$ [dBA]) aircraft noise level can either be the SEL or L_{Amax}. It should be noted that a positive value of ΔL indicates an overestimation of the aircraft noise level by the aircraft noise model and a negative value of indicates an underestimation of the aircraft noise level by the aircraft noise model.

$$\Delta L = L_{calculated} - L_{measured} \tag{6.1}$$

Meteorological Effects

Even though the ISO 20906 weather requirements have been imposed on the aircraft noise measurements, there could be an effect of one of the weather condition parameters on the observed level differences. Therefore, it is necessary to check the influence of the atmospheric conditions within the ISO 20906 specified weather condition requirements. The weather conditions under consideration are:

- Wind speed,
- Temperature, and
- Relative humidity.

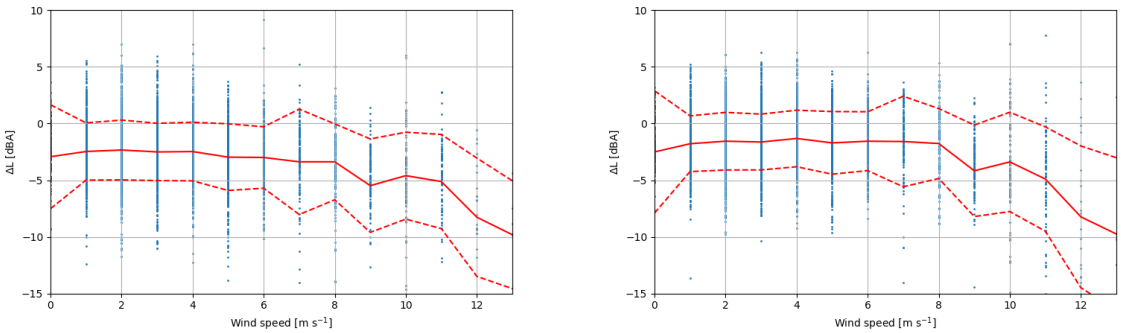

(a) L_{Amax} (b) SEL

Figure 6.5: Influence of wind speed on the observed difference between the calculated and measured aircraft noise level.

The influence of the local wind speed on the difference between the calculated and measured aircraft noise level is shown in Figure 6.5. The solid red line through the both figures indicates the mean observed difference and the dashed red lines indicate the mean plus and minus the standard deviation of the observed difference. It is observed that there is a clear effect of wind on the difference between the calculated and measured aircraft noise level at a wind speed larger than $8m\ s^{-1}$. It is therefore concluded that the requirements on the maximum allowable wind speed during an aircraft noise measurement should be decreased from $10m\ s^{-1}$ to $8m\ s^{-1}$.

The effect of the ambient air temperature (T_{air} [°]) on the observed difference between the calculated and measured aircraft noise level is shown in Figure 6.6. For the normal temperature range occurring around Schiphol at night (0°C < T_{air} < 20°C) there is no clear effect of temperature on the observed level differences.

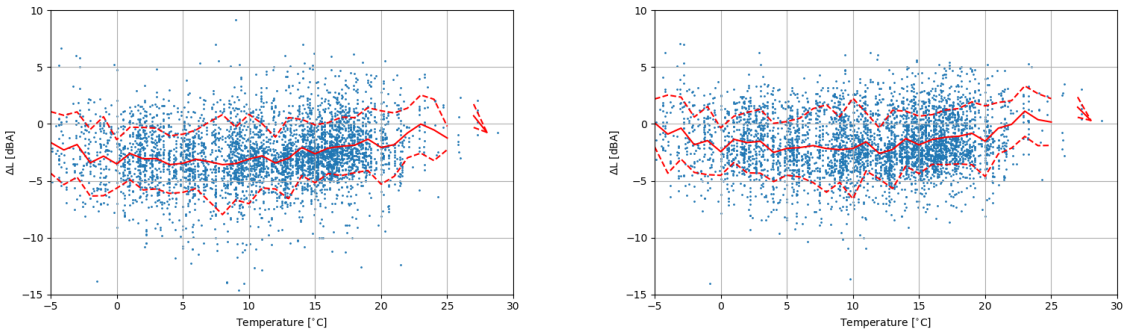

(a) L_{Amax} (b) SEL

Figure 6.6: Influence of temperature on the observed difference between the calculated and measured aircraft noise level.

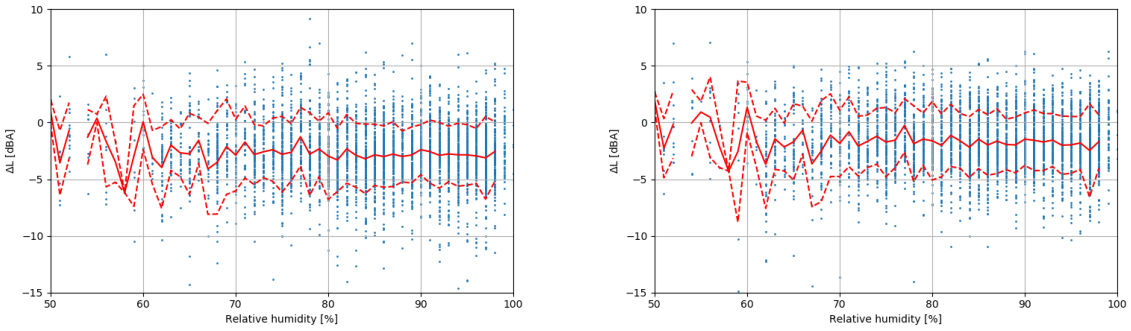

(a) L_{Amax} (b) SEL

Figure 6.7: Influence of relative humidity on the observed difference between the calculated and measured aircraft noise level.

Only for low temperatures there is an indication, but this is most likely due to a shortage of data for temperatures below -5 °C. Therefore, it is concluded that the ambient air temperature has no significant effect on the difference between the calculated and measured aircraft noise level.

The last weather influence on the sound propagation under consideration here is the relative humidity. The effect of the relative humidity is shown in Figure 6.7. From this figure it is concluded that there is no clear effect of the relative humidity on the observed differences between calculated and measured aircraft noise.

There is no clear indication that any of the weather parameters besides the wind speed have an effect on the observed differences between calculated and measured aircraft noise. The effect of the wind speed on the measured aircraft noise level is mitigated by posing a more stringent requirement on the maximum allowable wind speed during an aircraft noise measurement. Therefore, the decision is made to not further investigate the effects of meteorological conditions on the observed level difference between the calculated and measured aircraft noise level.

Geometric Effects

The geometric parameter used for the estimation of the noise level from the NPD tables is the slant distance between the aircraft and the measurement device location. Therefore, if an effect of the distance on the level differences is observed, the effect most likely originates from the NPD tables.

The effect of the minimum distance between the measurement device and the aircraft on the difference between the measured and calculated aircraft noise level is presented in Figure 6.8. From this figure it is observed that the mean difference between the calculated and measured aircraft noise model is strongly affected by the distance between the aircraft and the observer. As a result it is concluded that there is a strong effect of one of the NPD table input parameters on the difference between the calculated and measured aircraft noise level. This points towards the ANP database as one of the sources of discrepancies between the calculated and measured aircraft noise level.

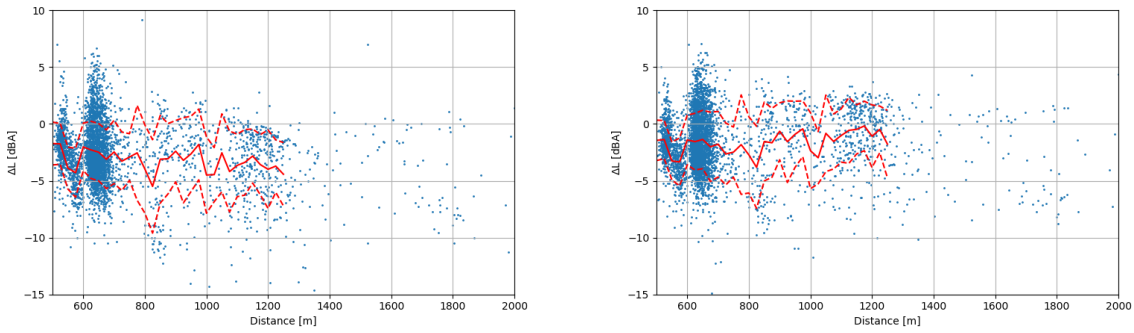

(a) L_{Amax} (b) SEL

Figure 6.8: Influence of distance between the aircraft and observer on the observed difference between the calculated and measured aircraft noise level.

Operational Effects

The operational effects are divided in the effect of the type of operation and the effect of aircraft type on the difference between the calculated and measured aircraft noise level. In order to check for statistical significance of the influence of the operation and aircraft type a T-test is performed.

T-test

The basic idea of the T-test is to check whether the null hypothesis that two distributions have the same mean (μ_0) holds. The T-value is calculated according to:

$$T = \frac{\bar{X} - \mu_0}{\frac{S}{\sqrt{n}}}$$

Where $\bar{X}$ is the mean of the distribution to be tested and S is the corresponding standard deviation. The probability (p-value) that the null hypothesis holds is given by:

$$p = f(df, T)$$

The p-value is a function of the degrees of freedom of the distribution under consideration (n-1) and the T-value found using the first equation. If the p-value is lower than a predefined confidence level the null hypothesis is rejected. The p-value used as confidence level is generally 0.05, which means that a statistically significant difference between two distributions is found if the p-value is lower than this confidence level.

The results of the T-test for the type of operation, arrival and departure, alone are presented in Table 6.2. Based on the T-test a statistically significant effect of the type of operation on the noise level differences between the calculated and measured aircraft noise level for both the SEL and L_{Amax} is observed.

Table 6.2: T-test results for the type of operation.

Metric	T-value	p-value
L_{Amax}	2.110	0.035
SEL	2.414	0.016

The next effect is the effect of the type of aircraft on the observed level differences. The distribution of the level differences for different aircraft types is shown in Figure 6.9. Based on visual observations from these figures it is already apparent that there is an effect of the type of aircraft on the observed level differences. These visual observations are supported by the p-values reported in Table A.1 for the L_{Amax} and Table A.2 for the SEL. Statistically significant differences in the mean difference between the calculated and measured aircraft noise level for different aircraft types indicate that the aircraft type itself is a strong driver for the

difference between the calculated and measured aircraft noise level. The only difference for the aircraft noise calculations for two aircraft with the same engine type and location is the ANP database. This indicates that the ANP database is a source of differences in the calculated aircraft noise level.

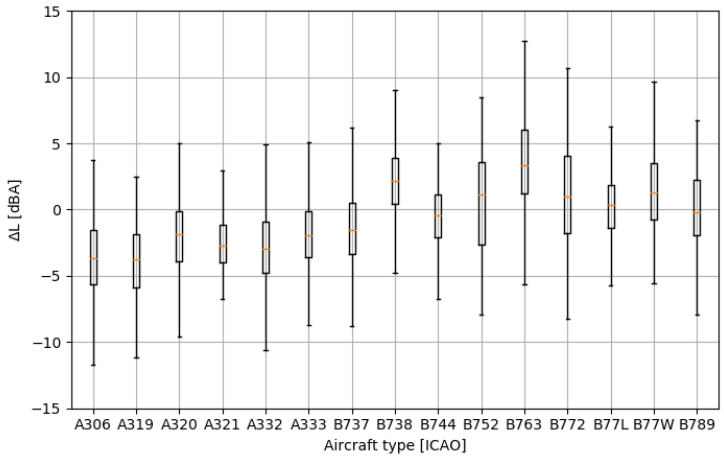

(a) L_{Amax}

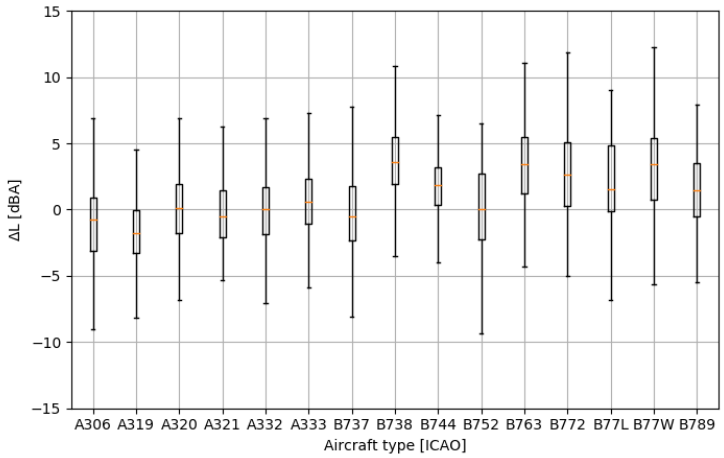

(b) SEL

Figure 6.9: Influence the type of the aircraft on the observed difference between the calculated and measured aircraft noise level.

Conclusion

Based on the observations of the baseline aircraft noise model comparison with aircraft noise measurements several conclusions are drawn. The first conclusion is that the wind speed has a strong effect on the difference between the aircraft noise calculations and measurements at a wind speed lower than the maximum allowable wind speed based on ISO 20906. This effect is mitigated by lowering the maximum allowable wind speed during an aircraft noise measurement to $8ms^{-1}$.

Secondly, the three main parameters having a statistically significant effect on the difference between the calculated and measured aircraft noise level are the slant distance between the aircraft and the measurement location, the type of aircraft operation, and the type of aircraft. All three parameters are directly associated with the input for the different parts of the ANP database. Therefore, the focus of further research is on the calibration and validation of the ANP database. The calibration and validation of the ANP database consists of two consecutive steps, which are performed subsequently:

1. Aircraft performance calibration, and

2. NPD table calibration.

6.2. ANP Calibration

This section focuses on the aircraft noise and performance calibration for the B738 aircraft during approach. The aircraft noise and performance calibration for the B772 aircraft is presented in Appendix B. The calibration of the aircraft noise and performance is only considered for flights landing at Schiphol as a consequence of the low number of departures from Schiphol during the nighttime. The calibration of the aircraft noise and performance database is divided in two steps as mentioned previously. First the calibration of the aircraft performance is considered. Thereafter, the calibration of the NPD tables is discussed. For the calibration of the aircraft performance of the B738 aircraft a total of 42 Aircraft Condition and Monitoring System (ACMS) logs have been provided by KLM. These logs contain the flight information of seven flights conducted with the B738 aircraft. The following parameters are available in the ACMS records:

- Time (t [s]),
- Latitude (λ [°]) and Longitude (ϕ [°]),
- Altitude (h [m or ft]),
- Gross weight (W [kg]),
- Fan rotational speed ($N1$ [rpm]),
- Flap handle selection (δ_{flap} [°]),
- Fuel flow (f_{fuel} [kg hr^{-1}]),
- True airspeed (V_{TAS} [kts]),
- Mach number (M [-]), and
- Total air temperature (T_{tot} [°C]).

Based on the ACMS records the assumptions made for the aircraft performance of the B738 are checked and the input parameters for the determination of the aircraft performance are calibrated. The first element of the aircraft performance input to be calibrated is the weight estimation method, which is compared with a radar based weight estimation method. Secondly, the default flap scheduling of the ANP is calibrated based on the data contained in the ACMS records. Finally, the aerodynamic coefficients corresponding to the different flap settings are calibrated.

An important element of aircraft performance calibration is also the validation of the calibrated aircraft performance. It is decided to use 75% of the ACMS records for the calibration of the aircraft performance and the remaining 25% of the records for subsequent validation. A correction of the aircraft performance is only accepted if both the calibration performs statistically significant better on the validation ACMS records than the default aircraft performance.

6.2.1. Weight Estimation

As described in chapter 5, several methods can be used for the estimation of the aircraft weight for an arriving aircraft. The current method for aircraft weight estimation used in the aircraft noise calculations for arriving aircraft is based on a mass fraction (90% MLW), as is described in the ECAC Doc.29 aircraft noise model guidelines. Another possible method for the estimation of the aircraft mass from radar data is based on the final approach speed of the aircraft (V_{app} [kts]).

First the performance of the mass fraction based weight estimation method is determined and the mass fraction based weight estimation method is calibrated. Subsequently, the performance the final approach speed based weight estimation method is determined. Thereafter the results of both weight estimation methods are compared and the best performing weight estimation method is selected. Finally, the effect of the best performing calibrated and validated weight estimation method on the aircraft noise calculations is discussed.

Mass Fraction

The current approach weight estimation of the implementation of the Doc.29 aircraft noise model guidelines is based on the maximum landing weight (MLW) of the aircraft. The current approach weight estimation method stipulates that the aircraft weight is approximated by 90% of the MLW. The distribution of the aircraft landing weight taken from the ACMS records is shown in Figure 6.10.

The approach weight distribution indicates that the approach weight estimation based on 90% of the MLW is inadequate. Calibration of the mass fraction based approach weight estimation method results in a mass fraction of 76.0% of the MLW. The performance of the default and calibrated mass fraction based weight estimation method is presented in Table 6.3. The first conclusion is that the default mass fraction aircraft weigh estimation method strongly overestimates the aircraft approach weight. This is supported by the distribution of the aircraft approach weight presented in Figure 6.10, where most ACMS records indicate an approach weight much lower than 90% of the MLW. The ACMS records used for validation indicate that

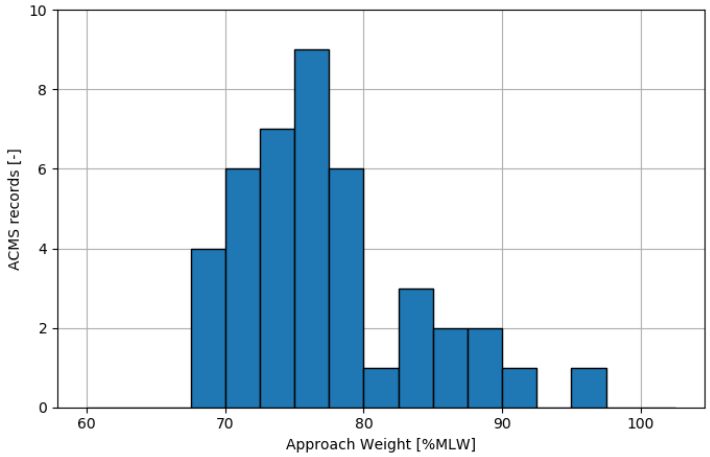

Figure 6.10: Distribution of the aircraft approach weight taken retrieved from the ACMS records. It should be noted that both the calibration and the validation ACMS records are included in the data in this figure.

large discrepancies between the calibrated mass fraction based weight estimation method and the validation data remains.

Table 6.3: Calibration of mass fraction based approach weight estimation.

Mass fraction	Calibration		Validation	
	μ [lb]	σ [lb]	μ [lb]	σ [lb]
Default	20426	6875	11093	11216
Calibrated	0	6875	-9333	11216

Landing Speed

The aircraft approach weight can also be estimated by making use of the aircraft final approach speed in combination with the aircraft specific weight estimation parameter (D [kts lbs$^{-\frac{1}{2}}$]) as given by the equation below. It should be noted that the final approach speed (V_{app} [kts]) to be used for this equation is in terms of true airspeed and not the ground speed as measured by radar.

$$W = \left(\frac{V_{app}}{D}\right)^2 \tag{6.2}$$

True Airspeed

The ground speed (V_g [kts]) is a combination of the relative velocity of the aircraft with respect to the local column of air (V_{air} [kts]) and the relative velocity of that same column of air and the ground (V_w [kts]). The addition of the two speed vectors is shown in the figure below.

$$\mathbf{V_g} = \mathbf{V_{TAS}} + \mathbf{V_w}$$

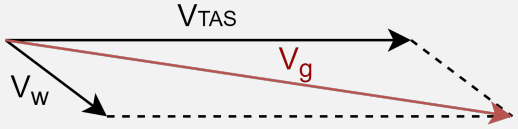

Figure 6.11: Addition of the true airspeed and wind vector to obtain the ground speed vector.

In order for the approach speed based landing weight estimation equation to be usable the aircraft specific weight estimation parameter has to be determined. The final approach speed is taken to be the average

true airspeed between 1.000 ft and the crossing of the runway threshold at 70 ft above the ground. The correlation between the final approach speed and the actual landing weight from the ACMS data recorders is shown in Figure 6.12. The aircraft specific weight estimation parameter is calibrated such that the mean difference between the calculated and actual aircraft weight is minimised. The results of the calibration of the approach speed weight estimation method are presented in Table 6.4.

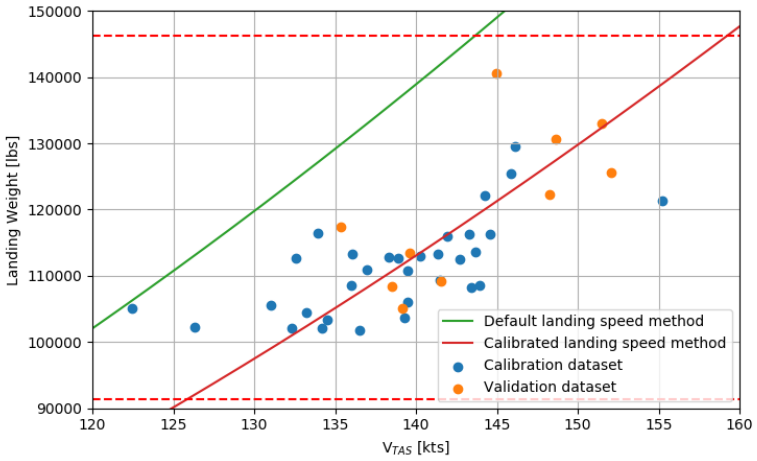

Figure 6.12: Relation between the final approach speed and the actual aircraft landing weight for the B738 flights. The bottom and top red dashed line indicate the Operational Empty Weight (OEW) and the MLW of the B738 aircraft respectively.

Table 6.4: Calibration of final approach speed based approach weight estimation.

Approach speed method	Calibration		Validation	
	μ [lb]	σ [lb]	μ [lb]	σ [lb]
Default	25441	9085	26522	8922
Calibrated	0	7294	-858	8265

For the verification of the final approach speed weight estimation method it is checked how often the resulting weight exceeds the weight range between the Operational Empty Weight (OEW) and MLW. The weight distribution resulting from the final approach speed method with the calibrated aircraft specific weight estimation coefficient is shown in Figure 6.13. From this figure it is observed that the estimated landing weight lies between the OEW and MLW for 97.48% of the flights under consideration. Therefore, the final approach speed based weight estimation method is considered to be verified.

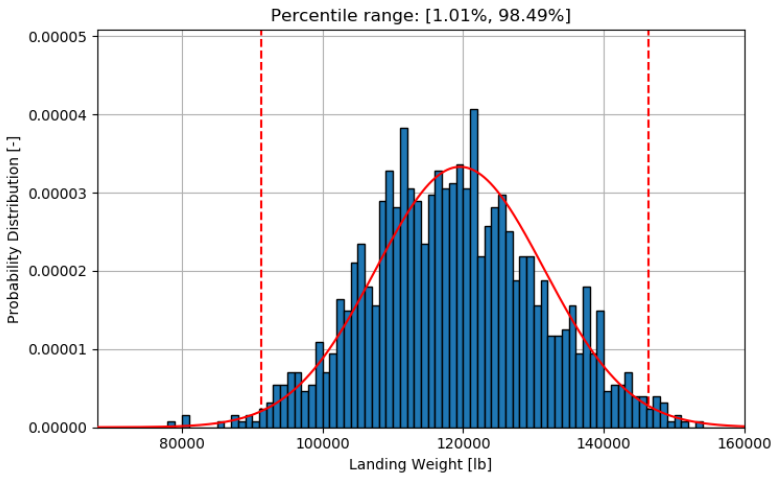

Figure 6.13: Results of the final approach speed weight estimation method for the nighttime B738 approaches of 2018 with a landing weight coefficient of 0.4164. The left dashed red line indicates the operational empty weight of the B738 and the right dashed red line indicates the maximum landing weight. The red curve indicates the normal distribution as an approximation of the landing weight distribution (μ = 119556 lbs, σ = 11976 lbs).

Weight Estimation Comparison

The performance of the two weight estimation methods after calibration is presented in Table 6.5. It is observed that for the validation case the approach speed method performs better than the mass fraction method. A T-test was performed to determine the statistical significance of the calibrated weight estimation methods with respect to the default weight estimation method. It is found that a statistically significant difference exists between the default weight estimation method for both the calibration ($p < 0.001$) and the validation ($p = 0.019$) case. Therefore, it is concluded that the best performing aircraft weight estimation method of the methods under consideration here is the calibrated approach speed weight estimation method. The calibrated approach speed weight estimation method is used in this thesis for aircraft noise calculations with calibrated aircraft performance in favour of the default mass fraction weight estimation method.

Table 6.5: Performance of calibrated weight estimation methods with respect to the Doc.29 standard.

Weight estimation method	Calibration		Validation	
	μ [lb]	σ [lb]	μ [lb]	σ [lb]
Mass fraction (Default)	20426	6875	11093	11216
Mass fraction (Calibrated)	0	6875	-9333	11216
Approach speed (Calibrated	0	7294	-858	8265

Effect on Noise Calculations

The effect of the calibrated approach aircraft weight estimation method on the noise calculations is presented in Figure 6.14. From the comparison between the calculated aircraft noise level resulting from the default and calibrated weight estimation method it is observed that the noise modelling accuracy is improved. This visual observation is supported by the aircraft noise model performance indicators for the default and calibrated weight estimation case presented in Table 6.6.

Table 6.6: Effect of the calibrated weight estimation method on the aircraft noise calculations.

Weight estimation method	μ [dBA]	σ [dBA]
Default	1.73	2.72
Calibrated	1.40	2.70

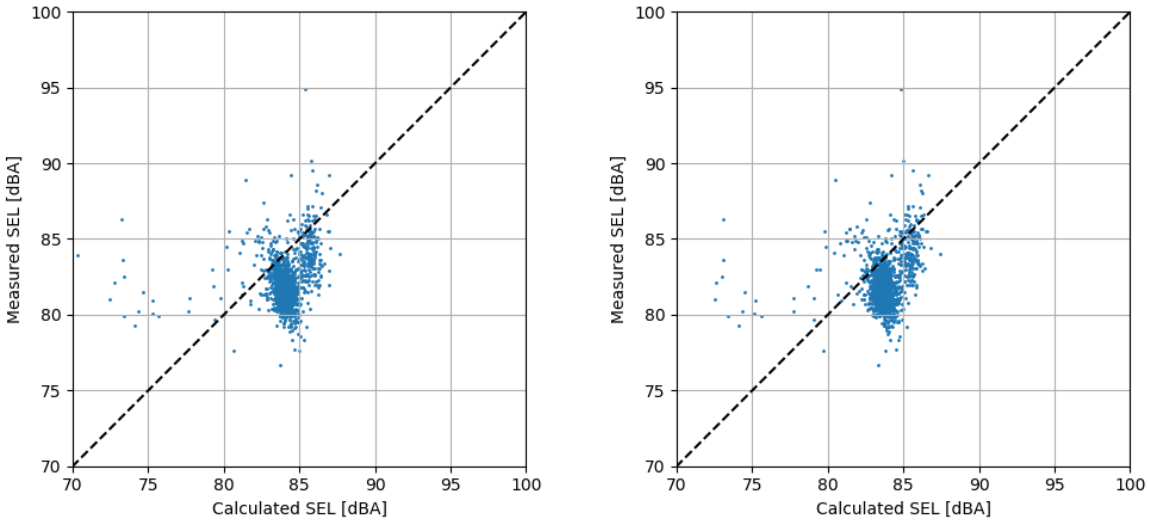

(a) Reference aircraft performance

(b) Calibrated weight estimation method

Figure 6.14: Effect of the calibrated weight estimation method on the aircraft noise calculations.

6.2.2. Flap Scheduling Estimation

The amount of drag generated by the aircraft is directly related to the configuration of the aircraft. Through the principle of the balance of forces the drag is strongly related to the thrust setting. The aircraft performance database contains a default flap scheduling during approach for each aircraft type, which is used for the current noise modelling. The two parameters which can be used for the estimation of the flap setting available from radar are the aircraft altitude and the calibrated airspeed.

First the default and calibrated flap estimation using the aircraft altitude is discussed. Secondly the default and calibrated flap estimation using the calibrated airspeed is discussed. Finally, a comparison between the two flap estimation method is made and the best performing method is determined.

Altitude

The default and calibrated altitude based flap setting estimation for the B738 aircraft is presented in Table 6.7. It should be noted that the default altitude based flap estimation method jumps from a 0° flap setting to a 15° flap setting once the aircraft altitude drops below 3,000 ft. This jump in flap setting is also visualised in Figure 6.15. From the flap setting obtained from the ACMS logs it is already concluded that such a jump in flap setting from 0° to 15° is not realistic.

Table 6.7: Default and calibrated flap setting estimation based on flap setting start altitude for the approaching B738 aircraft.

Flap Setting [°]	Default [ft]	Calibrated [ft]
0	6000	37000
1	3000	-
5	3000	3900
15	3000	2250
30	-	1800
40	2828	-

Based on visual inspection alone of Figure 6.15 it is already concluded that a large spread exists in the altitude based flap estimation. Furthermore, it is observed that a flap setting of 40° is only selected in 6 of the 32 flights, whereas a the other 26 flights land with a flap setting of 30°. Therefore, it is selected to limit the flap setting estimation to 30° rather than 40°. It is noted that for the B738 aircraft the default altitude based flap estimation method strongly overestimates the flap setting for altitudes lower than 3,000 ft. This overestimation of the flap setting is reduced by calibration of the flap setting estimation method.

Calibrated Airspeed

Not only altitude, but also calibrated airspeed (V_{CAS} [kts]) can be used as a proxy for the aircraft flap setting[6]. The flap setting estimation based on V_{CAS} is also incorporated in the ANP database. The default start V_{CAS} value for a certain flap setting is presented in Table 6.8.

Table 6.8: Default and calibrated flap setting estimation based on flap setting start calibrated airspeed for the approaching B738 aircraft.

Flap Setting [°]	Default [kts]	Calibrated [kts]
0	250	500.0
1	187	-
5	174.5	196.2
15	152	173.2
30	-	156.8
40	139	-

From visual inspection of Figure 6.15 it is observed that the spread of the flap setting in relation to the V_{CAS} seems lower than the spread in the relationship between the flap setting and the altitude. Furthermore, it is observed that the default V_{CAS} based flap setting estimation method underestimates the flap setting with respect to the actual flap setting. This effect is corrected for through the calibration of the V_{CAS} based flap setting estimation method as can be seen in Figure 6.15. The V_{CAS} levels associated with the flap setting for the calibrated flap setting method are presented in Table 6.8. For the calibration of the V_{CAS} based flap setting estimation method the flap setting has, similarly to the calibration of the altitude based flap setting estimation method, an upper bound of 30°.

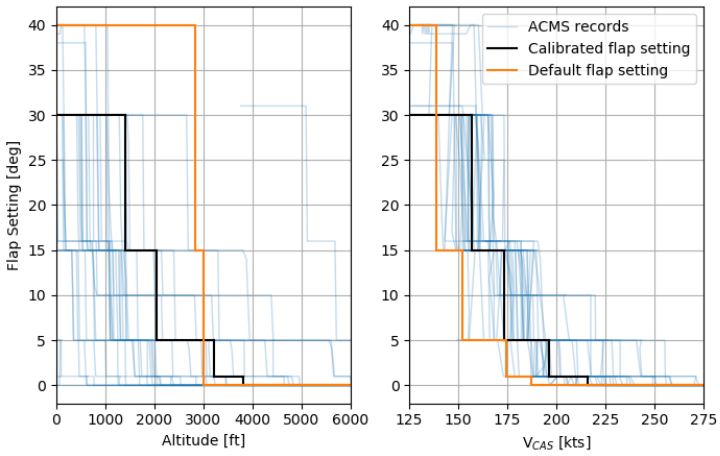

Figure 6.15: Altitude based (left) and V_{CAS} based (right) flap setting estimation method. The blue lines represent the data retrieved from the ACMS records. The orange and black lines are the default and calibrated flap setting estimation respectively.

Flap Estimation Comparison

The performance of the altitude and calibrated airspeed as estimation methods for the flap scheduling can not be compared directly. This is a consequence of the fact that the altitude and V_{CAS} can not be expressed in the same physical quantity. An alternative method for the comparison of the two different flap setting estimation methods is through the dimensionless coefficient of determination (R^2 [-]).

The coefficients of determination associated with default and calibrated altitude and airspeed based flap setting estimation methods are presented in Table 6.9. It is concluded from the results presented in this table that the calibrated airspeed based flap setting estimation method is the best performing estimation method. From statistical analysis it is also found that the better performance of the calibrated airspeed based flap estimation method with respect to the default airspeed flap estimation method (p<0.001) and the calibrated altitude flap estimation method (p<0.001) is statistically significant for both the calibration and validation datasets. Therefore, the V_{CAS} is used for the flap setting estimation when the calibrated aircraft performance is considered.

Table 6.9: Resulting coefficient of determination (R^2 [-]) of default and calibrated flap setting estimation methods.

Flap setting estimation method	Calibration	Validation
Altitude (Default)	-0.895	0.551
Altitude (Calibrated)	0.554	0.907
V_{CAS} (Default)	0.703	0.872
V_{CAS} (Calibrated)	0.912	0.965

From visual inspection of Figure 6.16 it is concluded that the default altitude based flap estimation method also overestimates the flap setting and the V_{CAS} based flap estimation method underestimates the flap setting. Both these effects are mitigated through the calibration using the ACMS records used for calibration. It should be noted that the calibrated flap setting presented in Figure 6.16 is not based on the ACMS records presented in this figure. These visual observations are in line with the related coefficients of determination presented in Table 6.9.

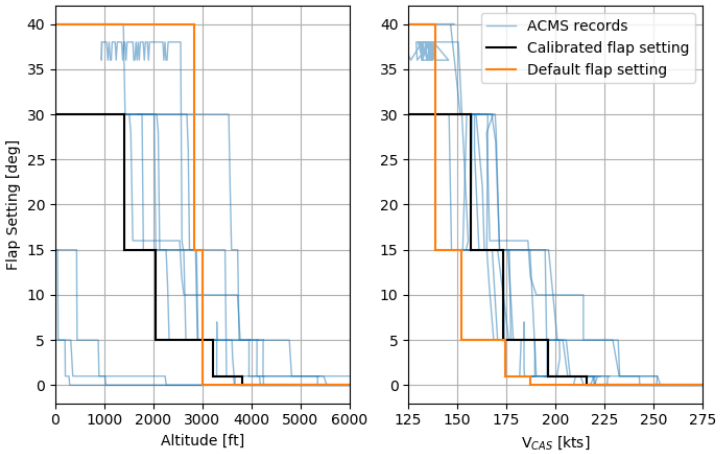

Figure 6.16: Validation of the altitude based (left) and V_{CAS} based (right) flap setting estimation method. The blue lines represent the data retrieved from the ACMS records used for validation. The orange and black lines are the default and calibrated flap setting estimation respectively.

Effect on Noise Calculations

The effect of calibration of the flap setting estimation method on the calculated aircraft noise level is presented in Figure 6.17. It is observed from this figure that the calibration of the flap setting estimation reduces the systematic error in the aircraft noise calculations. This visual observation is supported by the aircraft noise model performance metrics for the calibrated flap setting estimation method presented in Table 6.10. Even though the systematic error is decreased by the calibration of the flap setting estimation method, the spread of the difference between the calculated and measured aircraft noise level is not decreased.

Table 6.10: Effect of the calibrated flap setting estimation method on the aircraft noise calculations.

Flap setting estimation method	μ [dBA]	σ [dBA]
Default	1.73	2.72
Calibrated	0.81	2.74

6.2.3. Thrust Estimation

The thrust setting itself is not directly available from the ACMS logs. However, the fan rotational speed and the fuel flow to both engines are logged. The fuel flow is, in combination with the known engine type, used to recover the thrust setting in percentage of the maximum thrust level through the ICAO Aircraft Engine

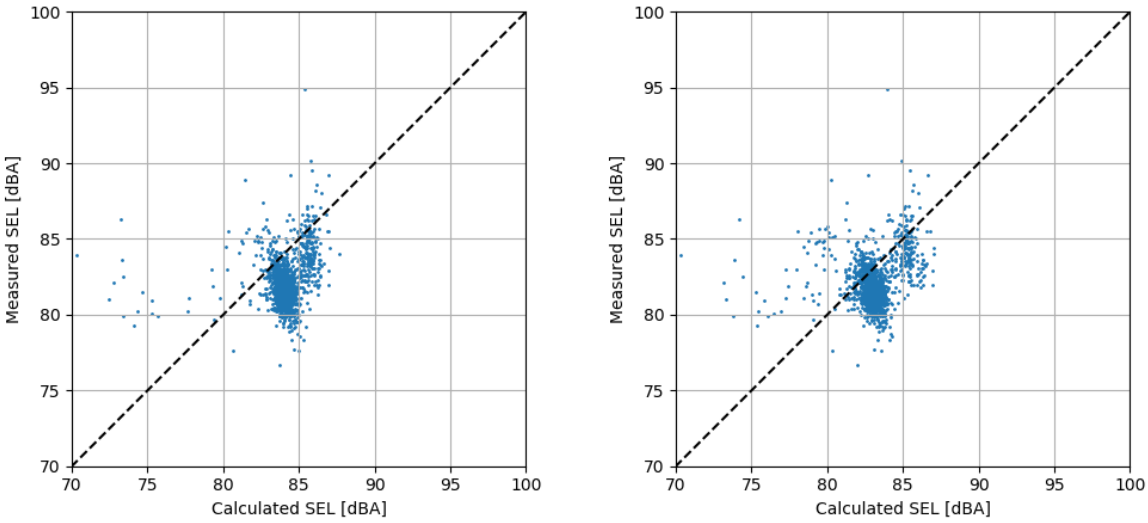

(a) Reference aircraft performance

(b) Calibrated flap setting estimation method

Figure 6.17: Effect of the calibrated flap setting estimation method on the aircraft noise calculations.

Emissions Databank. Therefore, for the calibration of the thrust estimation the fuel flow to the engine is used as a proxy for the thrust setting.

ICAO Aircraft Engine Emissions Databank[a]
For certification purposes all aircraft engines are tested by ICAO for emissions. For different engine settings the fuel flow and engine emissions are measured and reported. The engine settings and the corresponding percentage of maximum thrust setting used for the certification of the engine emissions are:

- Take-off thrust setting (100%),
- Climb-out thrust setting (85%),
- Approach thrust setting (30%), and
- Idle thrust setting (7%).

These recorded parameters are subsequently used to translate the fuel flow in the ACMS data to thrust setting, or vice versa if the thrust setting is available[64]. The engine most commonly used on the B738 aircraft is the CFM56-7B26/3 engine manufactured by CFM International. The relation between the fuel flow to the engine (f_{fuel} [kg s^{-1}]) and the thrust setting (T [%T$_{max}$]) as a percentage of the maximum thrust setting (T_{max} [lb]) is shown in the figure below. This figure also includes a second order polynomial regression, which is used thrust estimation based on fuel flow. For this specific engine type the relation between the fuel flow to the engine and the thrust setting is given by the equation below.

$$F_n = T_{max}\left(-0.2105\, f_{fuel}^2 + 111.89\, f_{fuel} - 0.048\right)$$

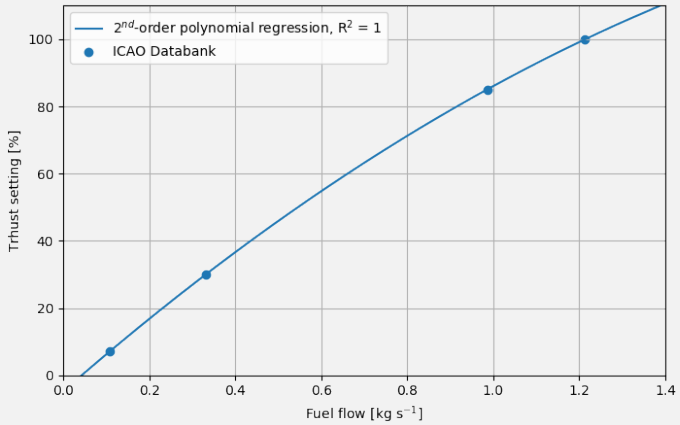

Figure 6.18: Relation between the fuel flow and the thrust as ratio of maximum available thrust for the CFM56-7B26/3 engine.

[a]Data retrieved from https://www.easa.europa.eu/easa-and-you/environment/icao-aircraft-engine-emissions-databank, accessed on 02-04-2020

As mentioned previously, there are three methods which can be used for the estimation of the thrust setting based on the data available from radar. The three methods for thrust estimation are:

1. Radar based
2. N1 estimation based
3. Performance based

Radar Based

The radar based thrust estimation is given by the equation below. The coefficients for the radar based thrust estimation method (E [lb], F [lb kts^{-1}], G_A [lb ft^{-1}], G_B [lb ft^{-2}], H [lb °C]) taken from the aircraft performance database are presented in Table 6.11. As mentioned previously, this thrust estimation method does not take the conservation of energy into account.

$$\frac{F_n}{\delta} = E + F\ V_{CAS} + G_A\ h + G_B\ h^2 + H\ T_{air} \tag{6.3}$$

The ambient, or static, air temperature is not available from the ACMS records, but the total air temperature (T_{tot} [°C]). The static air temperature (T_{stat} [°C]) can be determined based on the total air temperature and the Mach number at which the aircraft is flying.

Total air temperature

In a temperature probe of an aircraft the air is brought to rest with respect to the aircraft. The kinetic energy of the air is converted to internal energy as the air is brought to rest, which compresses the air. As a result of the compression of the air it experiences an adiabatic temperature increase. Therefore, the total air temperature (T_{tot} [°K]) measured by the temperature probe of the aircraft is higher than the static air temperature (T_{stat} [°K]). The relation between the total air temperature and static air temperature is given by the equation below.

$$T_{tot} = T_{stat}\left(1 + \frac{\gamma_{air} - 1}{2}\ M^2\right)$$

The relation between the total air temperature and static air temperature depends on the specific heat ratio (γ_{air} [-]), which is 1.4 for dry air, and the Mach number (M [-]). From the figure below it is observed that the total air temperature with respect to the static air temperature increases as the Mach number increases, which is in line with the expectations from the conversion of kinetic to internal energy. Furthermore it is observed that the difference between the total air temperature and the static air temperature is less than 2% for a Mach number lower than 0.3, which means that the

total air temperature and static air temperature can be used interchangeably during the approach flight phase of the aircraft.

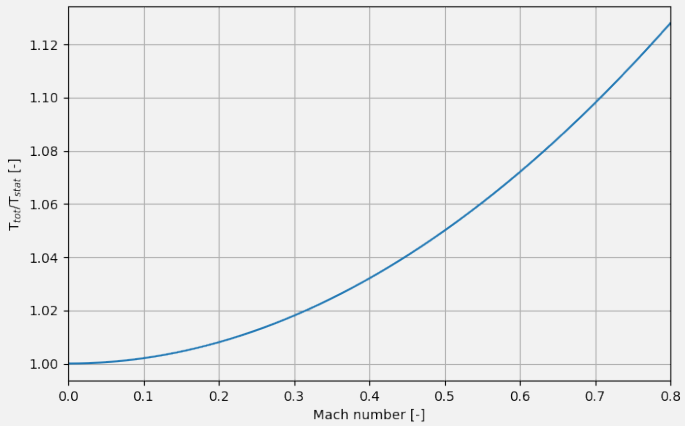

Figure 6.19: Relation between the Mach number and the ratio between T_{tot} and T_{stat}.

Table 6.11: Default and calibrated radar based thrust estimation method coefficients for the B738 aircraft.

Coefficient	Default	Calibrated
E	22404	1722
F	-27.26	-5.600
G_A	0.3056	-0.9532
G_B	0	$6.456\ 10^{-5}$
H	0	20.01

The thrust estimation resulting from the radar based thrust estimation method using the default coefficients is presented in Figure 6.20. From visual inspection of this figure it already becomes clear that large systematic discrepancies exist between the modelled and actual thrust setting. This statement is supported by the mean difference between the estimated and actual thrust setting presented in Table 6.12. These observed differences are mitigated through the calibration of the coefficients used for the radar based thrust setting estimation as is presented in Figure 6.21. The calibrated coefficients are presented in Table 6.11 and their effect on the mean difference and standard deviation are presented in Table 6.12. It is observed that not only the mean difference is affected by the calibration, but also the standard deviation for both the calibration and validation ACMS datasets is reduced.

Table 6.12: Performance of the radar based thrust estimation method using default and calibrated coefficients.

Coefficients	Calibration		Validation	
	μ [lb]	σ [lb]	μ [lb]	σ [lb]
default	14554	2161	14149	2204
calibrated	0	1695	-419	1894

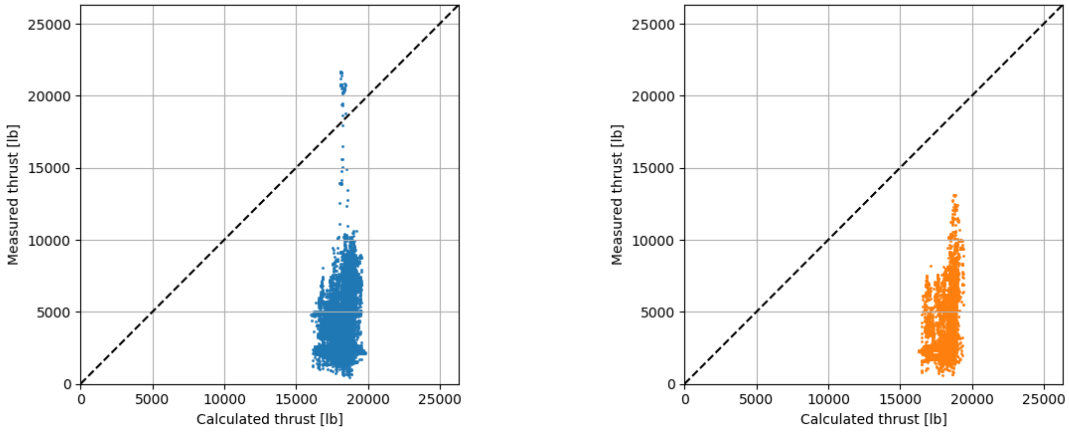

(a) Calibration ACMS logs

(b) Validation ACMS logs

Figure 6.20: Performance of the radar based thrust estimation method using default coefficients.

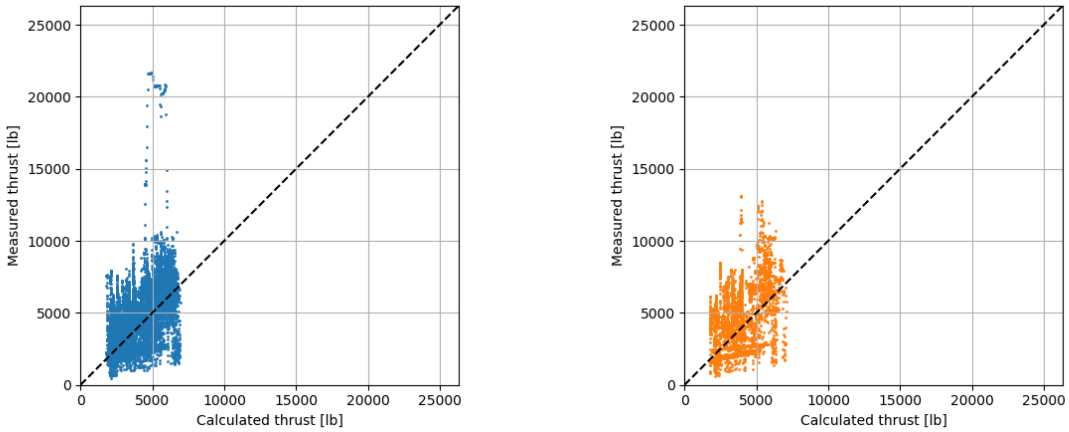

(a) Calibration ACMS logs

(b) Validation ACMS logs

Figure 6.21: Performance of the radar based thrust estimation method using calibrated coefficients.

N1 Estimation Based

The N1 based thrust estimation method is an extension of the radar based thrust estimation method given by the equation below. The aircraft performance database, however, does not contain the K_3 and K_4 coefficients for the B738 aircraft. Therefore, the N1 based thrust estimation method can not be applied to the B738 aircraft.

$$\frac{F_n}{\delta} = E + F\ V_{CAS} + G_A\ h + G_B\ h^2 + H\ T + K_3 \left(\frac{N1}{\sqrt{\theta}}\right) + K_4 \left(\frac{N1}{\sqrt{\theta}}\right)^2 \tag{6.4}$$

However, the relationship between the fan rotational speed and thrust setting can still be determined based on the data available from the ACMS logs. The relationship between the N1 parameter obtained from the ACMS logs and the associated thrust is presented in Figure 6.22. From this figure it is observed that a correlation exists between the N1 parameter and the thrust setting of the aircraft. The performance of the calibrated N1 parameter based thrust estimation method, the blue line in Figure 6.22, is presented in Table 6.13.

A close correlation between the N1 parameter and the aircraft thrust setting is observed. However, it should be noted that the N1 parameter is not directly available from radar data. The N1 parameter can be estimated only if sufficient quality aircraft noise measurements are available. This means that aircraft noise

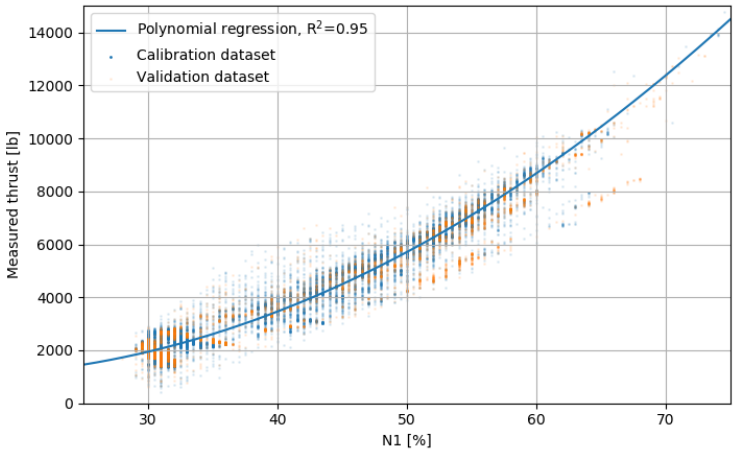

Figure 6.22: Relation between the fan rotational speed (N1) and the thrust.

Table 6.13: Performance of the N1 parameter based thrust estimation method.

ACMS data	μ [lb]	σ [lb]
Calibration	0	493
Validation	134	605

measurements can be used for the determination of the thrust setting of the aircraft. For the data under consideration for this research the required quality of aircraft noise measurements is not achieved and therefore the N1 parameter based thrust setting estimation is not implemented in the aircraft noise model.

Performance Based

The performance based thrust estimation method uses the dynamic equations of motion of the aircraft. This balances, on the left side of the equation, the amount of thrust with, on the right side of the equation, aerodynamic drag (dissipative force), change in altitude (potential force) and change in velocity (kinetic force). The thrust delivered by each engine is estimated by Equation 4.10, which is restated below.

$$\frac{F_n}{\delta} = W \frac{R \frac{\cos(\gamma)}{\cos(\varepsilon)} + \sin(\gamma) + \frac{a}{g}}{N \delta} \tag{6.5}$$

For the determination of the performance of this thrust estimation method the actual flap setting from the ACMS recordings is used rather than the estimated flap setting as presented in Table 6.8. The default and calibrated aerodynamic coefficients from the ANP database associated with a specific flap setting are presented in Table 6.14. For flap settings in the ACMS recordings for which there is no available data the value of the aerodynamic coefficient is obtained by interpolation between the nearest upper and lower value.

Table 6.14: Default and calibrated aerodynamic coefficient associated with the aircraft configuration for the B738 aircraft.

Flap setting [°]	Default	Calibrated
0	0.0767	0.0979
1	0.0914	-
5	0.1066	0.1119
15	0.1658	0.1553
30	-	0.1704
40	0.1897	-

The performance of the performance based thrust estimation using the default aerodynamic coefficients presented in Table 6.14 is presented visually in Figure 6.23. It is observed by visual inspection that the performance based thrust estimation method using the default aerodynamic coefficients tends to underestimate

the thrust setting of the aircraft. This observation is supported by the mean difference between the estimated and actual thrust setting reported in Table 6.15.

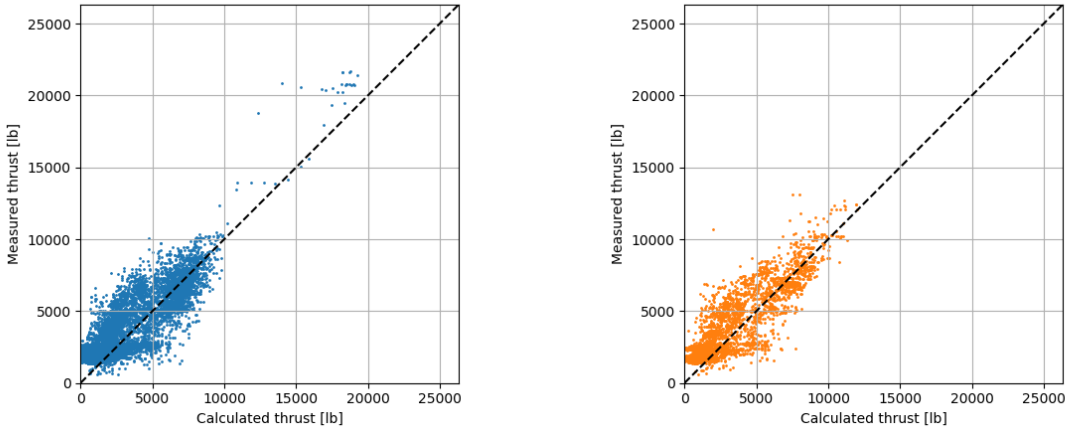

(a) Calibration ACMS logs

(b) Validation ACMS logs

Figure 6.23: Performance of the of the aircraft performance based thrust estimation method using default aerodynamic coefficients.

The validation of the performance based thrust estimation using the calibrated aerodynamic coefficients is presented in Figure 6.24. It is observed from this figure that a closer correlation between the estimated and actual thrust setting is found when compared to the thrust setting estimation using the default aerodynamic coefficients. This is both the case for the calibration and the validation ACMS datasets, which is in line with the thrust estimation method performance indicators presented in Table 6.15. It is observed that the mean difference and the standard deviation of the estimated thrust setting using the calibrated aerodynamic coefficients both are significantly lower (p<0.001) when compared to the estimated thrust setting using the default aerodynamic coefficients. Therefore, the calibrated aerodynamic coefficients are favoured over the default aerodynamic coefficients.

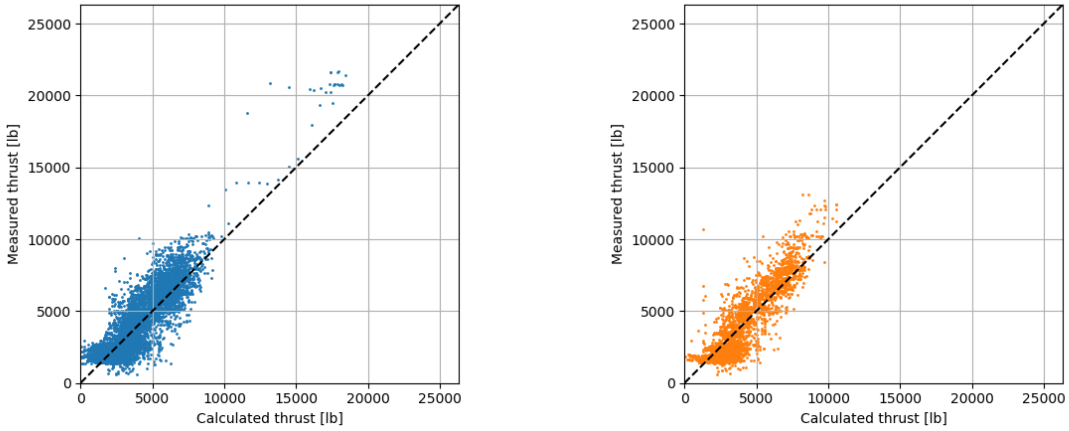

(a) Calibration ACMS logs

(b) Validation ACMS logs

Figure 6.24: Performance of the of the aircraft performance based thrust estimation method using calibrated aerodynamic coefficients.

Table 6.15: Performance of the aircraft performance based thrust estimation method using default and calibrated aerodynamic coefficients.

Coefficients	Calibration		Validation	
	μ [lb]	σ [lb]	μ [lb]	σ [lb]
default	-699	1263	-676	1296
calibrated	0	1023	52	1132

Thrust Estimation Comparison

Now that the performance characteristics of the different thrust estimation methods have been determined, the different thrust estimation methods are compared. The summary of the default and calibrated thrust estimation methods discussed above is provided in Table 6.16.

Table 6.16: Summary of the thrust estimation methods performances with default and calibrated coefficients for the approaching B738 aircraft.

Thrust estimation method	Calibration		Validation	
	μ [lb]	σ [lb]	μ [lb]	σ [lb]
Radar (Default)	14554	2161	14149	2204
Radar (Calibrated)	0	1695	-419	1894
N1 (Default)	-	-	-	-
N1 (Calibrated)	0	493	134	605
Performance (Default)	-699	1263	-676	1296
Performance (Calibrated)	0	1023	52	1132

Based on the results of the different thrust estimation methods presented in the table above it is concluded that the calibrated N1 based thrust estimation method is the best performing method for thrust estimation. For this thrust estimation method the lowest spread is observed and the mean difference for the validation dataset is comparable to the performance based thrust estimation method. However, the N1 based thrust estimation method requires the either the ACMS records of the flight of interest or the recorded pressure level during the aircraft noise event. As the recorded pressure level is not available for the aircraft noise events under consideration for this research, the effect of the N1 based thrust estimation method on the aircraft noise calculations is not investigated further.

The next best performing thrust estimation method is the performance based thrust estimation method. This method relies only on input parameters which either are either directly available in or can be determined based on the radar track. Therefore, the calibrated performance based thrust estimation method is the thrust estimation used when the calibrated aircraft performance is considered.

Effect on Noise Calculations

The effect of the calibration of the aerodynamic coefficient can not be assessed without also implementing the calibrated flap setting estimation method because the aerodynamic coefficient is directly linked to the flap setting. Therefore the combined effect of the calibrated flap setting estimation method and the calibrated aerodynamic coefficients on the aircraft noise calculations is presented in Figure 6.25. From comparison between the calculated and measured aircraft noise level using default aircraft performance and calibrated flap setting estimation method and calibrated aerodynamic coefficients it is clear that the calibration strongly affects the aircraft noise calculations. From the aircraft noise model performance for the default aircraft performance and the calibrated flap setting estimation method and the calibrated aerodynamic coefficients presented in Table 6.17 it is observed that the calibration of the aerodynamic coefficients reduces both the systematic error and the spread of the aircraft noise calculations.

Table 6.17: Effect of the calibrated flap setting estimation method and calibrated aerodynamic coefficients on the aircraft noise calculations.

Aerodynamic coefficients	μ [dBA]	σ [dBA]
Default	1.73	2.72
Calibrated	-0.20	2.64

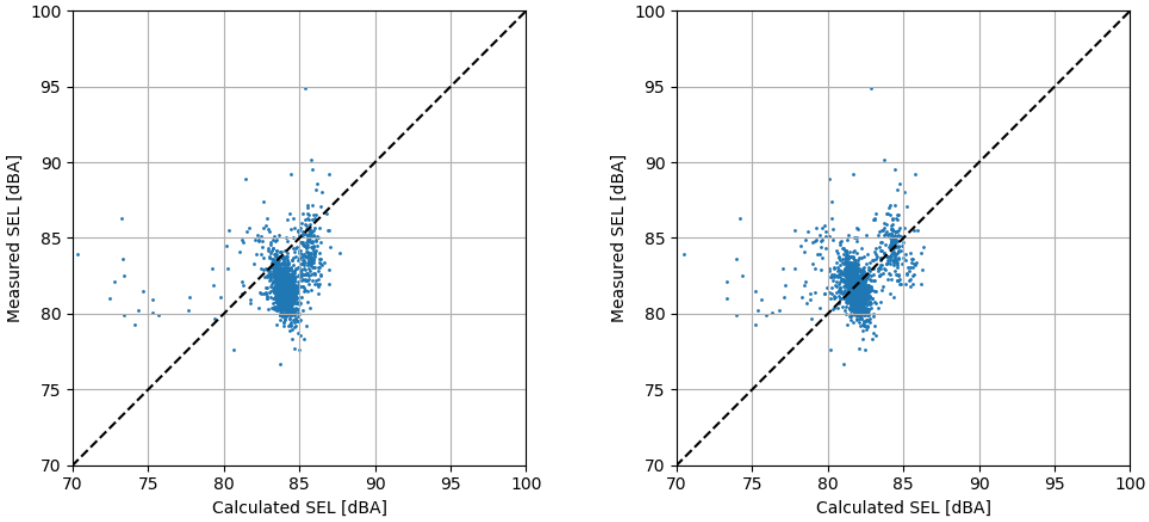

(a) Reference aircraft performance

(b) Calibrated flap setting estimation method and calibrated aerodynamic coefficients

Figure 6.25: Effect of the calibrated flap setting estimation method and calibrated aerodynamic coefficients on the aircraft noise calculations.

6.2.4. Combined Aircraft Performance Calibration

Here the effect of the combined aircraft performance calibration is presented. First, the main conclusions of the aircraft performance calibration are restated. Thereafter, the effect of the combined aircraft performance calibration on the aircraft noise calculations is assessed.

Aircraft Performance Calibration Conclusion

Two methods for the aircraft weight estimation for an approaching B738 aircraft have been considered. Based on the information available in the ACMS logs it is concluded that the approach speed based weight estimation method is most accurate. Therefore, the approach speed based weight estimation method with calibrated aircraft weight estimation coefficient is used for the combined calibrated aircraft performance estimation.

For the estimation of the flap setting for an approaching B738 aircraft two different proxies have been evaluated; the aircraft altitude and the calibrated airspeed. It has been determined that the best flap setting estimation is achieved when the calibrated airspeed is used as a proxy for the flap setting. Therefore, it is concluded that when the calibrated aircraft performance is considered the calibrated airspeed of the aircraft is used to estimate the flap setting of the aircraft.

Finally, three different methods for the determination of the thrust setting of the aircraft have been considered; the radar based, N1 parameter based, and aircraft performance based thrust setting estimation methods. Even though N1 parameter based thrust setting estimation method provides the highest accuracy, the determination of the N1 parameter requires data which is not always available. As a consequence the next best method, the aircraft performance based thrust setting estimation method, is used in combination with the calibrated aerodynamic coefficients when the calibrated aircraft performance is considered.

Effect on Noise Calculations

The effect of the combined aircraft performance calibration on the calculated aircraft noise level is presented in Figure 6.26 and Table 6.18. Where there is a mean overestimation of the aircraft noise level when the default aircraft performance is used, the use of the calibrated aircraft performance increases the accuracy of the aircraft noise model but also results in a slight underestimation of the aircraft noise level. Based on the aircraft noise model performance indicators presented in Table 6.18 it is concluded that using calibrated aircraft performance increases the accuracy of the aircraft noise model, but a systematic error in the aircraft noise calculations remains.

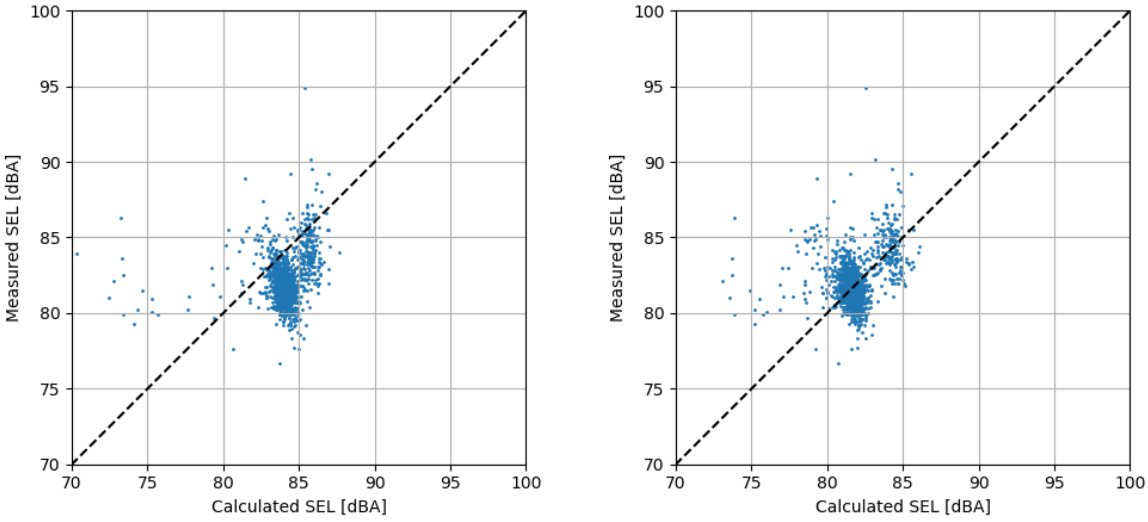

(a) Reference aircraft performance

(b) Calibrated aircraft performance

Figure 6.26: Effect of the combined aircraft performance calibration on the aircraft noise calculations.

Table 6.18: Effect of the calibrated aircraft performance on the aircraft noise calculations.

Aerodynamic coefficients	μ [dBA]	σ [dBA]
Default	1.73	2.72
Calibrated	-0.46	2.65

6.2.5. NPD Table Calibration

When the aircraft performance input parameters have been calibrated, the remaining systematic error can be handled through calibration of the NPD tables. As mentioned previously the NPD tables consist of a distance component and a thrust setting component, which can be seen in Table 6.19. Each aircraft noise event has a certain distance and power setting associated with it. First an example outlining the calibration of the NPD tables is presented. Thereafter the effect of the calibration of the NPD tables using both the default and calibrated aircraft performance on the aircraft noise calculations is discussed.

NPD Table Calibration Example

For example, an aircraft noise event with a calculated SEL value of 80.3dBA and a measured SEL value of 80.1dBA with a distance of 2,200 ft and a power setting of 4,150 lbs is associated with the SEL value indicated in Table 6.19. The two distances used for the NPD table, d_i and d_{i+1}, are 2,000 and 4,000 ft respectively. The two power settings used for the NPD table, P_i and P_{i+1}, are 4,000 and 5,000 lbs respectively. The mean difference in SEL or L_{Amax} between the calculated and measured aircraft noise level associated with each NPD table entry is determined, which is -0.2dBA in this example. For the NPD table entries where there are no corrections available an interpolation or extrapolation of the updated NPD table entries is performed. In

the case of this single aircraft noise event example the whole NPD table would be updated with a correction factor of -0.2dBA.

Table 6.19: Approach NPD table for the SEL of the B738 aircraft before NPD calibration.

	$200ft$	$400ft$	$630ft$	$1000ft$	$2000ft$	$4000ft$	$6300ft$	$10000ft$	$16000ft$	$25000ft$
$3000lb$	95.5	91.3	88.2	84.9	79.5	73.3	68.3	63.2	55.9	49.6
$4000lb$	96.2	91.9	88.8	85.6	80.2	74.1	69.4	64.3	56.8	50.7
$5000lb$	96.7	92.5	89.4	86.1	80.8	74.8	70.1	65.2	58	52.4
$6000lb$	97.2	93	89.9	86.7	81.4	75.5	70.9	66	59.4	54.3
$7000lb$	97.7	93.4	90.4	87.1	81.9	76	71.5	66.7	60.8	55.6

Calibration of the NPD tables can not be done indiscriminately. Two key requirements have to be kept in mind When performing the calibration of the NPD tables. The two requirements associated with the logic behind the NPD tables are:

1. The noise level shall decrease with increasing distance.
2. The noise level shall increase with an increasing power setting.

If conflicts occur in the logic of the NPD tables, priority is given to the updated entry with the largest amount of data points associated with that specific entry[30]. It is also noted that if conflicts still arise due to a similarity in the number of events associated with the conflicting entries, priority is given to aircraft noise events with a larger elevation angle.

Effect on Noise Calculations

The effect of the calibration of the NPD tables on the aircraft noise calculations is assessed twice. First the effect of calibration of the NPD tables using the default aircraft performance is determined and discussed. Subsequently, the effect of the calibration of the NPD tables using the combined calibrated aircraft performance is determined and discussed.

The effect of the calibrated NPD tables combined with default aircraft performance is presented in Figure 6.27 and Table 6.20. The first observation is that the mean difference between the calculated and measured aircraft noise level is strongly affected by calibration of the NPD tables. However, a small systematic error remains as NPD table calibration for a specific entry is only performed if sufficient aircraft noise events are associated with it and conflicts in NPD table logic. Furthermore, it is also observed that the spread of the aircraft noise calculations is reduced by calibration of the NPD tables.

Table 6.20: Effect of the calibrated NPD tables combined with default aircraft performance on the aircraft noise calculations.

NPD tables	μ [dBA]	σ [dBA]
Default	1.73	2.72
Calibrated	-0.29	2.45

The effect of the combination of aircraft performance calibration and calibration of the NPD tables is presented in Figure 6.28 and Table 6.21. It is observed that the combination of aircraft performance calibration and the calibration of the NPD tables results in an almost total mitigation of the systematic error in the aircraft noise calculations. Furthermore, the same magnitude of decrease in the spread of the aircraft noise calculation error is observed when compared to NPD table calibration with default aircraft performance. It is however strongly recommended to combine the calibration of the NPD tables with calibration of the aircraft performance. If the default aircraft performance is used for the calibration of the NPD tables it essentially means that the wrong NPD table entries are altered.

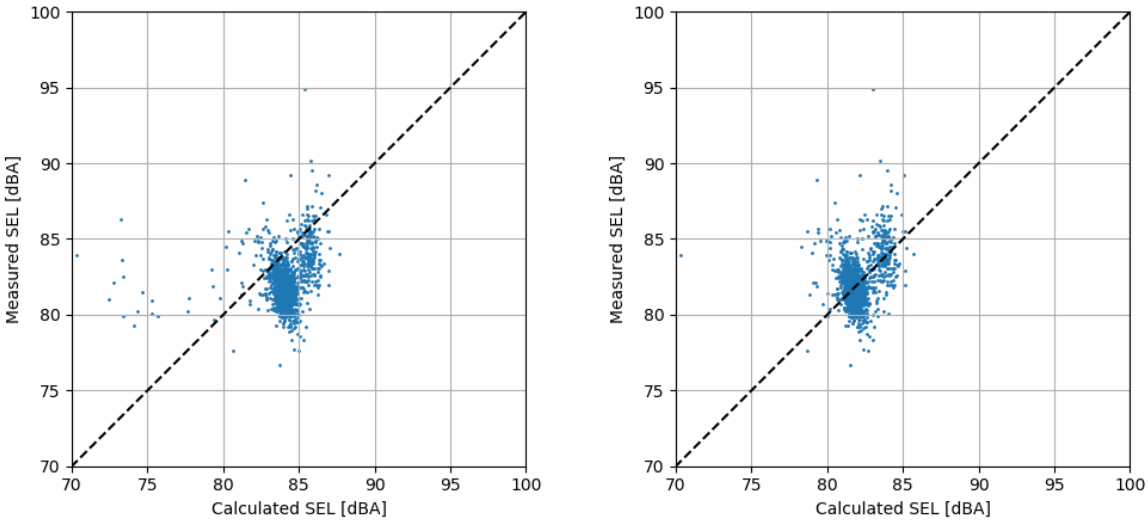

(a) Reference aircraft performance

(b) Calibrated NPD tables and default aircraft performance

Figure 6.27: Effect of the calibrated NPD tables combined with default aircraft performance on the aircraft noise calculations.

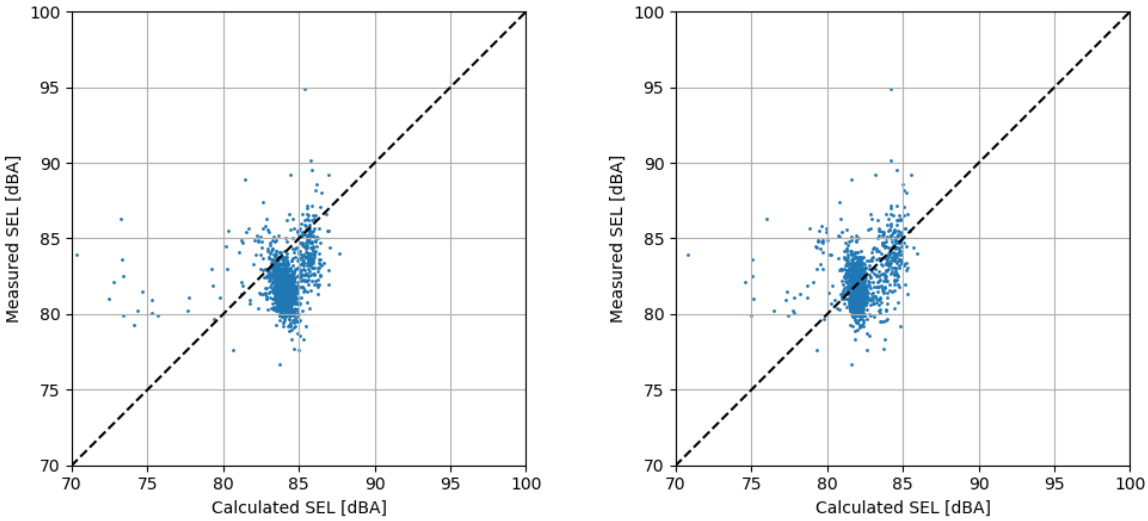

(a) Reference aircraft performance

(b) Calibrated NPD tables and calibrated aircraft performance

Figure 6.28: Effect of the calibrated NPD tables combined with calibrated aircraft performance on the aircraft noise calculations.

Table 6.21: Effect of the calibrated NPD tables combined with calibrated aircraft performance on the aircraft noise calculations.

NPD tables	μ [dBA]	σ [dBA]
Default	1.73	2.72
Calibrated	-0.01	2.44

6.3. Results Validation

The effects of the aircraft performance and NPD table calibration on the calculated aircraft noise level also have to be validated. For the validation of the NPD calibration an independent set of flights and aircraft noise events is used. The validation of the alterations to the aircraft noise model are considered both in

the temporal and spatial domain. For the temporal validation of the aircraft performance and NPD table calibration the selection is made to make use of the nighttime aircraft noise events of the year 2019. Secondly, the spatial validation of the effects of NPD table calibration is discussed. After the validation of the noise model improvements has been performed, the applications and limitations of these alterations are discussed.

6.3.1. Calibration Validation

The first step is to define the reference performance of the noise model with the default aircraft performance and NPD tables, which is subsequently used to quantify the effect of noise model improvements. Secondly, the effect of the calibration of the aircraft performance model is determined. Separately, the effect of the calibration of the NPD tables is also determined. Finally, the approaches of aircraft performance and NPD table calibration are combined. The aim of this section is to fill all entries in Table 6.22, after which statistical analysis is performed to determine the significance of model improvements.

Table 6.22: Results of aircraft performance and NPD calibration on the mean difference between the calculated and measured noise level for the calibration data (2018) and the validation data (2019) to be determined.

Aircraft Performance	NPD	2018		2019	
		μ [dBA]	σ [dBA]	μ [dBA]	σ [dBA]
Default	Default	-	-	-	-
Calibrated	Default	-	-	-	-
Default	Calibrated	-	-	-	-
Calibrated	Calibrated	-	-	-	-

Default Aircraft Performance and NPD

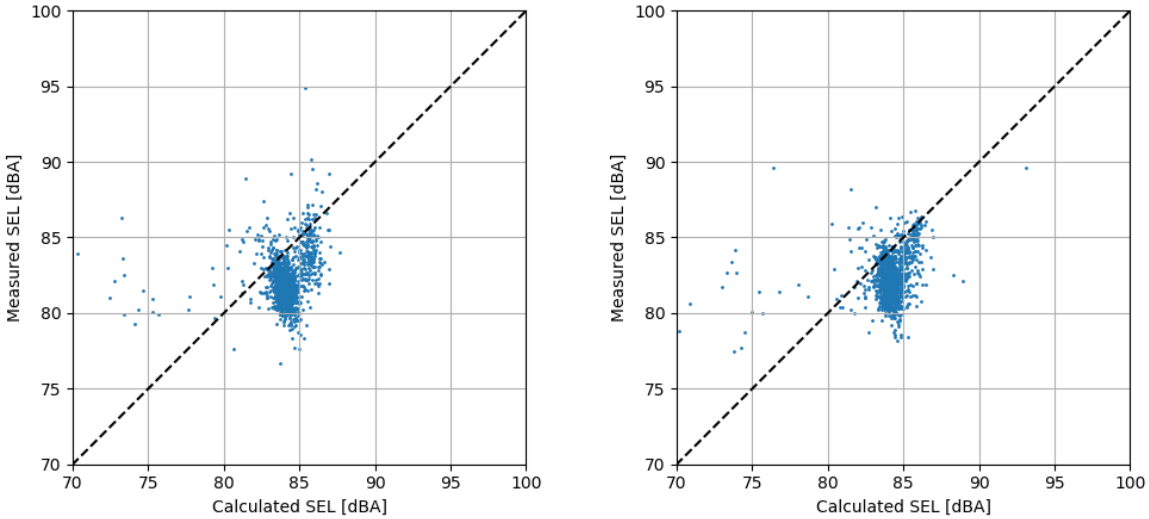

(a) 2018 (b) 2019

Figure 6.29: Default aircraft noise model performance for nighttime B738 aircraft operations in 2018 and 2019.

As mentioned previously, a baseline for the aircraft noise model performance has to be set in order to determine the effects of aircraft performance and NPD table calibration. The baseline noise model performance for the calibration year (2018) and validation year (2019) is shown in Table 6.23. The correlation between the calculated and measured SEL values is presented in Figure 6.29. From both the table and the figures it is apparent that the mean calculated aircraft noise event SEL is systematically higher than measured value for both the calibration and the validation year.

Table 6.23: Default aircraft noise model performance for nighttime B738 aircraft operations in 2018 and 2019.

Aircraft Performance	NPD	2018		2019	
		μ [dBA]	σ [dBA]	μ [dBA]	σ [dBA]
Default	Default	1.73	2.72	1.19	3.72

Calibrated Aircraft Performance

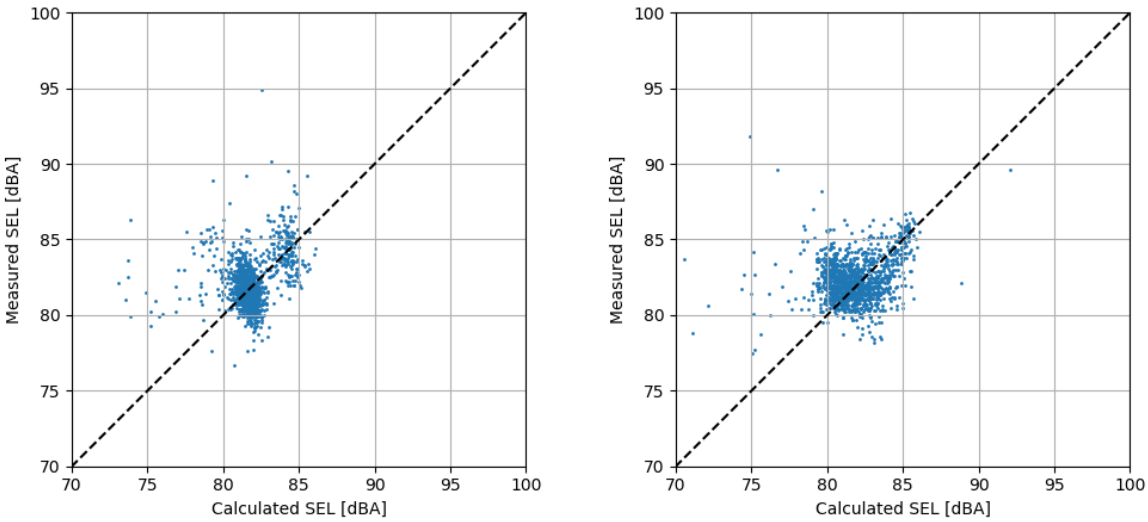

(a) 2018

(b) 2019

Figure 6.30: Aircraft noise model performance with calibrated aircraft performance modelling for nighttime B738 aircraft operations in 2018 and 2019.

The effect of the calibration of the aircraft performance database on the mean difference and the standard deviation is presented in Table 6.24. It is observed that the calibration of the aircraft performance based on the ACMS data leads to an underestimation instead of an overestimation of the mean aircraft noise level for both 2018 and 2019. This effect is also clearly observed in Figure 6.30, where the data points are shifted to the left with respect to the reference case. However, the absolute value of the mean difference between the calculated and measured aircraft noise level is decreased which indicates an increase in the aircraft noise model accuracy.

Furthermore, a reduction is observed in the standard deviation of the difference between the calculated and measured aircraft noise level. This implies that not only the systematic errors are reduced, but also the uncertainty bounds of the model itself are reduced. Therefore, using a calibrated aircraft performance database increases the accuracy of the aircraft noise prediction model. As mentioned previously, the quality of the result of the aircraft noise model can only be as good as the quality of the input in the aircraft noise model. With the calibrated and validated aircraft performance as input in the aircraft noise model the correctness of the noise model input is increased.

Table 6.24: Aircraft noise model performance with calibrated aircraft performance modelling for nighttime B738 aircraft operations in 2018 and 2019.

Aircraft Performance	NPD	2018		2019	
		μ [dBA]	σ [dBA]	μ [dBA]	σ [dBA]
Default	Default	1.73	2.72	1.19	3.72
Calibrated	Default	-0.46	2.65	-0.83	3.60

Calibrated NPD

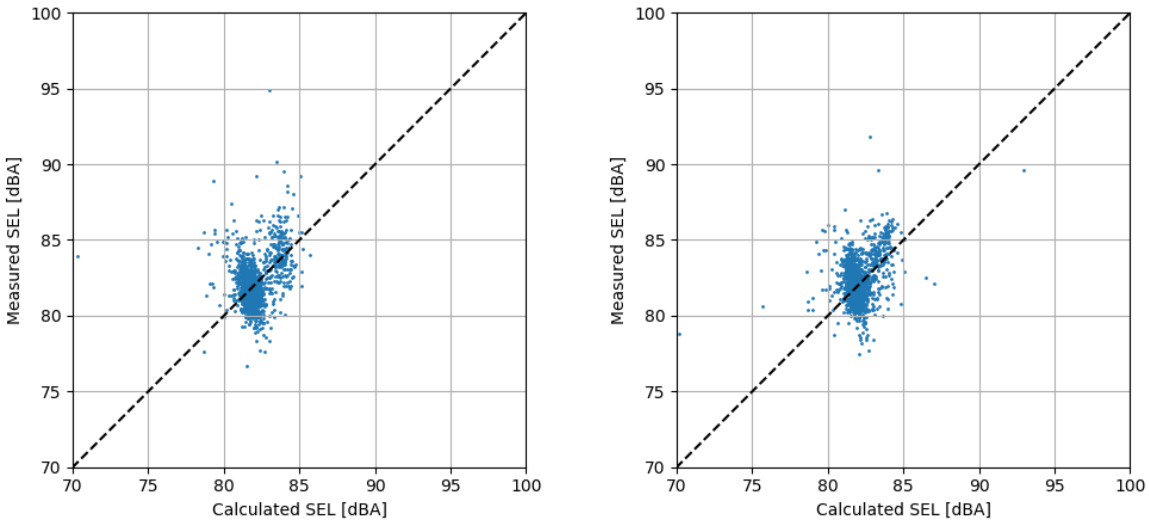

(a) 2018 (b) 2019

Figure 6.31: Aircraft noise model performance with calibrated NPD tables for nighttime B738 aircraft operations in 2018 and 2019.

As mentioned previously NPD calibration is performed to eliminate systematic errors using the comparison between aircraft noise calculations and measurements. However, as indicated in Table 6.25 there is a small remaining mean difference between aircraft noise calculations and measurements. The remaining mean difference is caused by conflicts in the NPD entries after the calibration. Nevertheless, the reduction of the mean difference as a result of the NPD calibration with respect to the reference cases is clearly visible in Figure 6.31 for both years.

The NPD table calibration does not only affect the systematic error, but also the spread of the calculation error. The effect of the NPD calibration on the systematic error and the spread of the calculation error is shown in Figure 6.31. Especially the outliers are reduced by the calibration of the NPD tables, which strongly affects the standard deviation.

Table 6.25: Aircraft noise model performance with calibrated NPD tables for nighttime B738 aircraft operations in 2018 and 2019.

Aircraft Performance	NPD	2018		2019	
		μ [dBA]	σ [dBA]	μ [dBA]	σ [dBA]
Default	Default	1.73	2.72	1.19	3.72
Default	Calibrated	-0.29	2.45	-0.60	3.28

Calibrated Aircraft Performance and NPD

The results of the combined aircraft performance and NPD table calibration is presented in Table 6.26. The combination of the aircraft performance and NPD calibration for the calibration year (2018) shows that mean difference is strongly reduced. However, the effect of the combined calibration for the validation year is less strong than for the calibration year. Furthermore, the standard deviation of the difference between the calculated and measured aircraft noise level is reduced with respect to the default noise calculations by calibration of the aircraft performance and NPD tables. This means that by calibration of both the aircraft performance and the NPD tables the accuracy of the aircraft noise calculations is increased.

Table 6.26: Aircraft noise model performance with calibrated aircraft performance and NPD tables for nighttime B738 aircraft operations in 2018 and 2019.

Aircraft Performance	NPD	2018		2019	
		μ [dBA]	σ [dBA]	μ [dBA]	σ [dBA]
Default	Default	1.73	2.72	1.19	3.72
Calibrated	Calibrated	-0.01	2.44	-0.45	3.43

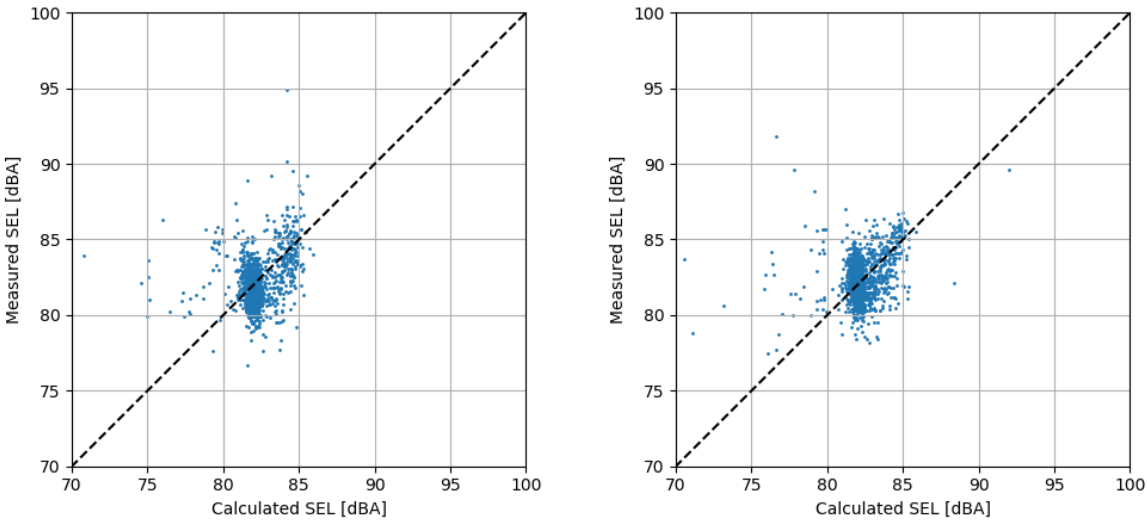

(a) 2018

(b) 2019

Figure 6.32: Aircraft noise model performance with calibrated aircraft performance and NPD tables for nighttime B738 aircraft operations in 2018 and 2019.

6.3.2. Spatial Validation

It is claimed by Bergmans et al. [11] that calibration of the NPD tables is only effective at the locations near the measurement site used for the calibration. This statement implies that the effects of NPD calibration are only valid for the locations where there is a measurement device nearby. The statement of Bergmans et al. is in their publication not supported by any evidence. In order to check the validity of this statement the following experiment has been designed.

In order to determine the spatial effect of calibration of the NPD tables the NOMOS Measurement Towers (NMT) are divided in two groups; a calibration and a validation group. The assignment to one of the two groups is done at random where 75% of the NMTs are used for NPD tables calibration and 25% of the NMTs are used for validation. Furthermore a division is made in the along track location of the NMTs. Based on the calibration of the Default Fixed Point Profiles (DFPP) in Appendix D it is observed that the power setting remains more or less constant until the aircraft is $9.3km$ ($5nm$) from the threshold for approaching aircraft. The decision has been made to divide the NMTs in two groups, one group located at an along track distance (S [nm]) of more than $9.3km$ and one group located at an along track distance less than $9.3km$. The division of the NMTs in the track distance based groups and calibration or validation group is presented in Table 6.27. For further information of the distribution of the along track distance for each individual NMT Appendix E can be consulted.

For this experiment it was decided to also include the daytime flights. It is common to fly set routes during the nighttime, which means that only several NMTs can provide noise measurements which satisfy all requirements, mainly the elevation angle requirement, posed for reliability. Including daytime operations, when a larger degree of vectoring is performed by air traffic control, results in more usable aircraft noise measurements at measurement locations which are not directly below a route. The inclusion of daytime aircraft operations does not strongly increase the number of valid aircraft noise events at the NMT locations which are positioned at less than $9.3km$ along track distance. This is a result of the fact that the aircraft trajectory from the interception of the ILS signal, at approximately $10.7nm$ from the threshold, to the threshold of the

Table 6.27: Division of NMTs in calibration and validation groups for along track distance greater than 9.3km (left) and less than 9.3km (right).

S <5nm		S >5nm	
Calibration	Validation	Calibration	Validation
1	12	4	14
2	26	7	16
10	29	13	21
15		20	25
17		23	28
18		24	32
19		27	45
40		30	
41		31	
		33	
		34	
		35	
		38	
		39	
		42	
		43	
		44	
		46	
		51	

runway is fixed. As a consequence low numbers of valid aircraft noise events with an elevation angle larger than 60° are obtained at these NMT locations. Therefore, the effect of NPD table calibration can only be accessed with sufficient certainty for NMT locations which are located at 9.3km or more from the threshold of the runway.

Different aircraft types are considered to eliminate the effect an individual aircraft type might have on the aircraft noise calculations. The aircraft used for this experiment are the A320, A333, A388, B744, B763, and B772 aircraft. This combination of aircraft provides a good coverage of the different aircraft weight categories and the aircraft manufacturers.

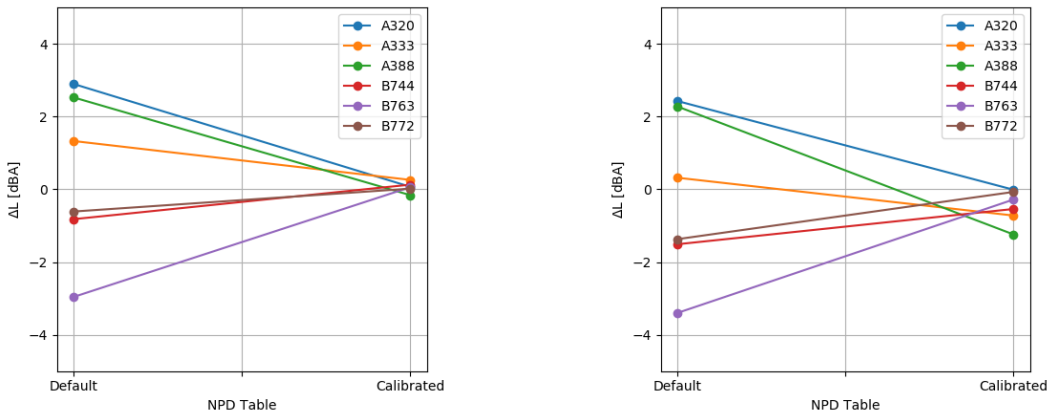

(a) Calibration NMTs

(b) Validation NMTs

Figure 6.33: Effect of NPD table calibration on the calibration NMTs (left) and validation NMTs (right) for different aircraft types.

The effect of calibration of the NPD tables on the mean difference between the calculated and measured aircraft noise level at the calibration and validation locations at more than 9.3km along track distance is presented in Figure 6.33. From the results presented in this figure it is clear that the calibration of the NPD

tables strongly reduces the mean difference between the calculated and measured aircraft noise level for the NMTs used for the calibration. This is in line with the expected behaviour of the calibration of the NPD tables. However, it is more interesting to observe what happens at the NMTs which are used for validation of the NPD table calibration. Here it is observed that even though the systematic errors in the aircraft noise calculations are not completely mitigated, as is the case for the NMTs used for calibration. The systematic error in the aircraft noise calculations is still reduced when compared to the default NPD tables, which means that calibration of the NPD tables also reduces the systematic error in aircraft noise calculations at locations where no noise measurements are performed. This observation disproves the claim made by Bergmans et al. [11] for the measurement site locations under consideration for this research.

6.3.3. Discussion

Here the effect of outliers on the aircraft noise calculations and the statistical significance of the aircraft noise model improvements are discussed. First the effect of the outliers on the performance of the calibrated NPD tables is discussed. subsequently, the implications of the statistical significance between the different cases presented in the previous section are outlined.

Outlier Effects

The combined results of the previous sections are presented in Table 6.28. It should be noted that the mean and standard deviation can be strongly affected by outliers. In order to eliminate the effect of outliers more outlier robust performance metrics are also considered.

Table 6.28: Results of aircraft performance and NPD calibration on the mean difference between the calculated and measured noise level for the calibration data (2018) and the validation data (2019).

Aircraft Performance	NPD	2018		2019	
		μ [dBA]	σ [dBA]	μ [dBA]	σ [dBA]
Default	Default	1.73	2.72	1.19	3.72
Calibrated	Default	-0.46	2.65	-0.83	3.60
Default	Calibrated	-0.29	2.45	-0.60	3.28
Calibrated	Calibrated	-0.01	2.44	-0.45	3.43

Outlier Robust Performance Metrics

Both the mean and the standard deviation of a dataset are rather sensitive to outliers[45]. This can be avoided by using the median and interquartile range (IQR) of the dataset based on the p^{th} emperical quantile, which is denoted by q_n. The p^{th} emperical quantile is given by the equation below for a dataset where $x_1 \leq x_2 \leq ... \leq x_n$[21], such that n is the number of elements in the dataset.

$$q_n(p) = x_k + \alpha \ (x_{k+1} - x_k)$$

where

$$k = \lfloor p\,(n+1) \rfloor$$

and

$$\alpha = p \ (n+1) - k$$

A good alternative for the mean of the dataset which is less sensitive to outliers is the median ($\tilde{x}$) [45]. The median is the middle of the dataset when put in ascending order, which corresponds with the value of the 50^{th} emperical quantile as presented below.

$$\tilde{x} = q_n(0.50)$$

Unlike the standard deviation, the interquartile range (IQR) is less sensitive to outliers. The IQR is bounded between the lower quartile (25%) and the upper quartile (75%). Because the IQR encompasses the middle half of the dataset, it is also referred to as the midspread.

$$IQR = q_n(0.75) - q_n(0.25)$$

The median and IQR values for each case are reported in Table 6.29. The comparison in this table also indicates a reduction in the spread for the combined calibrated aircraft performance and NPD case with respect to all other cases for the same year. Furthermore, an improvement of the noise modelling capacity in terms of median is observed between the default case and the fully calibrated case. It should be noted that the calibration of the NPD tables is based on the mean difference between the calculated and measured aircraft noise level, which means that the outliers also affect the calibration of the NPD tables. As a consequence of this way of NPD table calibration the median for the calibrated aircraft performance and calibrated NPD tables is not necessarily zero.

Table 6.29: Results of aircraft performance and NPD calibration on the mean difference between the calculated and measured noise level for the calibration data (2018) and the validation data (2019) using metrics less sensitive to outliers.

Aircraft Performance	NPD	2018		2019	
		$\tilde{x}$ [dBA]	IQR [dBA]	$\tilde{x}$ [dBA]	IQR [dBA]
Default	Default	2.14	1.97	1.81	2.06
Calibrated	Default	-0.23	2.40	-0.38	2.48
Default	Calibrated	0.00	1.90	-0.25	1.90
Calibrated	Calibrated	0.29	1.81	-0.02	1.84

Statistical Analysis

For each of the cases presented above, it is determined if the resulting differences between the calculated and measured aircraft noise level differ significantly from the other cases. From the results presented in Table 6.28 it can be determined if one method of calibrated aircraft noise calculations, namely only calibrated aircraft performance, only calibrated NPD tables, or both calibrated aircraft performance and NPD tables, provides a better estimation of the aircraft noise levels. If the difference between two cases is also found to be statistically significant, this indicates that one method is preferred over the other. The statistical significance levels for the comparison between the cases for 2018 and 2019 are provided in Table 6.30 and Table 6.31 respectively.

From Table 6.31 it is concluded that a statistical significant difference is observed between the default aircraft noise calculations and the calibrated aircraft performance and the calibrated NPD tables. For the validation aircraft noise dataset it is observed that there is no statistical significant difference between the default aircraft performance and calibrated NPD tables and the calibrated aircraft performance and calibrated NPD tables. However, it should be noted that using the default aircraft performance and calibrated NPD tables means that a the NPD table is calibrated wrongly based on unvalidated aircraft performance. Therefore, the calibrated aircraft performance should be favoured over the default, unvalidated, aircraft performance provided by the manufacturers.

Table 6.30: Statistical significance levels for the 2018 cases.

Aircraft Performance	NPD	Default Default	Calibrated Default	Default Calibrated	Calibrated Calibrated
Default	Default	-	<0.001	<0.001	<0.001
Calibrated	Default	<0.001	-	0.030	<0.001
Default	Calibrated	<0.001	0.030	-	<0.001
Calibrated	Calibrated	<0.001	<0.001	<0.001	-

Table 6.31: Statistical significance levels for the 2019 cases.

Aircraft Performance	NPD	Default Default	Calibrated Default	Default Calibrated	Calibrated Calibrated
Default	Default	-	<0.001	<0.001	<0.001
Calibrated	Default	<0.001	-	0.047	0.001
Default	Calibrated	<0.001	0.047	-	0.161
Calibrated	Calibrated	<0.001	0.001	0.161	-

7

Conclusion

It is concluded that differences occur between the calculated and measured values of single aircraft noise events exposure. When the differences between the calculated and measured aircraft noise levels are reported by the media, the perception of aviation and the corresponding noise annoyance is influenced. Reducing the magnitude of the calculation error increases trust in both local authorities and the aviation sector in general. This suggests that nuisance, a subjective matter, as a result of aircraft noise can be mitigated through the calibration and validation of the aircraft noise model.

Aircraft noise is measured and monitored by aircraft noise measurement systems at different airports. The most common purpose of those aircraft noise measurement systems is to provide information about the noise levels to the residents of communities around the airport. This is also the case for the NOMOS measurement system in place around Schiphol airport. However, large similarities are observed between the NOMOS system located around Schiphol airport and the ANOMS system located around Heathrow airport. As the ANOMS system is also used for model calibration, it is concluded that, at least several measurement device locations of, the NOMOS system can be used for model calibration.

The ECAC Doc.29 guidelines on the calculation of aircraft noise near airports has been implemented in Python for this research. This implementation is verified by comparing the model output to the expected output provided in 12 reference cases by ECAC. Based on the performance of the current implementation of the ECAC Doc.29 guidelines in comparison to the reference cases the current implementation is considered to be verified.

Based on the statistical analysis of the difference between the calculated and measured aircraft noise level it is concluded that both the aircraft type and the type of operation have a significant effect on these differences. The only difference in input data for different aircraft types and types of operation is the ANP database. Therefore it is concluded that the ANP database, which is not validated by Eurocontrol, is a source of significant differences between the calculated and measured aircraft noise level. Calibration and validation of the ANP database is necessary to increase the accuracy of the aircraft noise calculation model.

For the estimation of the aircraft noise model input during the approach phase a calibrated and validated estimation method for the aircraft weight, flap setting, and the thrust setting is required. The approach aircraft performance of the B738 aircraft has been calibrated and validated by a total of 42 ACMS logs provided by KLM. Based on the comparison between the ACMS logs and the aircraft performance estimation methods it is concluded that the weight estimation method most suited for the determination of the aircraft approach weight is based on the final approach speed. The approach flap setting estimation method best suited for the B738 aircraft is based on the calibrated airspeed. Furthermore, the aircraft performance based thrust setting estimation method is the best suited method for estimating the engine thrust setting based on radar tracks.

The effect of aircraft performance calibration on the comparison between the calculated and measured aircraft noise level is that the systematic error in the aircraft noise calculations is reduced from $1.73dBA$ to $-0.46dBA$. The accuracy of the aircraft noise calculations is increased by the calibration of the aircraft performance as the standard deviation decreases from $2.72dBA$ to $2.65dBA$. The spread of the calculated aircraft noise model is decreased from $2.72dBA$ to $2.45dBA$ and the systematic error is decreased from $1.73dBA$ to $-0.29dBA$ by only performing calibration on the NPD tables. The best results are obtained when the calibration of the aircraft performance and the calibration of the NPD tables is combined. In the case of combined

aircraft performance calibration and NPD table calibration the systematic error is reduced from 1.73dBA to -0.01dBA and the standard deviation is reduced by 10.3% from 2.72dBA to 2.44dBA.

The effect of the calibration of the aircraft performance and the NPD tables on the aircraft noise calculations was validated by using an independent set of aircraft operations. For the validation aircraft operations it is observed that the systematic error in the aircraft noise calculations is reduced from 1.19dBA using the default aircraft performance and NPD table to -0.45dBA using the calibrated aircraft performance and NPD table. The standard deviation of the aircraft noise calculations for the validation dataset using default aircraft performance and NPD tables is reduced by 7.8% from 3.72dBA to 3.43dBA. The standard deviation of the validation dataset using default aircraft performance is even lower at 3.28dBA and there is no statistically significant difference between the noise calculations using only the calibrated NPD tables and using the calibrated aircraft performance and calibrated NPD tables for the validation dataset. However, it is considered to be unwise to calibrate the NPD tables based on default aircraft performance. Calibration of the NPD tables based on the default aircraft performance means that an inaccurate thrust setting is used for alterations of the NPD tables, which is considered to be unwanted.

It was claimed by Bergmans et al. [11] that the calibration of NPD tables would only be valid in the vicinity of the measurement locations used for the calibration. The NMTs have been divided in groups of similar flight path characteristics, which were subsequently divided in a calibration and validation group. Even though the effect of NPD table calibration is more pronounced at the NMTs which are used for the calibration of the NPD tables, there is a clear mitigating effect on the systematic error in the aircraft noise calculations at the NMTs used for validation as well. Therefore, the claim by Bergmans et al. is considered to be disproved by the findings of this research. As a result the effects of NPD table calibration can with sufficient confidence be extrapolated to locations where no aircraft noise measurements are performed.

The final conclusion of this thesis is that a combined approach of aircraft performance calibration and NPD table calibration results in an increase of aircraft noise modelling accuracy. The validity of the results obtained aircraft performance calibration and NPD table calibration in both the temporal and spatial domain extends beyond the time span and the measurement locations used for the calibration.

Recommendations

The recommendations for data extension, future research and aircraft noise monitoring system alterations based on this research are presented below.

ANP Database Extension

Currently the ANP database does not contain all parameters of interest for every aircraft type. For the correct modelling of the aircraft performance it is recommended that data required to fill the entries which currently are unfilled in the ANP database is provided.

For aircraft types for which there is no available data in the ANP database a substitution is made based on the ICAO type code. This substitution is accompanied by one NPD correction factor for approach and one NPD correction factor for departure. No corrections are provided for the aircraft performance, meaning that the aircraft performance of another aircraft is used to determine the performance of the aircraft under consideration. This inevitably leads to an inadequate estimation of the aircraft performance, which subsequently leads to wrong input parameters in the aircraft noise calculation. Therefore, it is recommended that the ANP database is extended or the aircraft substitutions table is expanded to include aircraft performance correction parameters as well.

The calibration of the ANP database is strongly dependent on data which is not directly available from surveillance data. The aircraft parameters of interest; the aircraft weight, configuration, and thrust setting are commonly collected by a system as the ACMS. To allow for better calibration of the ANP database it is recommended that the operator of the aircraft, the airline, shares the anonymised ACMS logs with the user of the ANP data. This allows for more accurate aircraft noise calculations, which is considered to be beneficial for the aviation sector as a whole including the aircraft operators.

Future Research

Based on the data available from the ACMS logs it is observed that a strong correlation exists between the fan rotational speed (N1 [rpm]) and thrust setting for approaching aircraft. Hence, the thrust setting of the aircraft can accurately be estimated by the N1 parameter. Using the N1 parameter eliminates the need for the determination of the aircraft weight, flap setting, and aerodynamic coefficient. Therefore, NPD calibration

based on the thrust setting estimated obtained through the N1 parameter can be performed without the need for any other aircraft performance calibration. However, the need for flight recordings is not eliminated as these are the only reliable source for the determination of the correlation between the fan rotational speed and the engine thrust setting. It is expected that the fan rotational speed provides an accurate estimation of the aircraft thrust setting, reducing the input uncertainty for the aircraft noise model. A lower uncertainty in the input for the aircraft noise model results in a lower uncertainty in the calculated aircraft noise level. It is strongly recommended that the effect of N1 parameter based NPD table calibration is assessed.

Noise Monitoring System Improvements

During this research it was found that measured noise level assigned to an aircraft flyover event could have a cause other than an aircraft flyover event. This indicates that the aircraft noise detection algorithm used by NOMOS should be reevaluated. An example of an improved aircraft noise detection algorithm would include a check on the spectrum of the sound signal and identify certain aspects unique to aircraft noise. This can either be done manually or machine learning could be used for image recognition of the spectrogram.

The current application through which the NOMOS data is accessed is the ANOMS 9 application developed by Brüel & Kjær. This application does not support the use of APIs for the retrieval of noise event information, radar tracks, or audio files. Implementation of the possibility to retrieve information by use of an API would strongly decrease the time required for the acquisition of the right data for future research, especially if the machine learning based on the spectrogram of the aircraft noise event as mentioned above is considered.

Within the ANOMS 9 application it is currently only possible to retrieve the full dataset resulting from a set of query parameters. However, the ANOMS 9 application is a 32-bit application, meaning that there can be insufficient memory available for larger queries. Therefore, it is suggested to implement a random selection to obtain a subset which can still be considered representative for the full query.

The positioning of NOMOS measurement devices is until now mainly a political decision. This means that most measurement devices are positioned either in residential areas or commercial centres, which are not necessarily directly below an aircraft route. In order to increase the valid number of aircraft noise measurements, especially near the airport where the aircraft trajectories are fixed as a result of the ILS, it is recommended that the measurement devices are positioned directly below these routes. In this way the effect of the calibration of the NPD tables for higher thrust settings near the airport can also be evaluated.

A

Aircraft Type P-values

Table A.1: p-values resulting from the T-test on the aircraft type for the L_{Amax}.

ICAO Type	A306	A319	A320	A321	A332	A333	A359	A388	B734	B737	B738	B744	B748	B752	B763	B772	B77L	B77W	B789
A306	-	0.012	0.002	0.274	0.928	<0.001	0.262	0.023	<0.001	<0.001	0.008	<0.001	<0.001	<0.001	<0.001	<0.001	<0.001	<0.001	<0.001
A319	0.012	-	<0.001	0.001	0.007	<0.001	0.002	0.843	<0.001	<0.001	<0.001	<0.001	<0.001	<0.001	<0.001	<0.001	<0.001	<0.001	<0.001
A320	0.002	<0.001	-	0.194	<0.001	0.191	0.354	<0.001	<0.001	<0.001	0.063	<0.001	<0.001	<0.001	<0.001	<0.001	<0.001	<0.001	<0.001
A321	0.274	0.001	0.194	-	0.204	0.031	0.871	<0.001	<0.001	<0.001	0.705	<0.001	<0.001	<0.001	<0.001	<0.001	<0.001	<0.001	<0.001
A332	0.928	0.007	<0.001	0.204	-	<0.001	0.195	0.018	<0.001	<0.001	0.001	<0.001	<0.001	<0.001	<0.001	<0.001	<0.001	<0.001	<0.001
A333	<0.001	<0.001	0.191	0.031	<0.001	-	0.09	<0.001	<0.001	<0.001	<0.001	<0.001	<0.001	<0.001	<0.001	<0.001	<0.001	<0.001	<0.001
A359	0.262	0.002	0.354	0.871	0.195	0.09	-	0.002	<0.001	<0.001	0.916	<0.001	<0.001	<0.001	<0.001	<0.001	<0.001	<0.001	<0.001
A388	0.023	0.843	<0.001	<0.001	0.018	<0.001	0.002	-	<0.001	<0.001	<0.001	<0.001	<0.001	<0.001	<0.001	<0.001	<0.001	<0.001	<0.001
B734	<0.001	<0.001	<0.001	<0.001	<0.001	<0.001	<0.001	<0.001	-	0.781	<0.001	0.459	0.685	<0.001	<0.001	0.017	0.151	0.001	0.904
B737	<0.001	<0.001	<0.001	<0.001	<0.001	<0.001	<0.001	<0.001	0.781	-	<0.001	0.505	0.48	<0.001	<0.001	<0.001	0.026	<0.001	0.629
B738	0.008	<0.001	0.063	0.705	0.001	<0.001	0.916	<0.001	<0.001	<0.001	-	<0.001	<0.001	<0.001	<0.001	<0.001	<0.001	<0.001	<0.001
B744	<0.001	<0.001	<0.001	<0.001	<0.001	<0.001	<0.001	<0.001	0.459	0.505	<0.001	-	0.255	<0.001	<0.001	<0.001	0.002	<0.001	0.279
B748	<0.001	<0.001	<0.001	<0.001	<0.001	<0.001	<0.001	<0.001	0.685	0.48	<0.001	0.255	-	<0.001	<0.001	0.072	0.356	0.008	0.739
B752	<0.001	<0.001	<0.001	<0.001	<0.001	<0.001	<0.001	<0.001	<0.001	<0.001	<0.001	<0.001	<0.001	-	<0.001	0.003	<0.001	0.025	<0.001
B763	<0.001	<0.001	<0.001	<0.001	<0.001	<0.001	<0.001	<0.001	<0.001	<0.001	<0.001	<0.001	<0.001	<0.001	-	<0.001	<0.001	<0.001	<0.001
B772	<0.001	<0.001	<0.001	<0.001	<0.001	<0.001	<0.001	<0.001	0.017	<0.001	<0.001	<0.001	0.072	0.003	<0.001	-	0.187	0.323	0.005
B77L	<0.001	<0.001	<0.001	<0.001	<0.001	<0.001	<0.001	<0.001	0.151	0.026	<0.001	0.002	0.356	<0.001	<0.001	0.187	-	0.027	0.115
B77W	<0.001	<0.001	<0.001	<0.001	<0.001	<0.001	<0.001	<0.001	0.001	<0.001	<0.001	<0.001	0.008	0.025	<0.001	0.323	0.027	-	<0.001
B789	<0.001	<0.001	<0.001	<0.001	<0.001	<0.001	<0.001	<0.001	0.904	0.629	<0.001	0.279	0.739	<0.001	<0.001	0.005	0.115	<0.001	-

Table A.2: p-values resulting from the T-test on the aircraft type for the SEL.

ICAO Type	A306	A319	A320	A321	A332	A333	A359	A388	B734	B737	B738	B744	B748	B752	B763	B772	B77L	B77W	B789
A306	-	0.003	0.037	0.449	0.215	<0.001	0.239	0.002	0.001	<0.001	0.001	<0.001	<0.001	<0.001	<0.001	<0.001	<0.001	<0.001	<0.001
A319	0.003	-	<0.001	<0.001	<0.001	<0.001	0.262	0.412	<0.001	<0.001	0.265	<0.001	<0.001	<0.001	<0.001	<0.001	<0.001	<0.001	<0.001
A320	0.037	<0.001	-	0.383	0.329	<0.001	0.004	<0.001	0.018	0.016	<0.001	<0.001	0.003	<0.001	<0.001	<0.001	<0.001	<0.001	<0.001
A321	0.449	<0.001	0.383	-	0.877	0.002	0.077	<0.001	0.008	0.011	0.001	<0.001	<0.001	<0.001	<0.001	<0.001	<0.001	<0.001	<0.001
A332	0.215	<0.001	0.329	0.877	-	<0.001	0.028	<0.001	0.004	0.001	<0.001	<0.001	0.001	<0.001	<0.001	<0.001	<0.001	<0.001	<0.001
A333	<0.001	<0.001	<0.001	0.002	<0.001	-	<0.001	<0.001	0.819	0.517	<0.001	<0.001	0.337	0.048	<0.001	<0.001	<0.001	<0.001	0.373
A359	0.239	0.262	0.004	0.077	0.028	<0.001	-	0.103	<0.001	<0.001	0.57	<0.001	<0.001	<0.001	<0.001	<0.001	<0.001	<0.001	<0.001
A388	0.002	0.412	<0.001	<0.001	<0.001	<0.001	0.103	-	<0.001	<0.001	0.094	<0.001	<0.001	<0.001	<0.001	<0.001	<0.001	<0.001	<0.001
B734	0.001	<0.001	0.018	0.008	0.004	0.819	<0.001	<0.001	-	0.551	<0.001	0.034	0.533	0.196	<0.001	0.001	0.013	<0.001	0.669
B737	<0.001	<0.001	0.016	0.011	0.001	0.517	<0.001	<0.001	0.551	-	<0.001	<0.001	0.199	0.032	<0.001	<0.001	<0.001	<0.001	0.198
B738	0.001	0.265	<0.001	0.001	<0.001	<0.001	0.57	0.094	<0.001	<0.001	-	<0.001	<0.001	<0.001	<0.001	<0.001	<0.001	<0.001	<0.001
B744	<0.001	<0.001	<0.001	<0.001	<0.001	<0.001	<0.001	<0.001	0.034	<0.001	<0.001	-	0.217	0.782	<0.001	0.006	0.207	<0.001	0.033
B748	<0.001	<0.001	0.003	<0.001	0.001	0.337	<0.001	<0.001	0.533	0.199	<0.001	0.217	-	0.448	<0.001	0.01	0.073	<0.001	0.746
B752	<0.001	<0.001	<0.001	<0.001	<0.001	0.048	<0.001	<0.001	0.196	0.032	<0.001	0.782	0.448	-	<0.001	0.086	0.337	0.006	0.227
B763	<0.001	<0.001	<0.001	<0.001	<0.001	<0.001	<0.001	<0.001	<0.001	<0.001	<0.001	<0.001	<0.001	<0.001	-	<0.001	<0.001	<0.001	<0.001
B772	<0.001	<0.001	<0.001	<0.001	<0.001	<0.001	<0.001	<0.001	0.001	<0.001	<0.001	0.006	0.01	0.086	<0.001	-	0.371	0.136	<0.001
B77L	<0.001	<0.001	<0.001	<0.001	<0.001	<0.001	<0.001	<0.001	0.013	<0.001	<0.001	0.207	0.073	0.337	<0.001	0.371	-	0.034	0.007
B77W	<0.001	<0.001	<0.001	<0.001	<0.001	<0.001	<0.001	<0.001	<0.001	<0.001	<0.001	<0.001	<0.001	0.006	<0.001	0.136	0.034	-	<0.001
B789	<0.001	<0.001	<0.001	<0.001	<0.001	0.373	<0.001	<0.001	0.669	0.198	<0.001	0.033	0.746	0.227	<0.001	<0.001	0.007	<0.001	-

B

B772 Approach Calibration

B.1. Aircraft Performance Calibration

For the aircraft performance calibration of the B772 aircraft 40 ACMS logs have been provided by KLM. The 40 ACMS logs are divided in 30 ACMS logs for the calibration of the aircraft performance and 10 ACMS logs for the subsequent validation of the aircraft performance calibration. The ACMS logs of the B772 aircraft contain the same parameters as the ACMS logs of the B738 aircraft outlined in section 6.2.

The calibration of the aircraft performance database for the B772 aircraft is presented in the same order as the aircraft performance calibration for the B738 aircraft. First the aircraft weight estimation method is calibrated. Subsequently, the flap scheduling is estimated based on both the aircraft altitude and the V_{CAS}. Finally, the calibration of the aerodynamic coefficients associated with the different flap settings is discussed.

B.1.1. Weight Estimation

The distribution of the aircraft weight as a percentage of the MLW is presented in Figure B.1. It is observed from visual comparison between this figure and the distribution of the aircraft approach weight for the B738 aircraft that the spread of the B772 aircraft weight distribution is lower. Therefore, also the mass fraction based weight estimation method is considered for the B772 weight estimation.

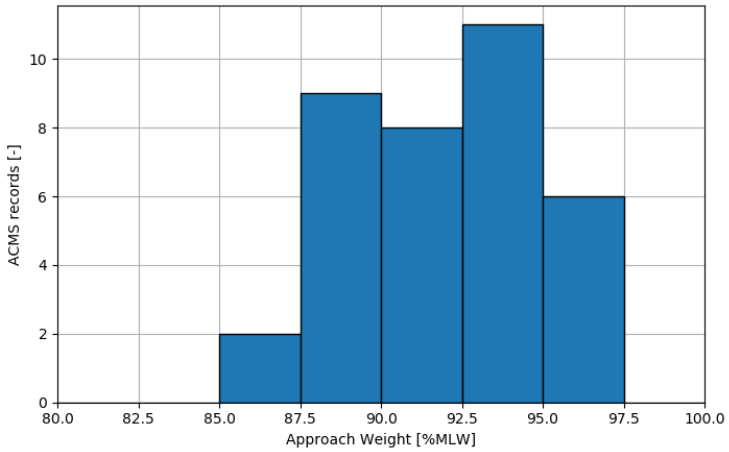

Figure B.1: Distribution of the aircraft approach weight taken retrieved from the ACMS records. It should be noted that both the calibration and the validation ACMS records are included in the data in this figure.

The performance of the weight estimation methods under consideration, the mass fraction and the approach speed based weight estimation methods, are presented in Table B.1. From the results presented in this table it is concluded that the calibrated mass fraction based weight estimation method performs better than the default mass fraction and the calibrated approach speed based weight estimation methods. When

the calibrated aircraft performance is considered for the B772 aircraft the aircraft weight during approach is estimated to be 92.0% of the MLW. This is in contrast with the results from the weight estimation calibration for the B738 aircraft, which indicates that the most suitable weight estimation method has to be determined for each aircraft type individually.

Table B.1: Performance of calibrated weight estimation methods with respect to the Doc.29 standard for the B772 aircraft.

Weight estimation method	Calibration		Validation	
	μ [lb]	σ [lb]	μ [lb]	σ [lb]
Mass fraction (Default)	-9441	12653	-11124	14527
Mass fraction (Calibrated)	0	12653	-1683	14527
Approach speed (Calibrated)	0	26327	13822	30561

B.1.2. Flap Setting Calibration

The flap setting as recorded in the ACMS logs does not directly contain the flap setting angle as also contained in the aircraft performance database. Instead the ACMS logs contain a flap handle selection parameter, which takes on the value of 1, 2, 4, 8, 16, 32, or 64. Therefore, the calibrated flap scheduling for the B772 aircraft cannot be compared to the default flap scheduling in the aircraft performance database.

The two parameters considered for the estimation of the flap setting are the altitude and the V_{CAS}. The flap setting as a function of both parameters is presented in Figure B.2. The start points of the average flap setting corresponding to the ACMS logs used for calibration as a function of both altitude and V_{CAS} are provided in Table B.2. From both Figure B.2 and the values provided in Table B.2 it is observed that the estimated flap setting increases with decreasing altitude or decreasing V_{CAS}.

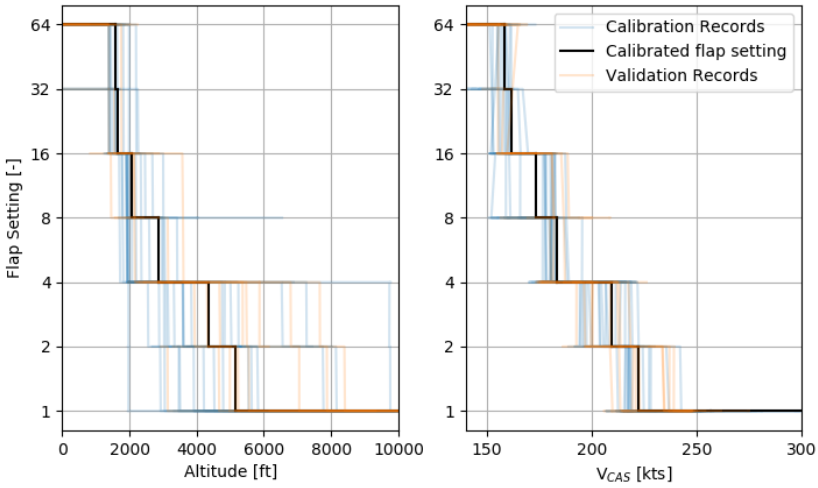

Figure B.2: Altitude based (left) and calibrated airspeed based (right) flap setting estimation method. The blue lines represent the data retrieved from the ACMS records for calibration. The orange lines represent the data retrieved form the ACMS records for validations. The black lines indicate the results of the flap scheduling calibration.

As mentioned in the case of the B738 flap setting estimation, the mean and standard deviation of flap setting estimation methods based on two different parameters cannot be compared directly. The coefficient of determination (R^2 [-]) was introduced to allow for the comparison of the two flap setting estimation methods. From the values of the coefficients of determination for the two calibrated flap setting estimation methods provided in Table B.3 it is determined that for the calibration case the V_{CAS} performs better than the altitude. However, when the validation cases are considered the performance of the two flap setting estimation methods is similar. Even though no large differences are observed it is decided to base the flap setting estimation method on V_{CAS} rather than the altitude.

Table B.2: Results for the calibration of the altitude and V_{CAS} based flap setting estimation methods for the B772 aircraft.

Flap setting	Altitude [ft]	Calibrated airspeed [kts]
1	37000	500
2	5160	222.1
4	4350	209.4
8	2880	183.4
16	2060	173.7
32	1660	161.7
64	1580	158.4

Table B.3: Resulting coefficient of determination (R^2 [-]) of the calibrated altitude and V_{CAS} based flap setting estimation methods.

Flap setting estimation method	Calibration	Validation
Altitude (Calibrated)	0.794	0.849
Calibrated airspeed (Calibrated)	0.882	0.839

B.1.3. Aerodynamic Coefficient Calibration

The final step in the calibration of the aircraft performance is the calibration of the aerodynamic coefficient of the aircraft. For the determination of the aerodynamic coefficient associated with a certain flap setting it is also required to have the thrust setting of the engines available. The thrust setting is not directly available from the ACMS logs, but is estimated as a function of the fuel flow to the engine. The relation between the fuel flow and the thrust setting for the GE90-94B engine obtained from the ICAO Aircraft Engine Emissions Databank is given by the equation below.

$$T = T_{max} \cdot \left(-0.0288\, f_{fuel}^2 + 0.3968\, f_{fuel} - 0.0418\right) \tag{B.1}$$

The aerodynamic coefficients for the distinct flap settings are presented in Table B.4. It is observed that the aerodynamic coefficients increase as the flap setting increases except for flap setting 8. Therefore, this flap setting is excluded from the calibrated aircraft performance data. The correlation between the calculated and actual thrust setting for both the calibration and validation ACMS logs using the calibrated aerodynamic coefficients is presented in Figure B.3.

Table B.4: Result of calibration of the aerodynamic coefficients for the B772 aircraft.

Flap setting	Calibrated
1	0.0832
2	0.0906
4	0.0960
16	0.1239
64	0.1718

The performance of the thrust estimation method using calibrated aerodynamic coefficients is presented in Table B.5. From the values provided in this table it is observed that the mean difference between the calculated and the actual thrust setting for the calibration case is 0.5% of the maximum thrust setting for this engine. Therefore, the thrust estimation method using calibrated aerodynamic coefficients is considered to be validated. This means that when the calibrated aircraft performance is considered the calibrated aerodynamic coefficients are used.

Table B.5: Results of the calibrated aerodynamic coefficients thrust estimation method for the B772 aircraft.

Aerodynamic coefficients	Calibration		Validation	
	μ [lb]	σ [lb]	μ [lb]	σ [lb]
Calibrated	0	4998	-503	5458

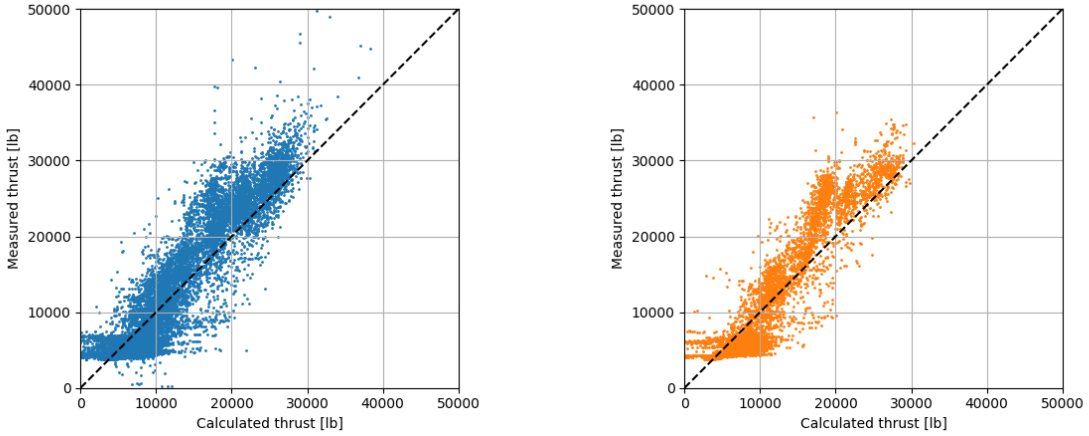

(a) Calibration

(b) Validation

Figure B.3: Calibration and validation of the relation between estimated and actual thrust for the performance based thrust estimation method using calibrated aerodynamic coefficients.

B.2. Results and Validation

The impact of aircraft performance calibration and NPD tables calibration is discussed in this section. The calibration of the NPD tables is validated by assessing the impact on an independent set of nighttime aircraft noise events of the B772 aircraft from 2019. First the reference performance of the aircraft noise model using the default aircraft performance and NPD tables is determined for the NPD calibration set (2018) and the NPD validation set (2019). The reference aircraft noise model performance for the B772 aircraft is shown in Figure B.4.

The resulting aircraft noise model performance for all cases under consideration are presented in Table B.6. The aircraft noise model performance for the reference cases indicate that the measured aircraft noise level is higher than the calculated aircraft noise level. After the implementation of the calibrated aircraft performance the calculated aircraft noise level is still lower than the measured aircraft noise level, but the mean difference is decreased. This conclusion is in line with the visual observations of Figure B.5. The effect of the calibration of the NPD tables using default aircraft performance is presented in Figure B.6. It is observed that much of the systematic error in the aircraft noise calculations is mitigated by calibration of the NPD tables, which is as expected. Finally, the effect of the calibrated aircraft performance and calibrated NPD tables on the aircraft noise calculations is presented in Figure B.7. Even though the spread of the aircraft noise calculations is in this case somewhat increased with respect to the calibrated NPD tables combined with the default aircraft performance, the systematic errors in the calculations are further reduced for both the calibration and validation dataset. Therefore, it is concluded that the best aircraft noise model performance is attained when the calibrated aircraft performance and the calibrated NPD tables are combined.

Table B.6: Results of aircraft performance and NPD calibration on the mean difference between the calculated and measured noise level for the calibration data (2018) and the validation data (2019) of the B772 aircraft.

Aircraft Performance	NPD Tables	2018		2019	
		μ [dBA]	σ [dBA]	μ [dBA]	σ [dBA]
Default	Default	-1.30	2.77	-1.47	2.76
Calibrated	Default	-0.89	3.03	1.05	3.09
Default	Calibrated	-0.29	2.87	-0.47	2.83
Calibrated	Calibrated	-0.08	2.96	-0.26	2.91

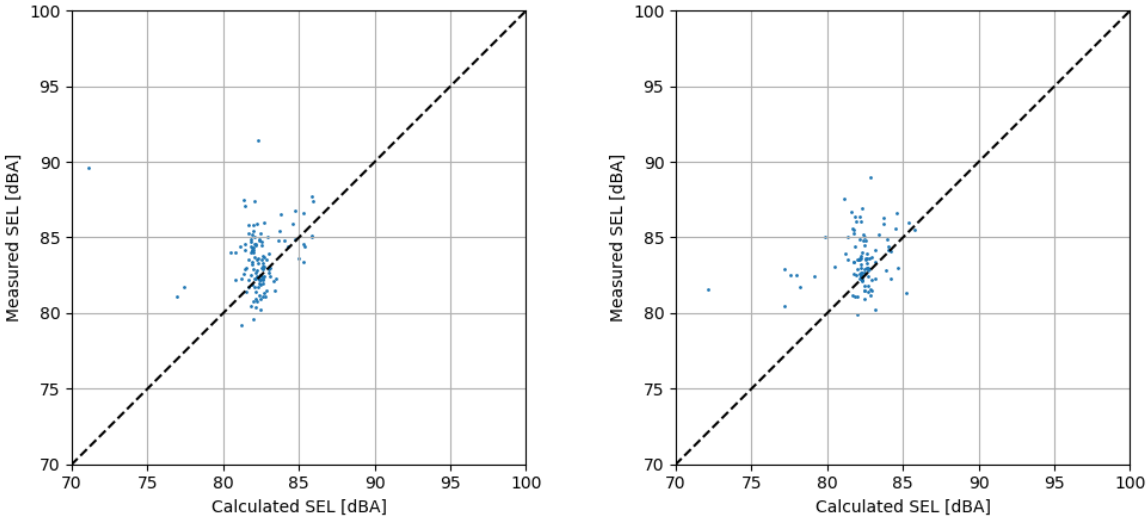

(a) 2018 (b) 2019

Figure B.4: Aircraft noise model performance with default aircraft performance and NPD tables for nighttime B772 aircraft operations in 2018 and 2019.

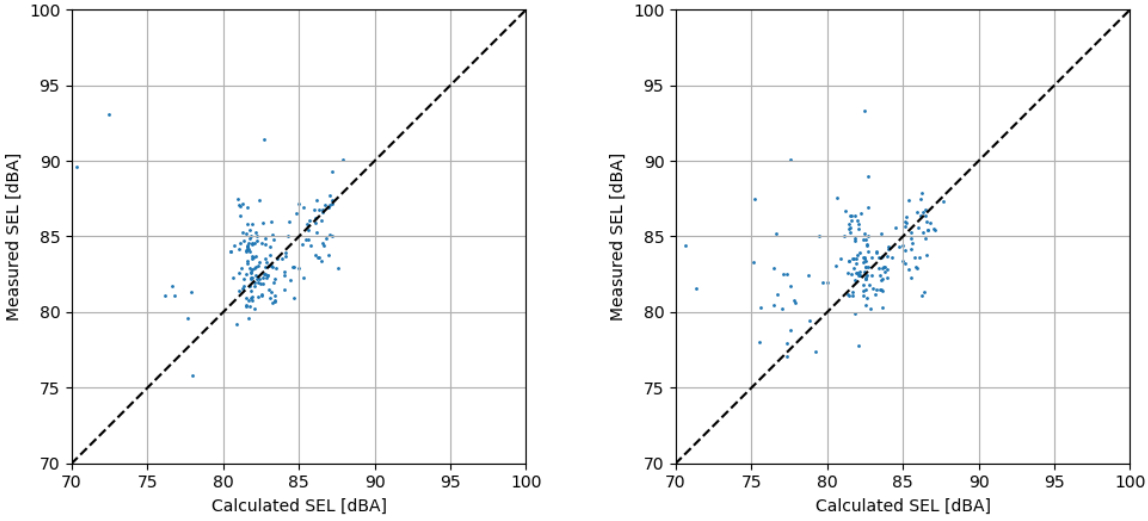

(a) 2018 (b) 2019

Figure B.5: Aircraft noise model performance with calibrated aircraft performance and default NPD tables for nighttime B772 aircraft operations in 2018 and 2019.

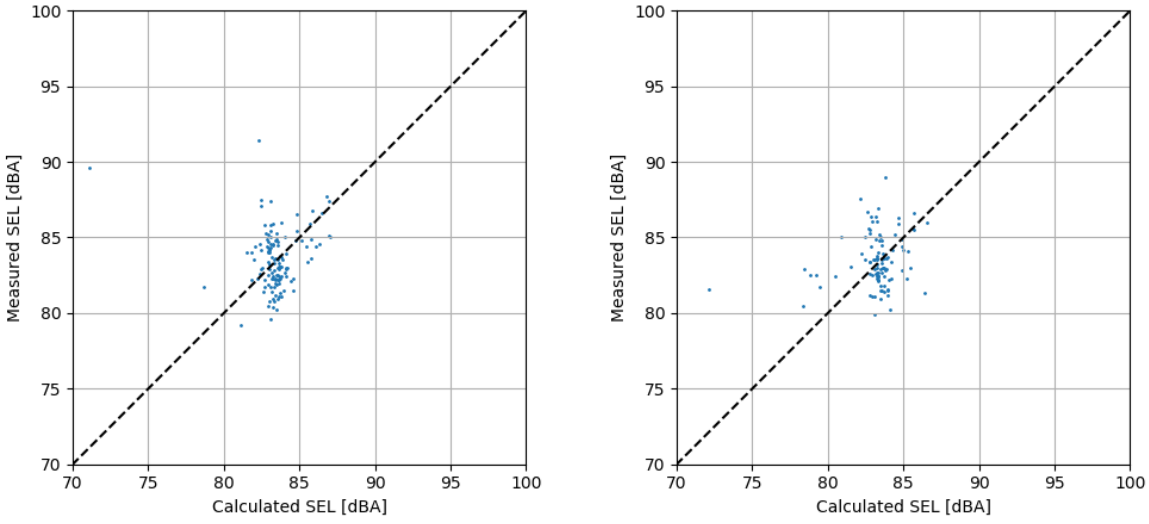

(a) 2018 (b) 2019

Figure B.6: Aircraft noise model performance with default aircraft performance and calibrated NPD tables for nighttime B772 aircraft operations in 2018 and 2019.

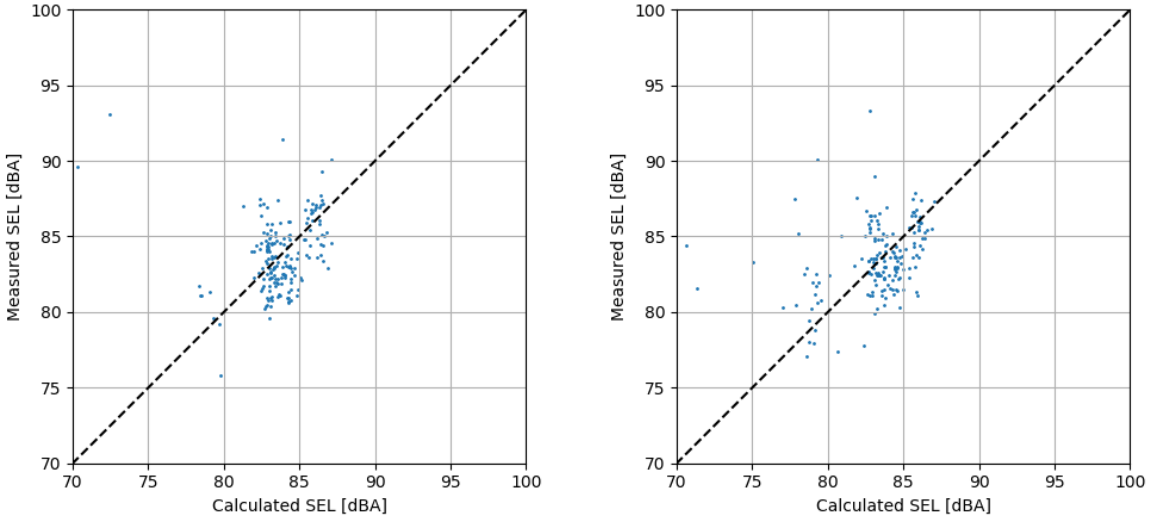

(a) 2018 (b) 2019

Figure B.7: Aircraft noise model performance with calibrated aircraft performance and NPD tables for nighttime B772 aircraft operations in 2018 and 2019.

C

Track Descriptions

In this appendix the aircraft tracks used for this research are presented visually. For each set of tracks the lateral track distribution is presented, along with the associated runway distribution, and speed and altitude profiles.

C.1. 2018 Nighttime Operations

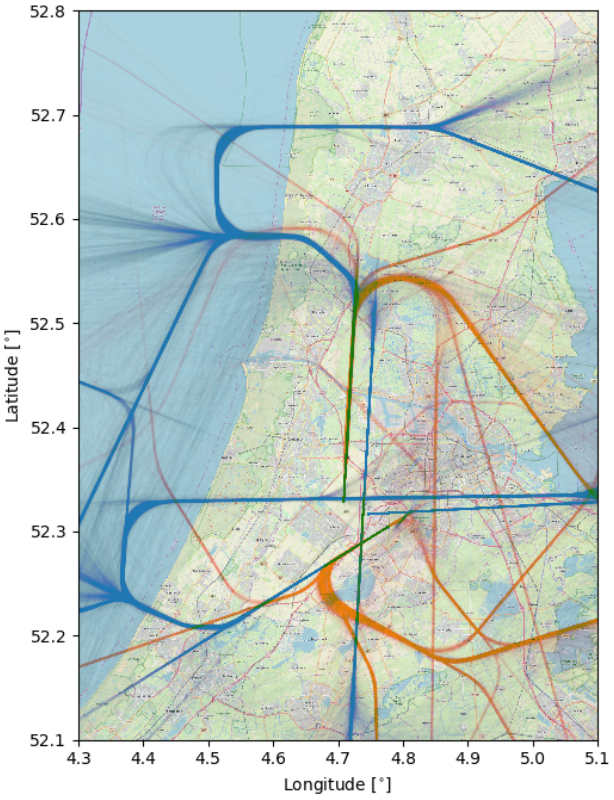

Figure C.1: Lateral tracks of the nighttime aircraft operations in 2018.

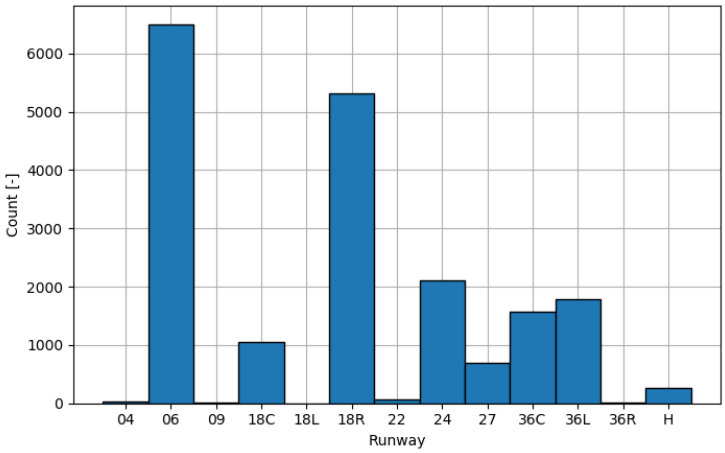

Figure C.2: Runway distribution of the nighttime aircraft operations in 2018.

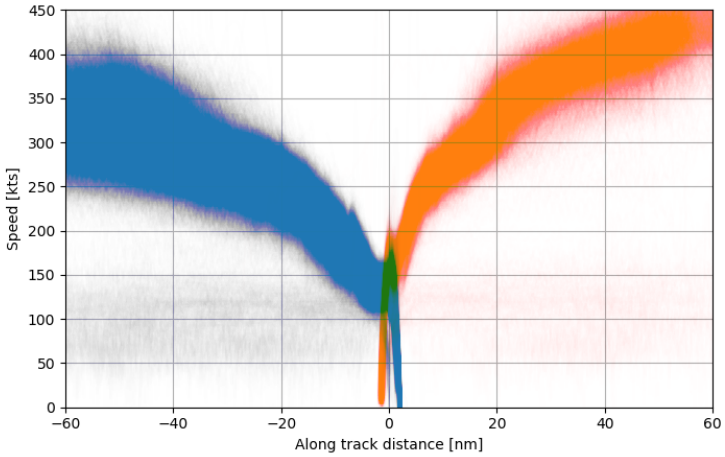

Figure C.3: Speed profiles of the nighttime aircraft operations in 2018.

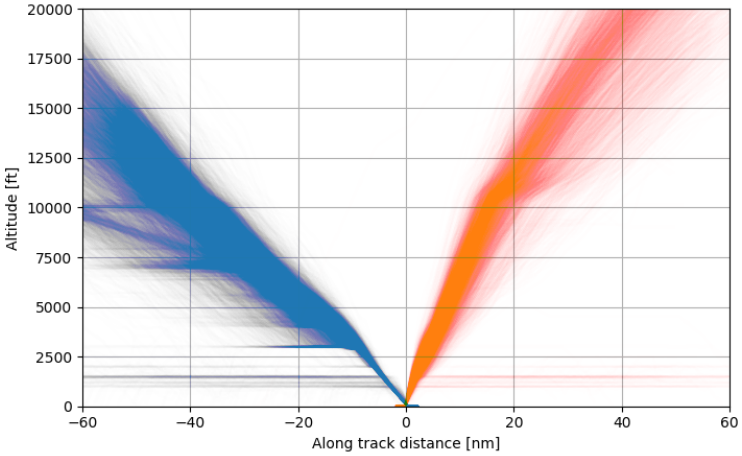

Figure C.4: Altitude profiles of the nighttime aircraft operations in 2018.

C.2. B738 Operations

C.2.1. 2018 Nighttime

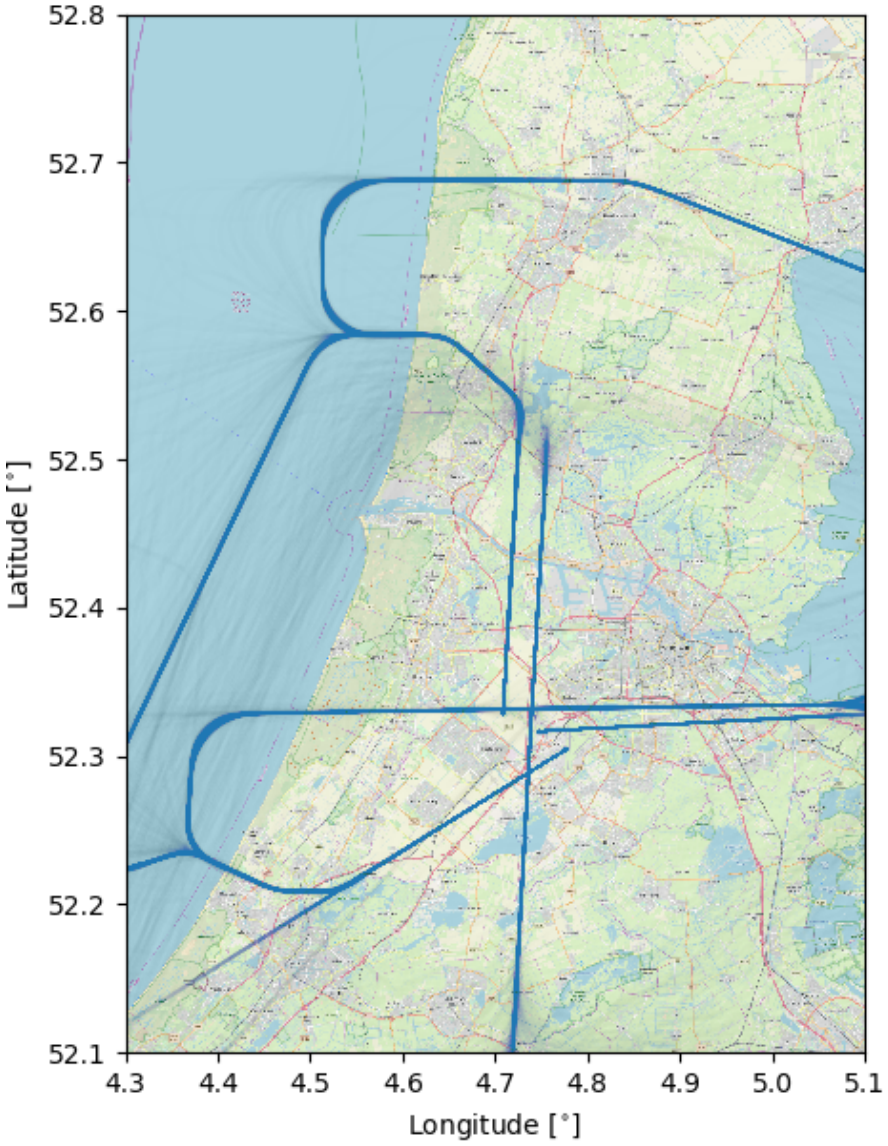

Figure C.5: Lateral tracks of the nighttime aircraft operations of the B738 aircraft in 2018.

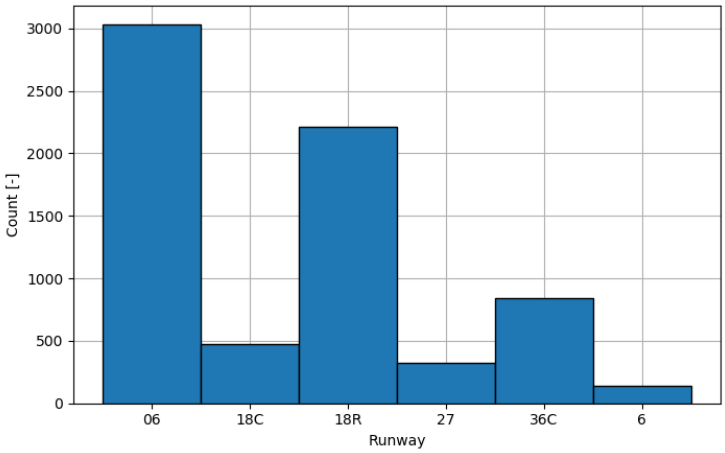

Figure C.6: Runway distribution of the nighttime aircraft operations of the B738 aircraft in 2018.

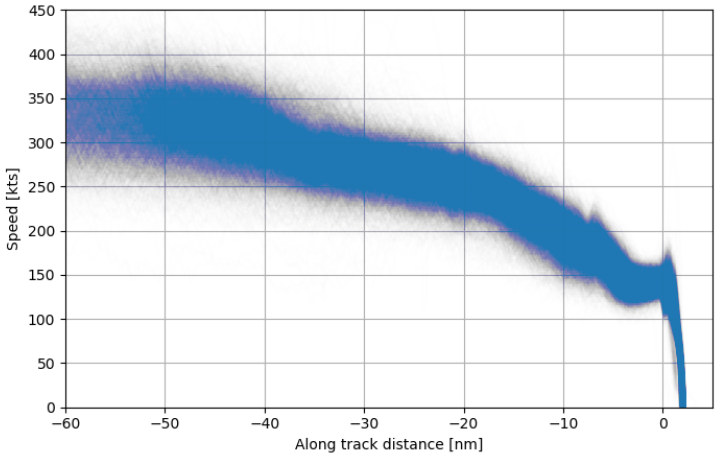

Figure C.7: Speed profiles of the nighttime aircraft operations of the B738 aircraft in 2018.

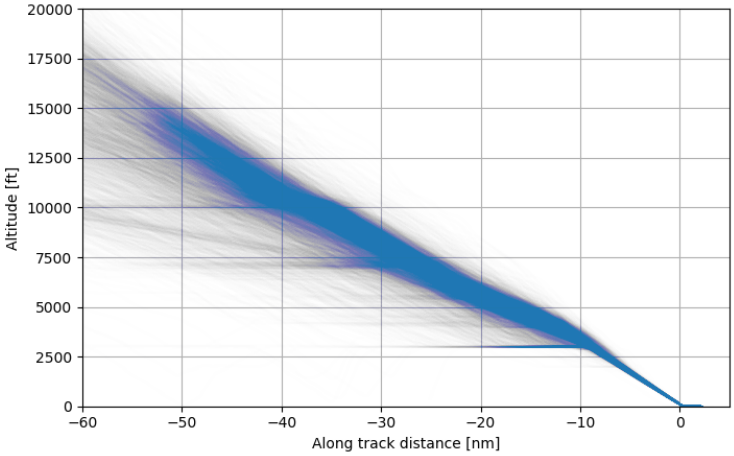

Figure C.8: Altitude profiles of the nighttime aircraft operations of the B738 aircraft in 2018.

C.2.2. 2019 Nighttime

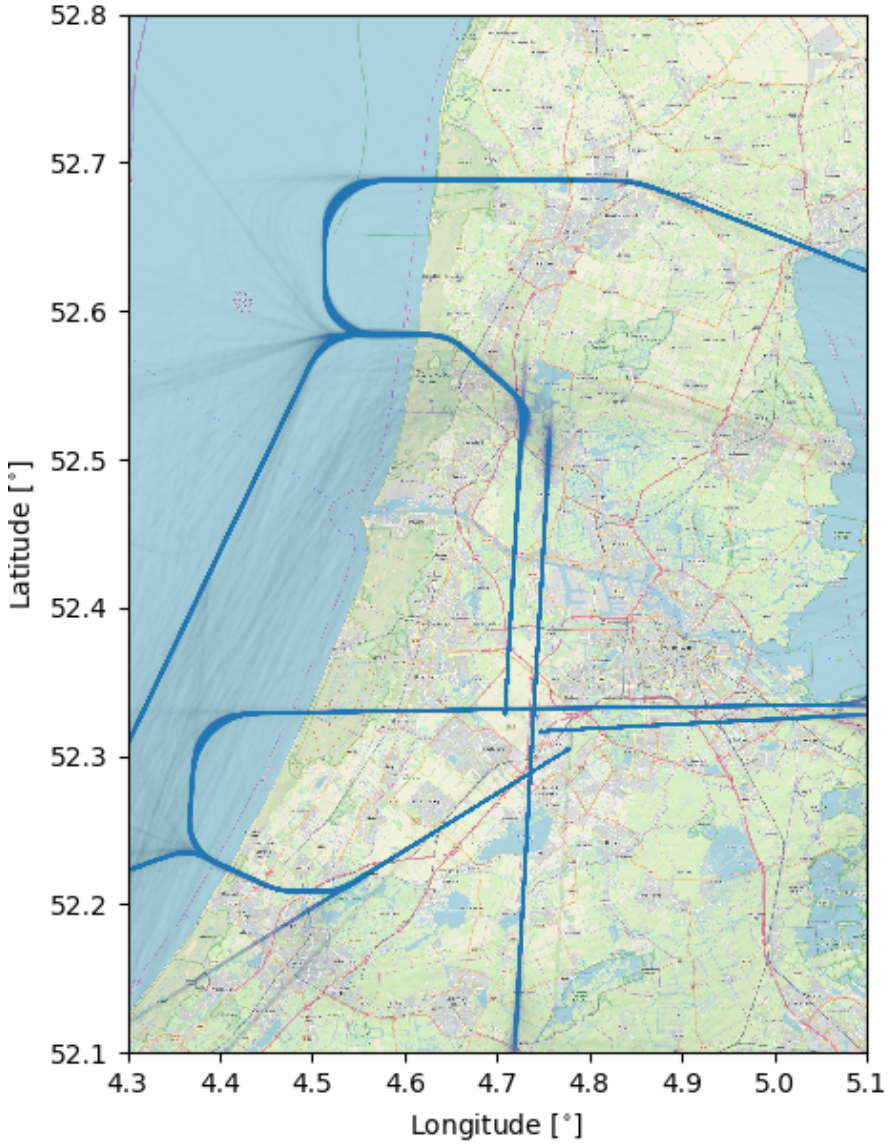

Figure C.9: Lateral tracks of the nighttime aircraft operations of the B738 aircraft in 2019.

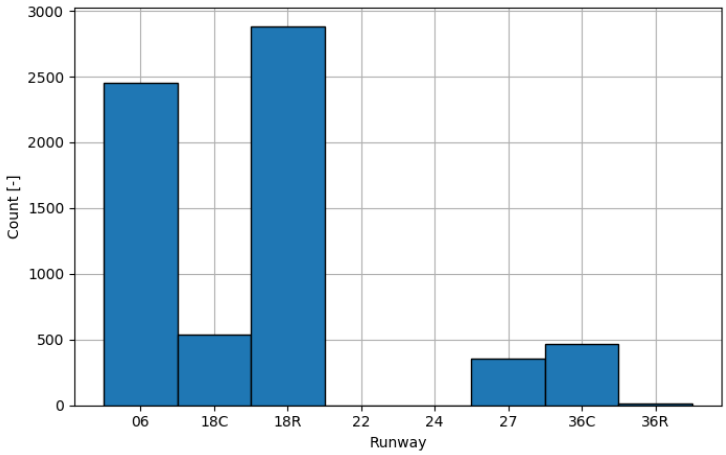

Figure C.10: Runway distribution of the nighttime aircraft operations of the B738 aircraft in 2019.

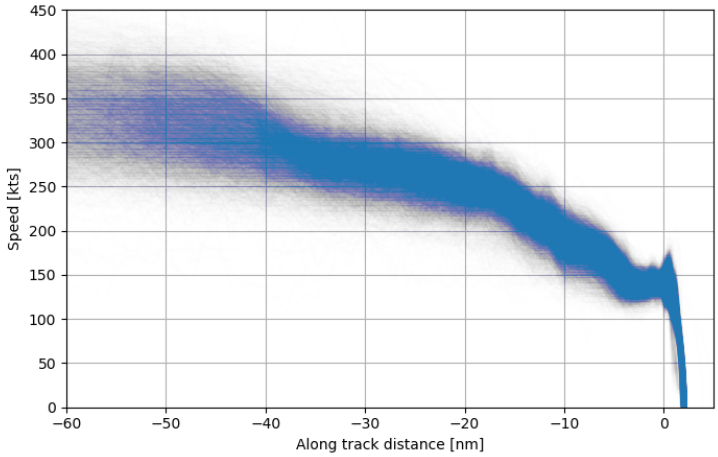

Figure C.11: Speed profiles of the nighttime aircraft operations of the B738 aircraft in 2019.

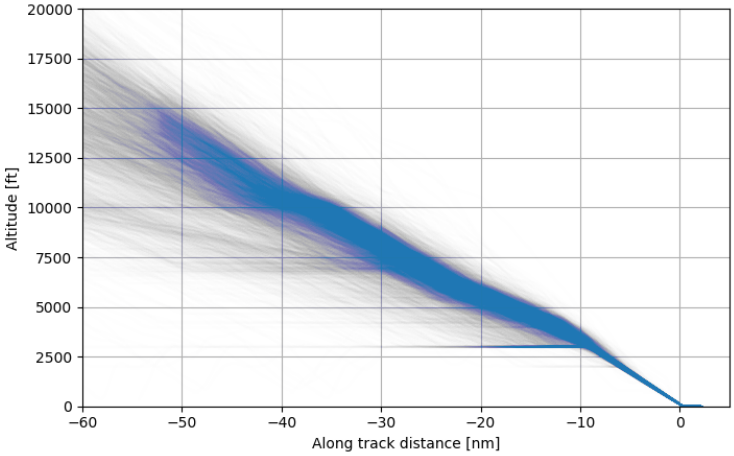

Figure C.12: Altitude profiles of the nighttime aircraft operations of the B738 aircraft in 2019.

C.3. B772 Operations

C.3.1. 2018 Nighttime

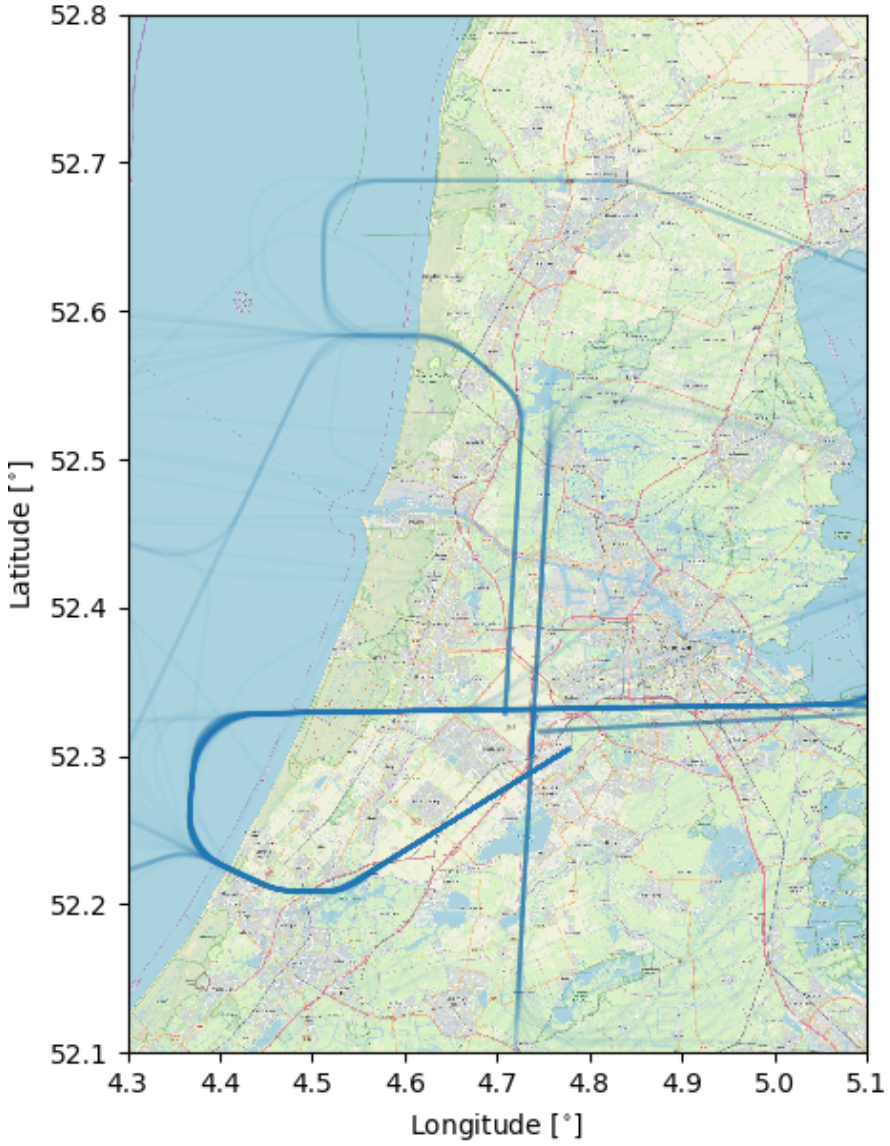

Figure C.13: Lateral tracks of the nighttime aircraft operations of the B772 aircraft in 2018.

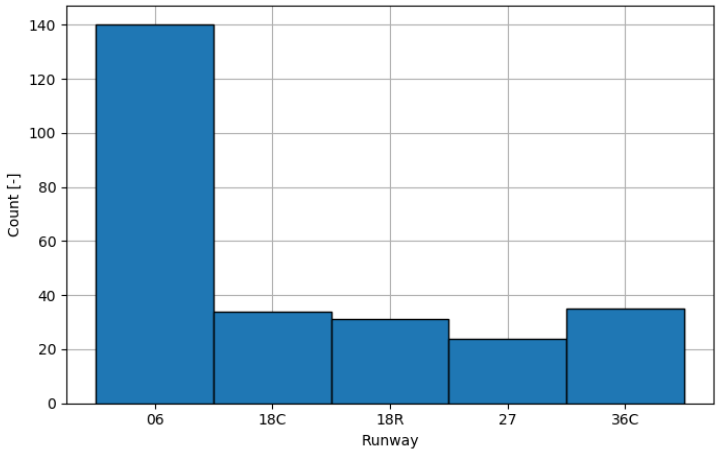

Figure C.14: Runway distribution of the nighttime aircraft operations of the B772 aircraft in 2018.

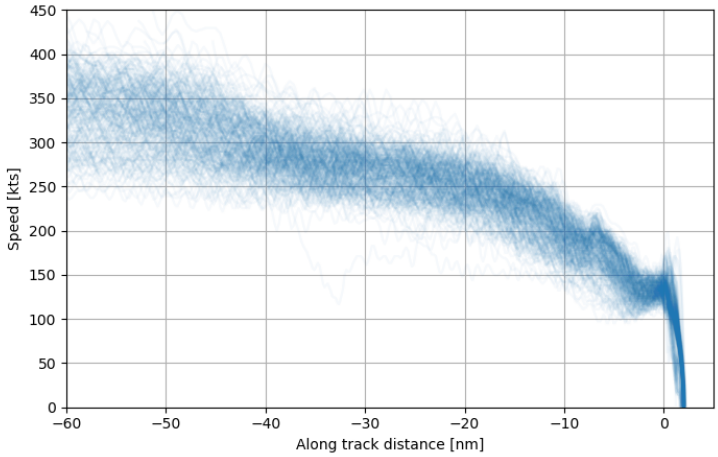

Figure C.15: Speed profiles of the nighttime aircraft operations of the B772 aircraft in 2018.

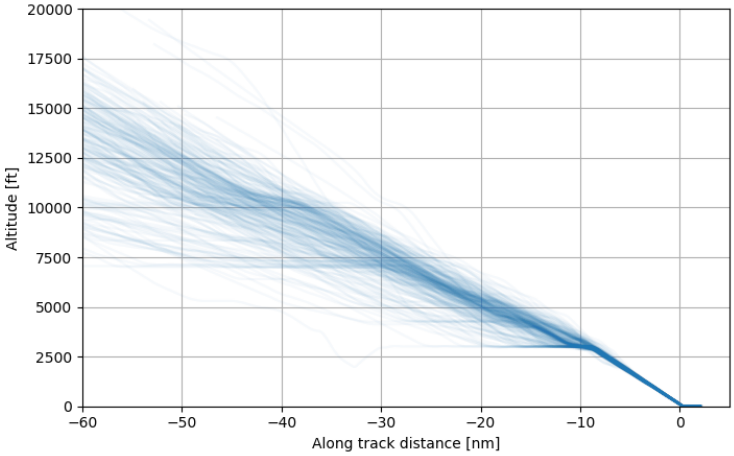

Figure C.16: Altitude profiles of the nighttime aircraft operations of the B772 aircraft in 2018.

C.3.2. 2019 Nighttime

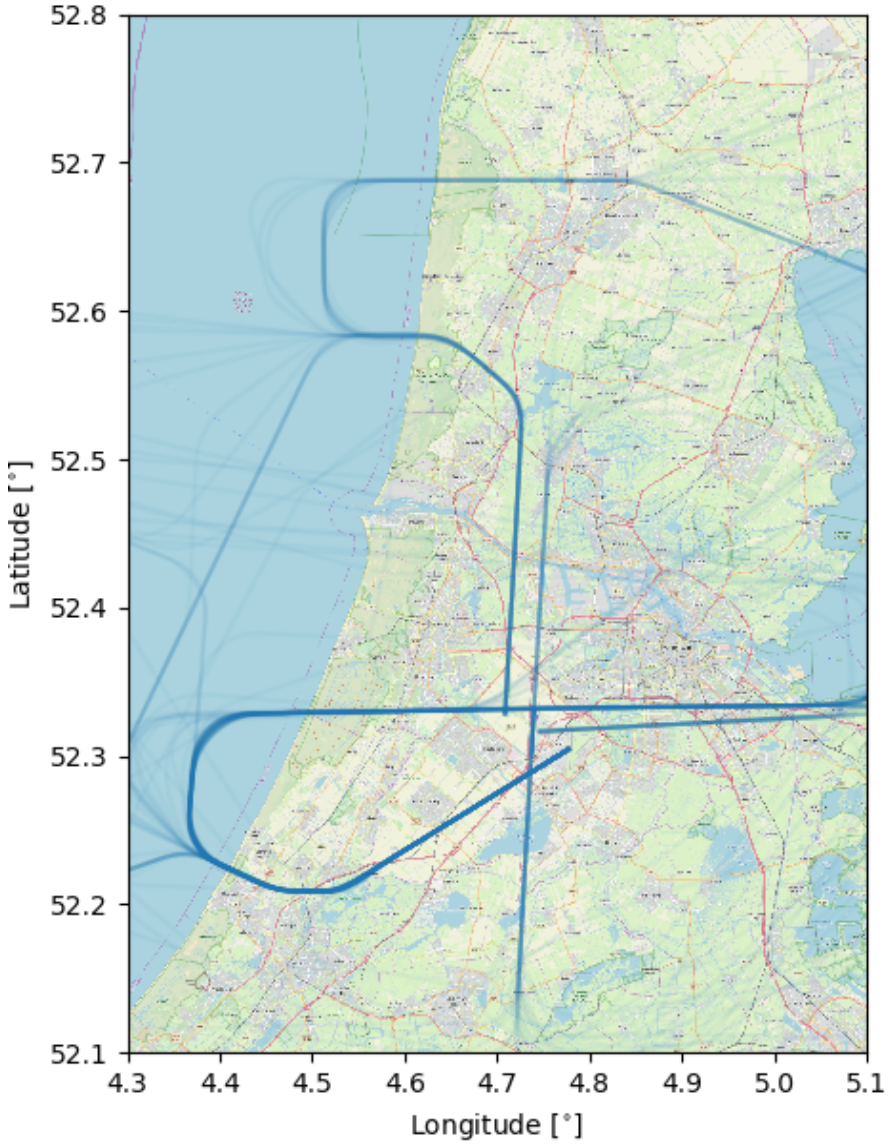

Figure C.17: Lateral tracks of the nighttime aircraft operations of the B772 aircraft in 2019.

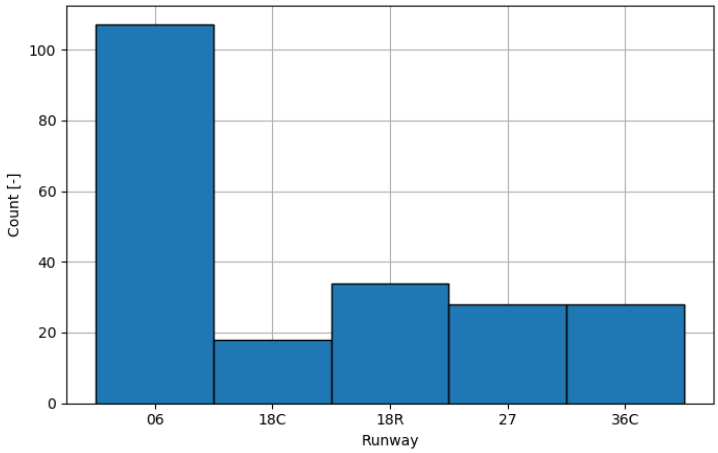

Figure C.18: Runway distribution of the nighttime aircraft operations of the B772 aircraft in 2019.

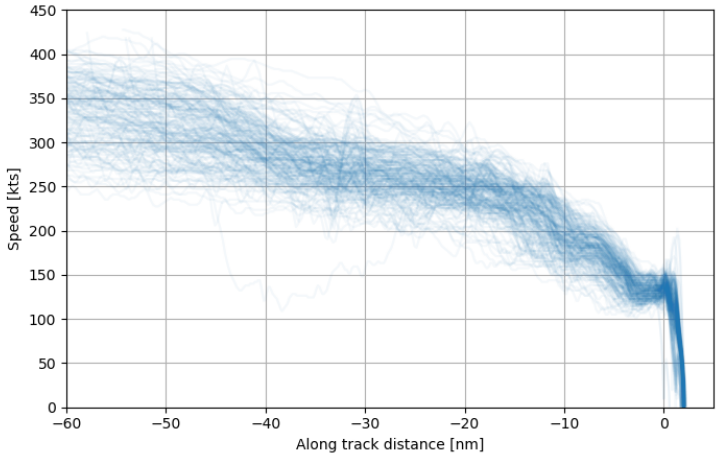

Figure C.19: Speed profiles of the nighttime aircraft operations of the B772 aircraft in 2019.

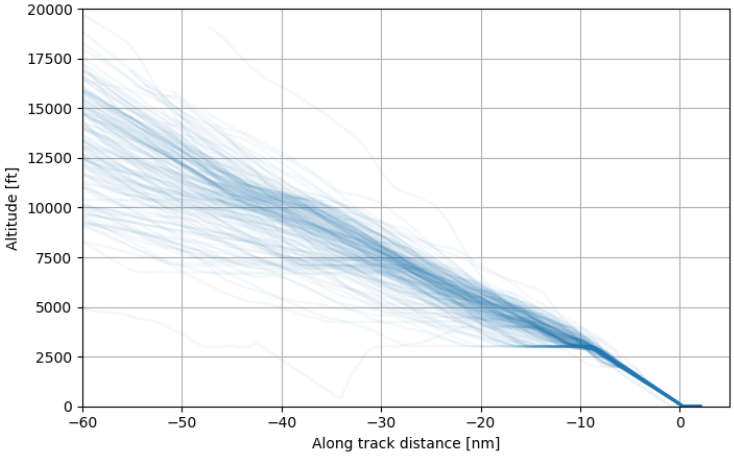

Figure C.20: Altitude profiles of the nighttime aircraft operations of the B772 aircraft in 2019.

D

Default Fixed Point Profile Calibration

For the calculation of the aircraft noise impact of future operations there are no radar tracks yet available for the determination of the aircraft noise level. In this case so called Default Fixed Point Profiles (DFPPs) are used. DFPPs contain the aircraft altitude, the power setting and true airspeed as a function of along track distance to the threshold location of the runway.

D.1. B738 Aircraft

The only DFPP available for the B738 aircraft is a profile for arrivals of the B738 aircraft. The altitude and airspeed profiles of the DFPP can be calibrated using either the ACMS logs or the radar tracks. The thrust setting profiles of the DFPP can be calibrated with the known thrust setting from the ACMS logs as the actual thrust setting cannot be obtained from radar data alone. The calibration of the altitude, true airspeed and thrust setting profile is presented in subsequent order. Due to the large amount of radar tracks for B738 aircraft approaching at Schiphol (54,225 during the year 2018) a random sample of 2,000 tracks from the set of tracks is used for calibration of the DFPP.

D.1.1. Altitude Profile

A comparison between the DFPP altitude profile and the altitude profile from the ACMS logs is presented in Figure D.1. From this figure it is observed that the predicted level segment between $15nm$ and $8nm$ until the threshold of the runway in the default FPP is not observed from the ACMS logs. Furthermore, the at an altitude lower than $3{,}000ft$ great similarity is observed between the default and calibrated altitude profile. This is caused by the interception of the signal of the Instrument Landing System (ILS).

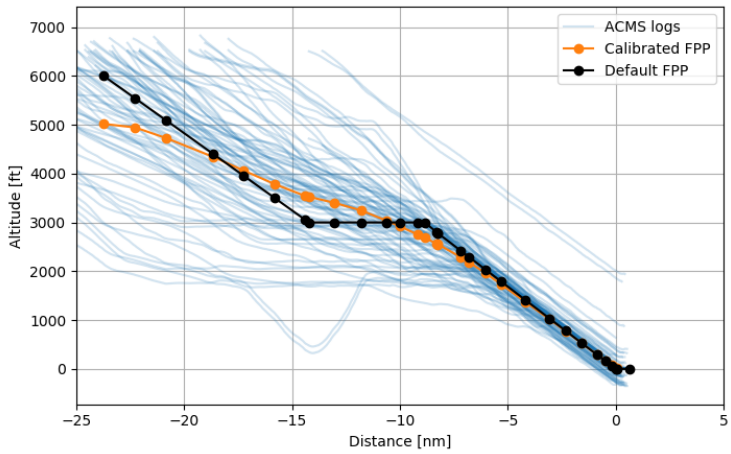

Figure D.1: Calibration of the FPP altitude profile for the B738 aircraft using ACMS logs.

From the comparison between the radar tracks and the default FPP for the B738 aircraft in Figure D.2 it is concluded that for some flights level segments do exist. Level flight segments during approach are observed at 3,000ft and 2,000ft. In order to accurately represent the routes associated with these level segments it is recommended that more than one FPP is defined, depending on the presence of a level segment.

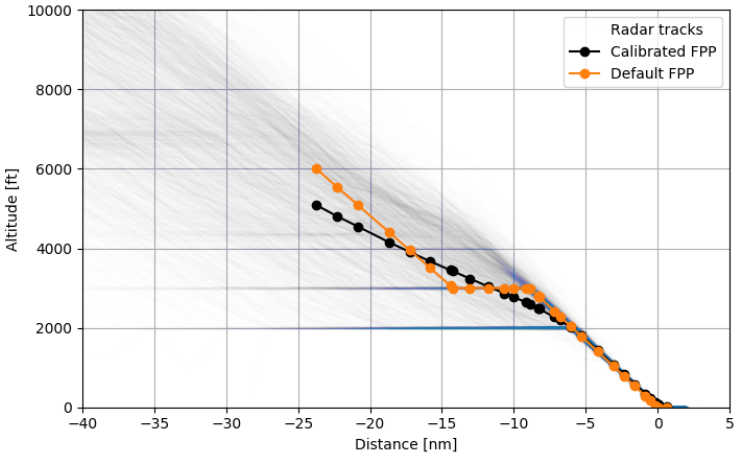

Figure D.2: Calibration of the FPP altitude profile for the B738 aircraft using radar tracks.

D.1.2. Airspeed Profile

The default V_{TAS} profile presented in Figure D.3 indicates a more or less constant true airspeed until the aircraft is 13nm from the threshold. After this point the true airspeed is strongly reduced until the aircraft is 8nm away from the threshold and remains constant from that point onward. However, both the calibrated true airspeed profiles based on the ACMS logs, presented in Figure D.3 and the radar data, presented in Figure D.4, indicate that this is not a representative profile. It is observed that the airspeed steadily decreases until the aircraft is approximately 5nm away from the threshold of the runway and remains constant afterwards.

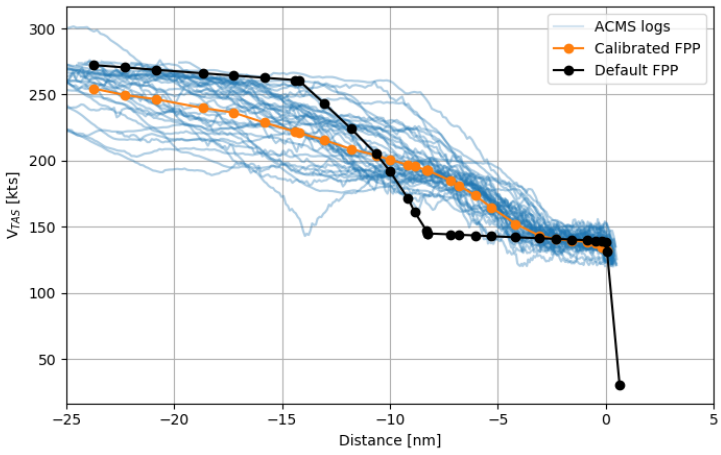

Figure D.3: Calibration of the FPP true airspeed profile for the B738 aircraft using ACMS logs.

D.1.3. Thrust Profile

The comparison between the default FPP thrust setting estimation and the actual thrust setting from the ACMS logs is presented in Figure D.5. The default FPP thrust setting contains a jump in thrust setting at 8nm from the threshold. This corresponds to the point in the default FPP altitude where the ILS is intercepted

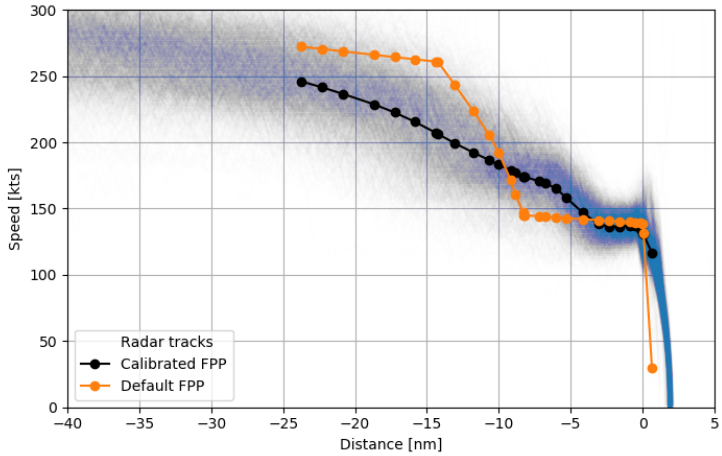

Figure D.4: Calibration of the FPP true airspeed profile for the B738 aircraft using radar.

and the true airspeed is kept constant. However, it was concluded from the calibrated FPP true airspeed, presented Figure D.3 and Figure D.4, that the airspeed still decreases between $8nm$ and $5nm$ from the threshold of the runway and is kept constant after $5nm$. This is in line with the calibrated FPP thrust setting, where the thrust is strongly increased at the point where the aircraft is $5nm$ from the threshold.

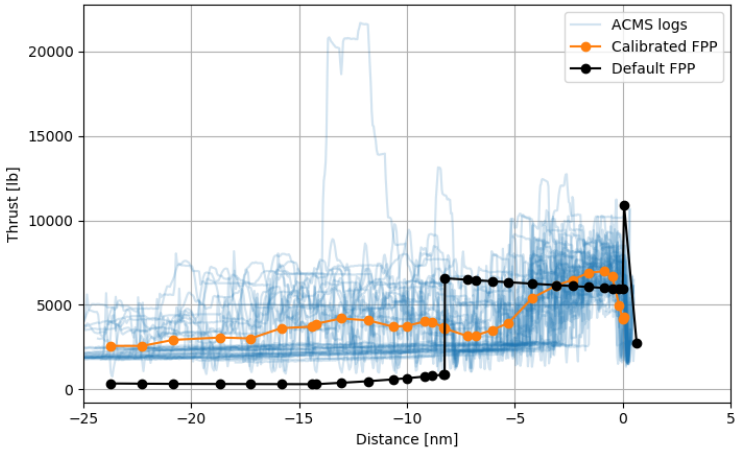

Figure D.5: Calibration of the FPP thrust profile for the B738 aircraft using ACMS logs.

D.2. B772 Aircraft

The only DFPP available for the B772 aircraft is a profile for arrivals of the B772 aircraft. The altitude and airspeed profiles of the DFPP can be calibrated using either the ACMS logs or the radar tracks. The thrust setting profiles of the DFPP can be calibrated with the known thrust setting from the ACMS logs as the actual thrust setting cannot be obtained from radar data alone. The calibration of the altitude, true airspeed and thrust setting profile is presented in subsequent order.

D.2.1. Altitude Profile

A comparison between the DFPP altitude profile and the altitude profile from the ACMS logs is presented in Figure D.6. From this figure it is observed that the predicted level segment between $15nm$ and $8nm$ until the threshold of the runway in the default FPP is not observed from the ACMS logs. Furthermore, the at an

altitude lower than 3,000ft great similarity is observed between the default and calibrated altitude profile. This is caused by the interception of the signal of the Instrument Landing System (ILS).

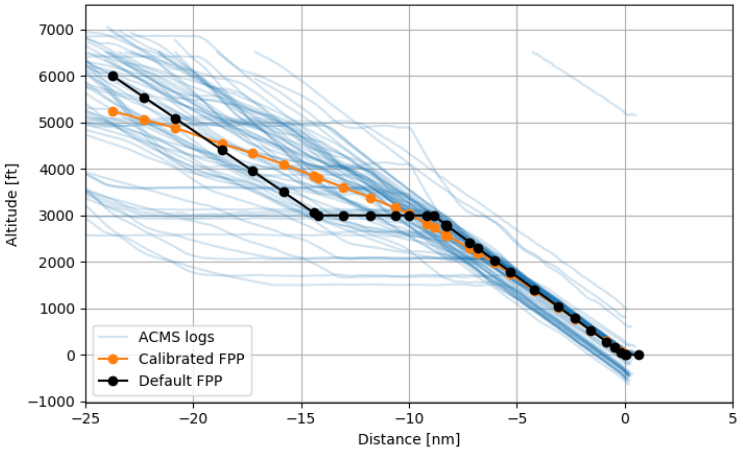

Figure D.6: Calibration of the FPP altitude profile for the B772 aircraft using ACMS logs.

From the comparison between the radar tracks and the default FPP for the B772 aircraft in Figure D.7 it is concluded that for some flights level segments do exist. Level flight segments during approach are observed at 3,000ft and 2,000ft. In order to accurately represent the routes associated with these level segments it is recommended that more than one FPP is defined, depending on the presence of a level segment.

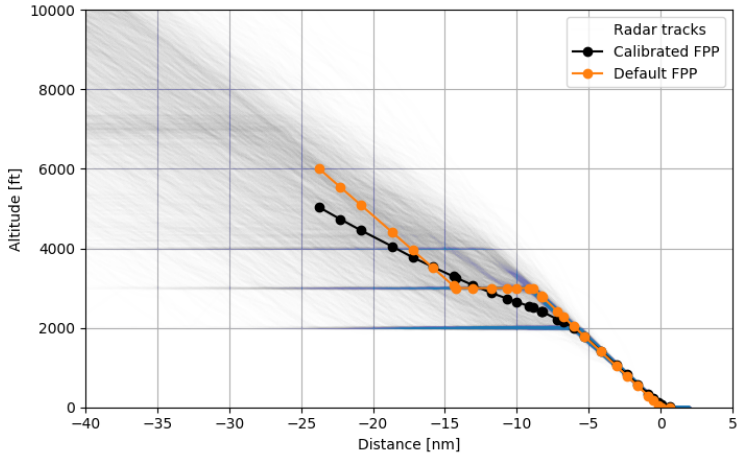

Figure D.7: Calibration of the FPP altitude profile for the B772 aircraft using radar tracks.

D.2.2. Airspeed Profile

The default V_{TAS} profile presented in Figure D.8 indicates a more or less constant true airspeed until the aircraft is 15nm from the threshold. After this point the true airspeed is strongly reduced until the aircraft is 8nm away from the threshold and remains constant from that point onward. However, both the calibrated true airspeed profiles based on the ACMS logs, presented in Figure D.8 and the radar data, presented in Figure D.9, indicate that this is not a representative profile. It is observed that the airspeed steadily decreases until the aircraft is approximately 5nm away from the threshold of the runway and remains constant afterwards.

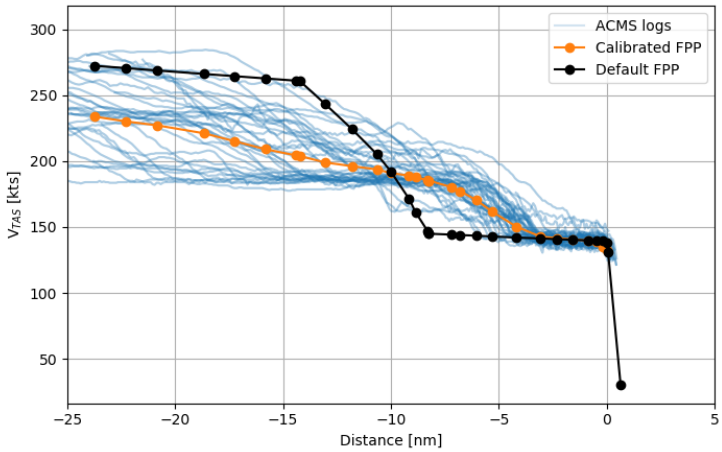

Figure D.8: Calibration of the FPP true airspeed profile for the B772 aircraft using ACMS logs.

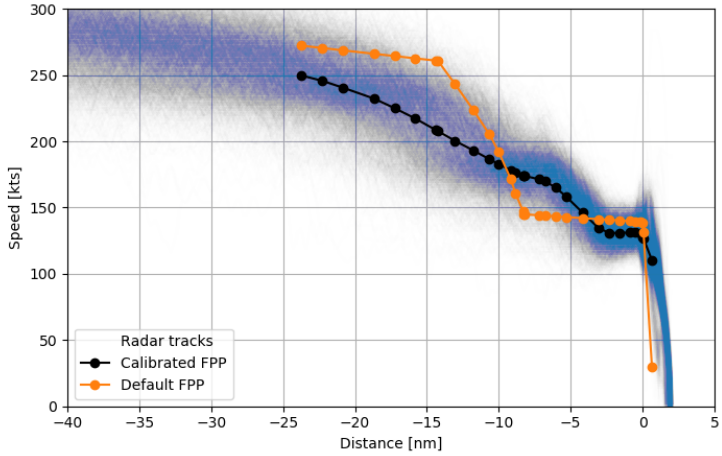

Figure D.9: Calibration of the FPP true airspeed profile for the B772 aircraft using radar.

D.2.3. Thrust Profile

The comparison between the default FPP thrust setting estimation and the actual thrust setting from the ACMS logs is presented in Figure D.10. The default FPP thrust setting contains a jump in thrust setting at $8nm$ from the threshold. This corresponds to the point in the default FPP altitude where the ILS is intercepted and the true airspeed is kept constant. However, it was concluded from the calibrated FPP true airspeed, presented Figure D.8 and Figure D.9, that the airspeed still decreases between $8nm$ and $5nm$ from the threshold of the runway and is kept constant after $5nm$. This is in line with the calibrated FPP thrust setting, where the thrust is strongly increased at the point where the aircraft is $5nm$ from the threshold.

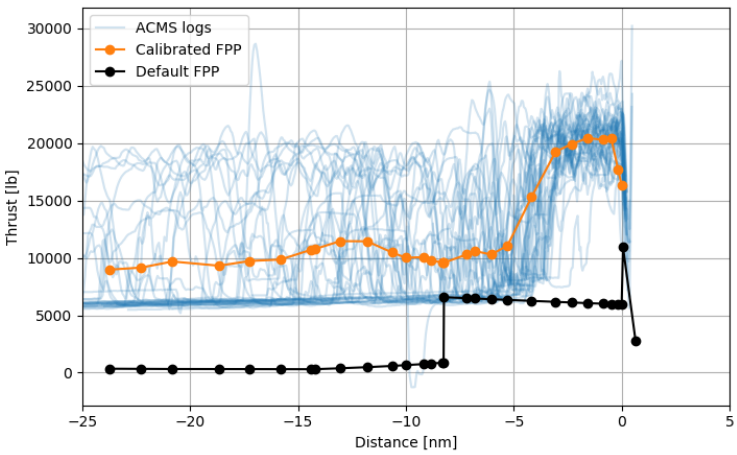

Figure D.10: Calibration of the FPP thrust profile for the B772 aircraft using ACMS logs.

E

NMT Track Distance

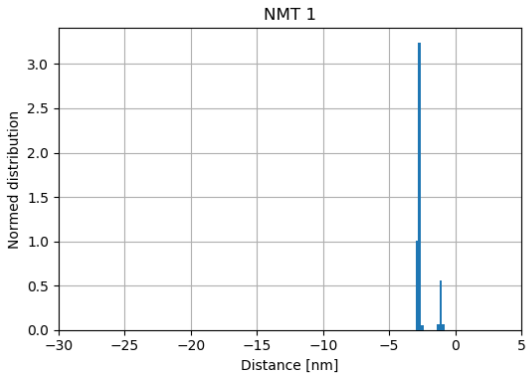

Figure E.1: Distribution of the distance to go till the runway threshold for NMT 1.

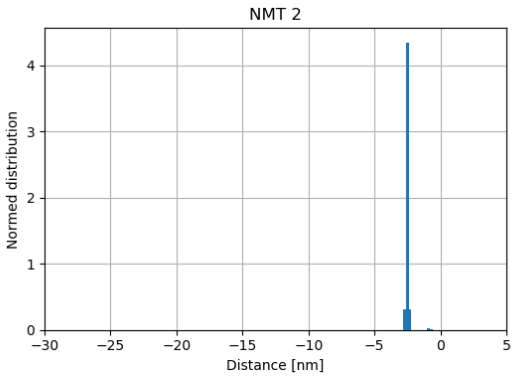

Figure E.2: Distribution of the distance to go till the runway threshold for NMT 2.

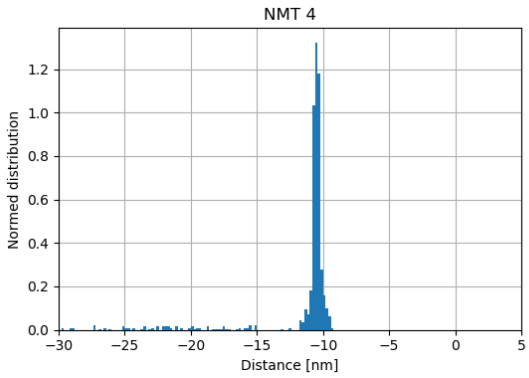

Figure E.3: Distribution of the distance to go till the runway threshold for NMT 4.

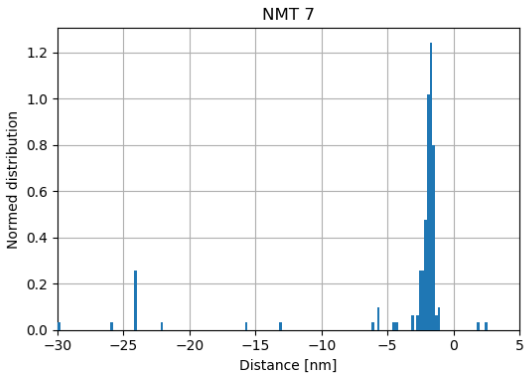

Figure E.4: Distribution of the distance to go till the runway threshold for NMT 7.

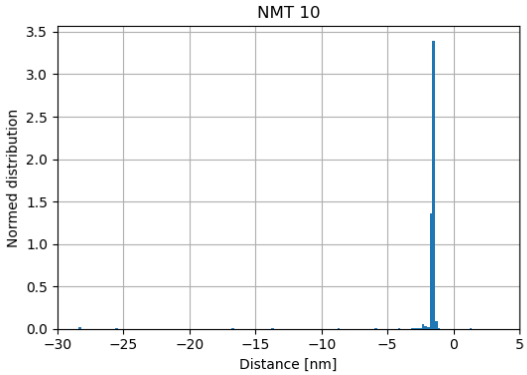

Figure E.5: Distribution of the distance to go till the runway threshold for NMT 10.

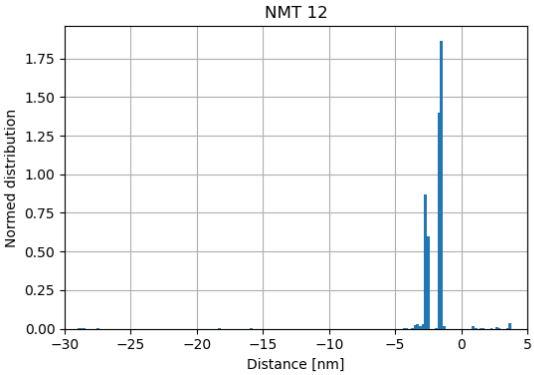

Figure E.6: Distribution of the distance to go till the runway threshold for NMT 12.

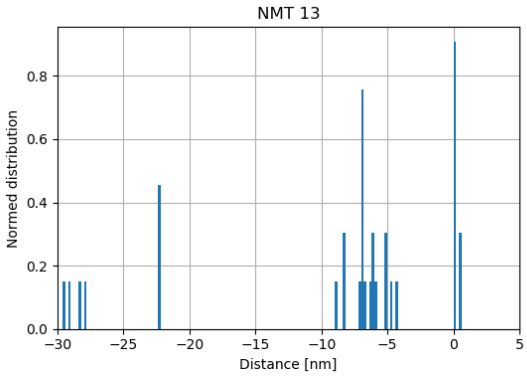

Figure E.7: Distribution of the distance to go till the runway threshold for NMT 13.

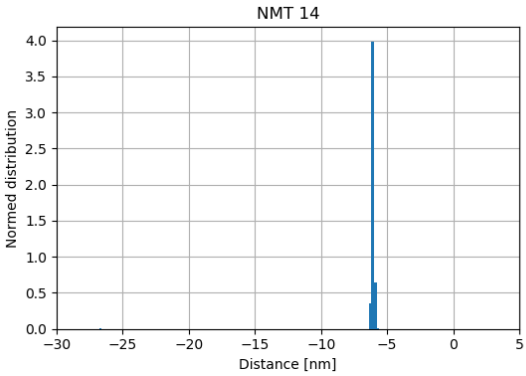

Figure E.8: Distribution of the distance to go till the runway threshold for NMT 14.

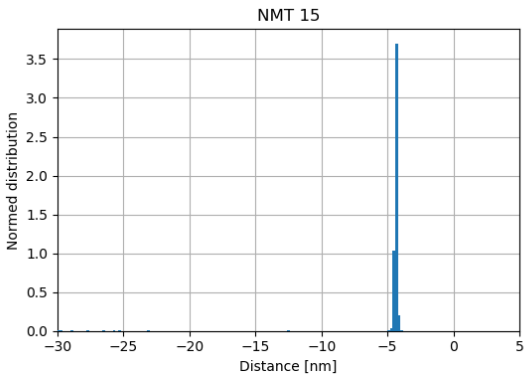

Figure E.9: Distribution of the distance to go till the runway threshold for NMT 15.

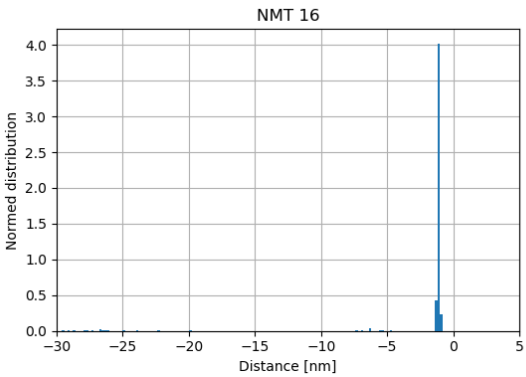

Figure E.10: Distribution of the distance to go till the runway threshold for NMT 16.

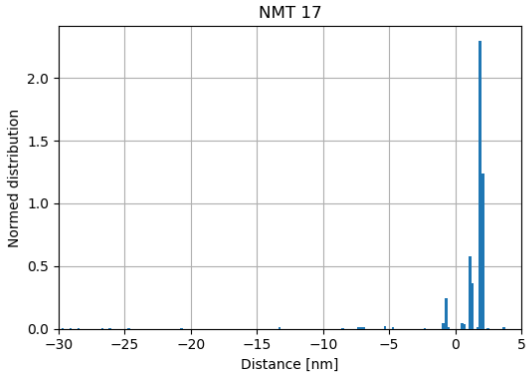

Figure E.11: Distribution of the distance to go till the runway threshold for NMT 17.

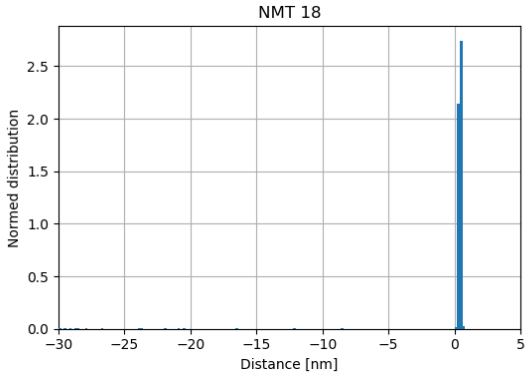

Figure E.12: Distribution of the distance to go till the runway threshold for NMT 18.

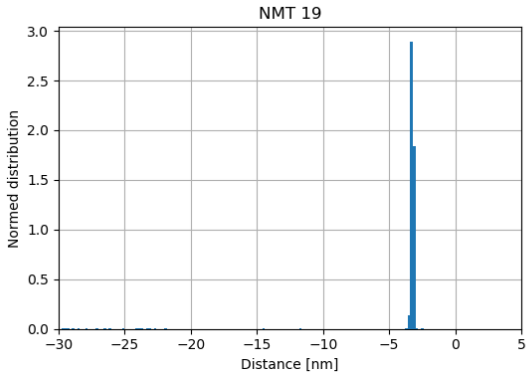

Figure E.13: Distribution of the distance to go till the runway threshold for NMT 19.

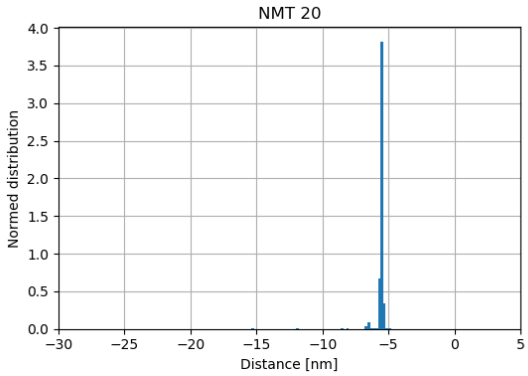

Figure E.14: Distribution of the distance to go till the runway threshold for NMT 20.

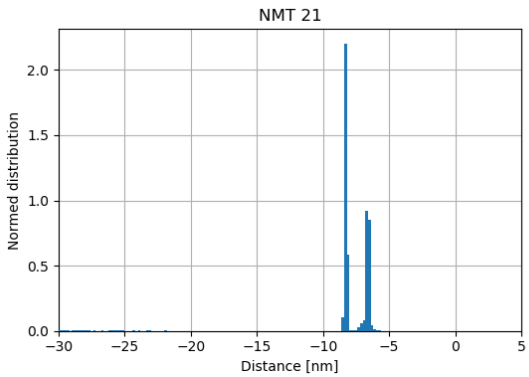

Figure E.15: Distribution of the distance to go till the runway threshold for NMT 21.

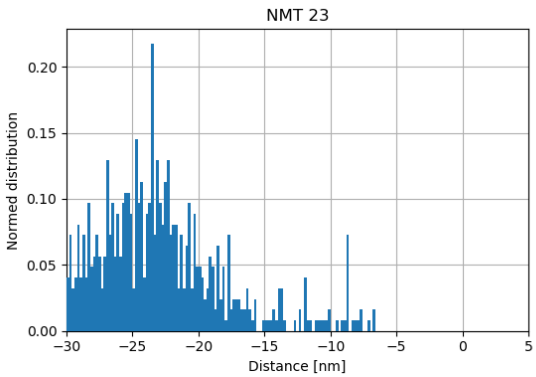

Figure E.16: Distribution of the distance to go till the runway threshold for NMT 23.

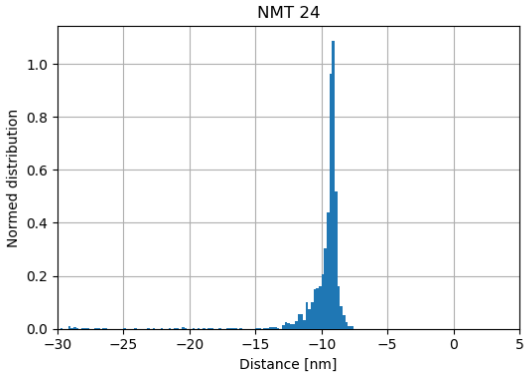

Figure E.17: Distribution of the distance to go till the runway threshold for NMT 24.

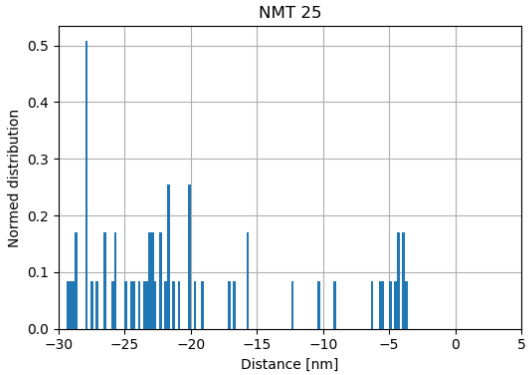

Figure E.18: Distribution of the distance to go till the runway threshold for NMT 25.

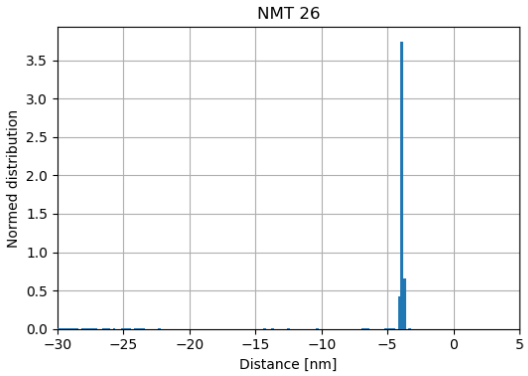

Figure E.19: Distribution of the distance to go till the runway threshold for NMT 26.

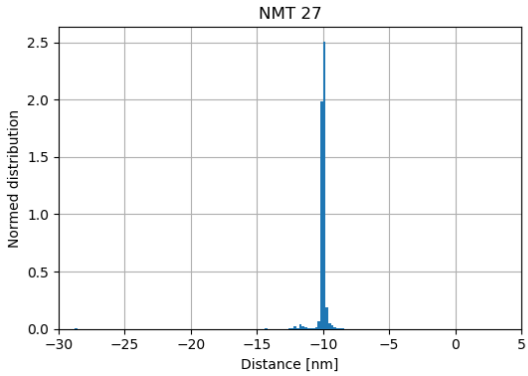

Figure E.20: Distribution of the distance to go till the runway threshold for NMT 27.

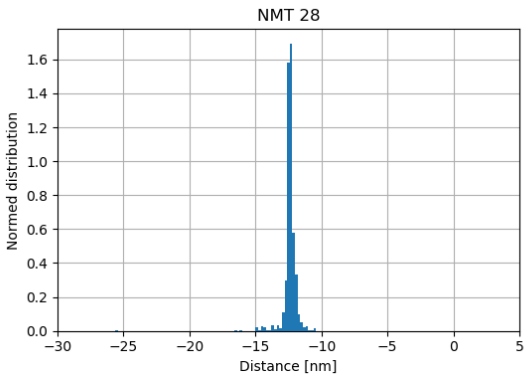

Figure E.21: Distribution of the distance to go till the runway threshold for NMT 28.

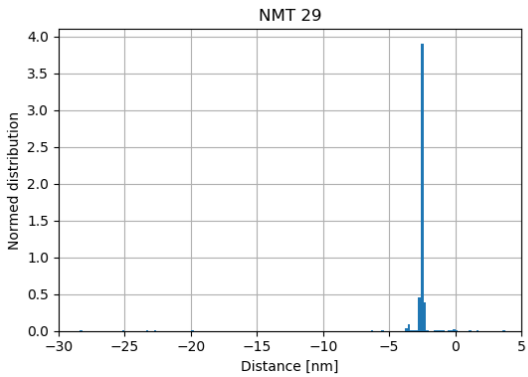

Figure E.22: Distribution of the distance to go till the runway threshold for NMT 29.

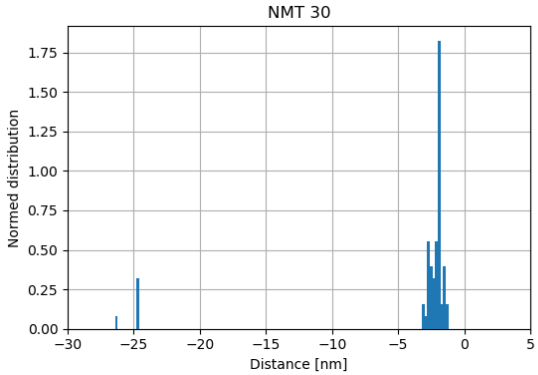

Figure E.23: Distribution of the distance to go till the runway threshold for NMT 30.

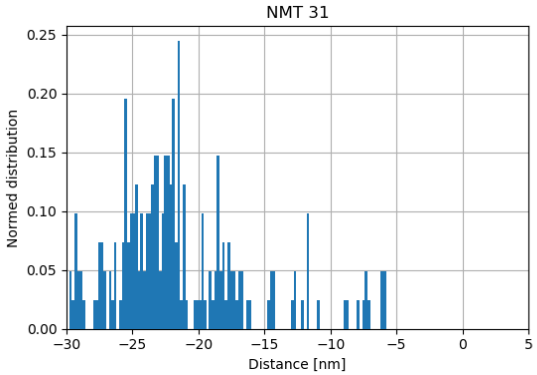

Figure E.24: Distribution of the distance to go till the runway threshold for NMT 31.

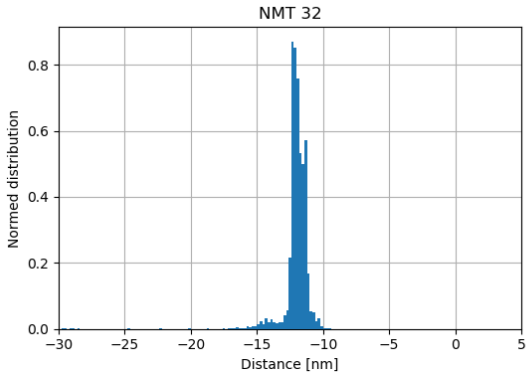

Figure E.25: Distribution of the distance to go till the runway threshold for NMT 32.

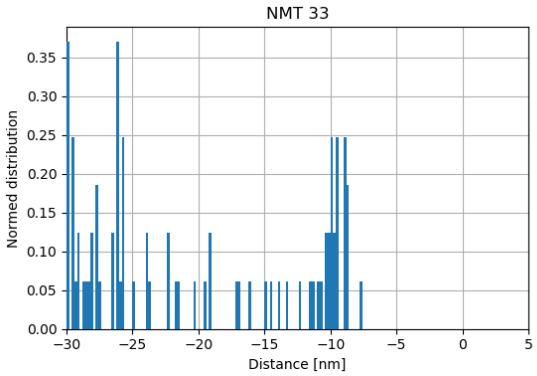

Figure E.26: Distribution of the distance to go till the runway threshold for NMT 33.

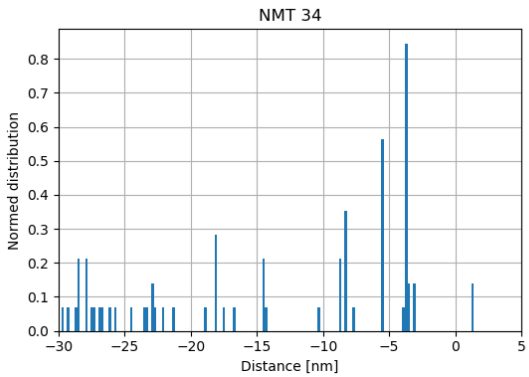

Figure E.27: Distribution of the distance to go till the runway threshold for NMT 34.

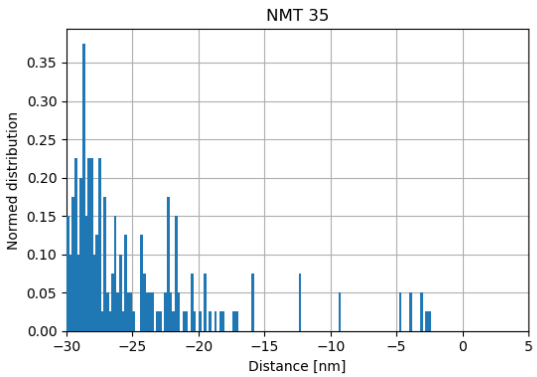

Figure E.28: Distribution of the distance to go till the runway threshold for NMT 35.

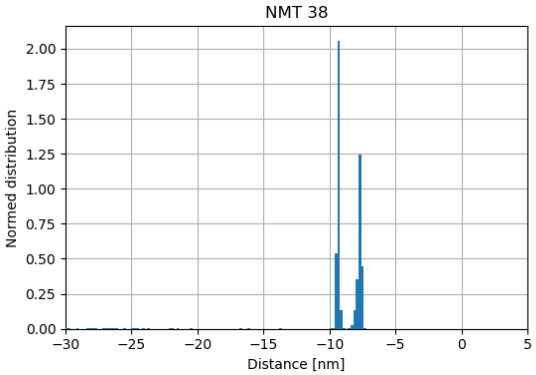

Figure E.29: Distribution of the distance to go till the runway threshold for NMT 38.

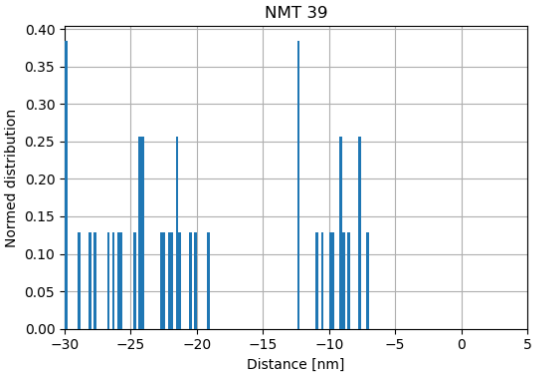

Figure E.30: Distribution of the distance to go till the runway threshold for NMT 39.

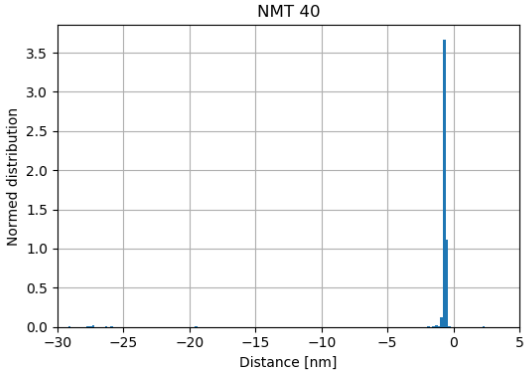

Figure E.31: Distribution of the distance to go till the runway threshold for NMT 40.

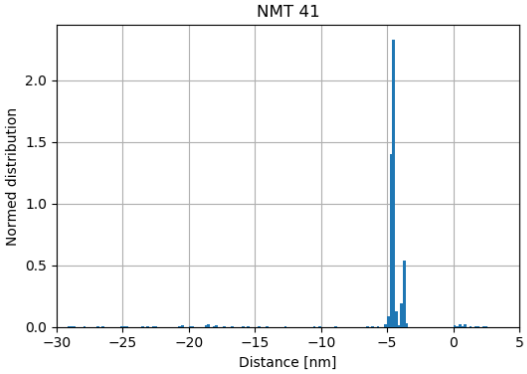

Figure E.32: Distribution of the distance to go till the runway threshold for NMT 41.

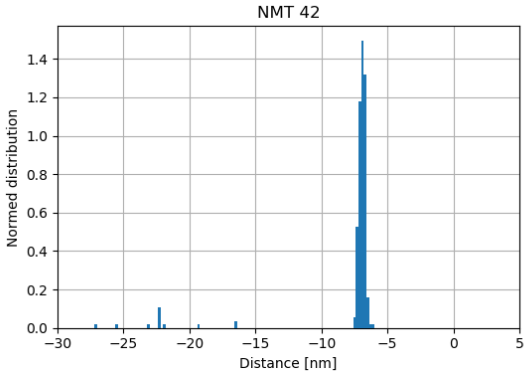

Figure E.33: Distribution of the distance to go till the runway threshold for NMT 42.

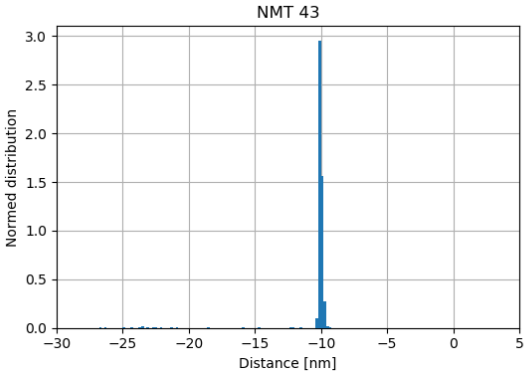

Figure E.34: Distribution of the distance to go till the runway threshold for NMT 43.

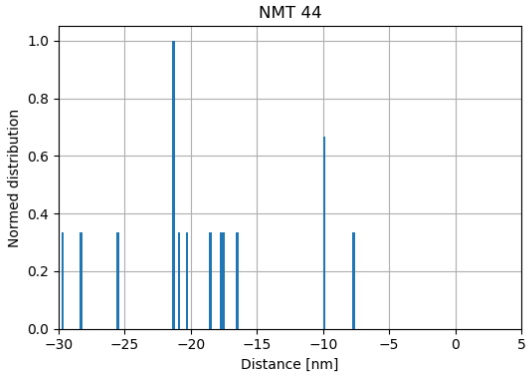

Figure E.35: Distribution of the distance to go till the runway threshold for NMT 44.

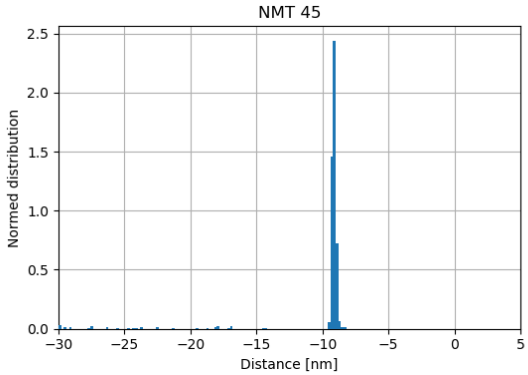

Figure E.36: Distribution of the distance to go till the runway threshold for NMT 45.

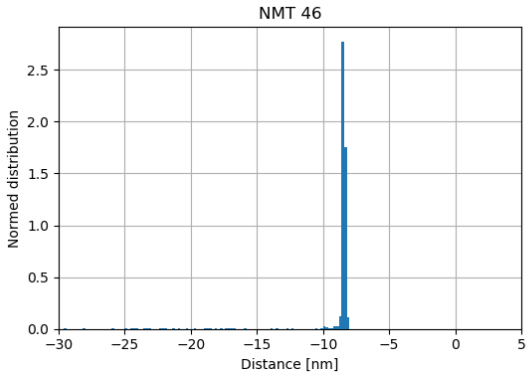

Figure E.37: Distribution of the distance to go till the runway threshold for NMT 46.

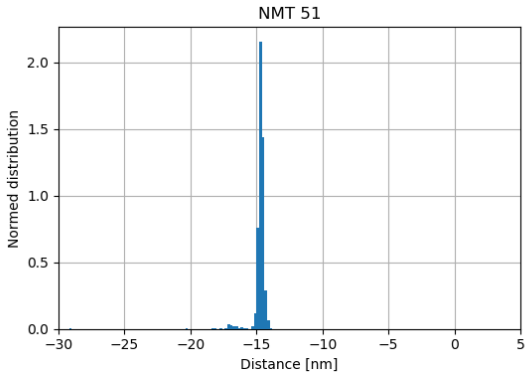

Figure E.38: Distribution of the distance to go till the runway threshold for NMT 51.

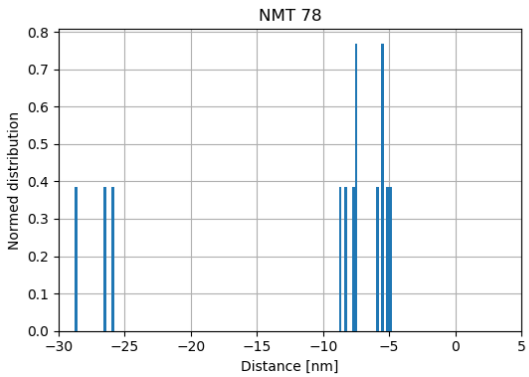

Figure E.39: Distribution of the distance to go till the runway threshold for NMT 78.

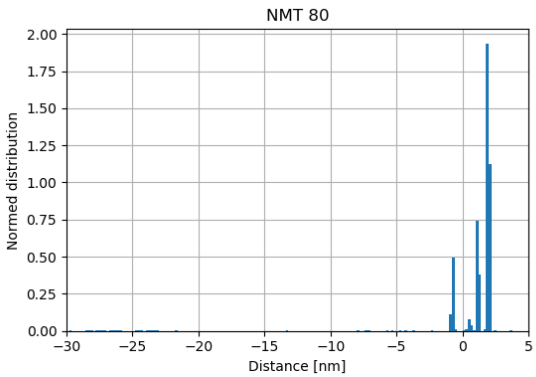

Figure E.40: Distribution of the distance to go till the runway threshold for NMT 80.

F

Unit Conversion Table

Table F.1: Conversion to SI units.

Unit	Name	SI Conversion
ft	foot,feet	0.3048 m
nm	nautical mile	1852 m
kt	knot	0.5144 ms-1
lb	pound	0.4536 kg
lbf	pound force	4.4482N

Bibliography

[1] J.E. Adair. *The art of creative thinking: How to be innovative and develop great ideas*. Kogan Page Publishers, 2007.

[2] D.H.T. Bergmans A.M. Kruger-Dokter. Een nieuwe berekeningsmethodiek voor vliegtuiggeluid in nederland. Technical report, NLR, 2010. NLR-TP-2010-208.

[3] A. Mast P. Balke A.R. Eisses, J. Golliard. Onderzoek naar verschillen tussen gemeten en berekend vliegtuiggeluid. Technical report, TNO, 2006.

[4] V. Bulc. European aviation environmental report. Technical report, EASA, 2016.

[5] R. Bütikofer. *Noise Mapping in the EU: Models and Procedures*. Taylor & Francis, 2013.

[6] R.E. Caves, L.R. Jenkinson, D.P. Rhodes, and J.B. Ollerhead. Estimation of civil aircraft performance and operating practices from radar data. 1998.

[7] European Civil Aviation Conference. *Report on Standard Method of Computing Noise Contours around Civil Airports*, 2016. Volume 1: Applications Guide 4th Edition.

[8] European Civil Aviation Conference. *Report on Standard Method of Computing Noise Contours around Civil Airports*, 2016. Volume 2: Technical Guide 4th Edition.

[9] European Civil Aviation Conference. *Report on Standard Method of Computing Noise Contours around Civil Airports*, 2016. Volume 3, Part 1: Reference Cases and Verification Framework 4th Edition.

[10] P. Havelock D. Rhodes, S. White. *Validating the CAA aircraft noise model with noise measurements*. UK Civil Aviation Authority, 2000.

[11] A. de Jong D.H.T. Bergmans, F. van Deventer. Voortgangsnotitie verbetering kwaliteit modelberekeningen vliegtuiggeluid. 2009.

[12] R.H. Hogenhuis D.H.T. Bergmans, H.W. Veerbeek. Het meten van vliegtuiggeluid. Technical report, NLR, 2014. NLR-TP-2014-037.

[13] E.P. Dinges. Feasibility of creating integrated noise model (inm) profiles from radar data. Technical report, FAA, 2002. FAA-AEE-02-02.

[14] J.B. Ollerhead D.P. Rhodes. Aircraft noise model validation. Technical report, Inter-Noise, 2001.

[15] M.P. Elliott. A methodology for determining aircraft fuel burn using air traffic control radar data. Master's thesis, Georgia Institute of Technology, 2011.

[16] *Directive 2002/49/EC Of the European Parliament and of the Council of 25 June 2002 relating to the assessment and management of environmental noise*. The European Parliament and the Council of the European Union, 2002.

[17] H. Fastl and E. Zwicker. *Psychoacoustics: facts and models*, volume 22. Springer Science & Business Media, 2006.

[18] JE Ffowcs Williams. The noise from turbulence convected at high speed. *Philosophical Transactions of the Royal Society of London. Series A, Mathematical and Physical Sciences*, 255(1061):469–503, 1963.

[19] A. Filippone. Aircraft noise prediction. *Progress in Aerospace Sciences*, 68:27–63, 2014.

[20] Antonio Filippone and Lothar Bertsch. Comparison of aircraft noise models with flyover data. *Journal of Aircraft*, 51(3):1043–1047, 2014.

[21] H.P. Lopuhaä L.E. Meester F.M. Dekking, C. Kraaikamp. *A Modern Introduction to Probability and Statistics*. Springer, 2005.

[22] L.M. Graves. *The theory of functions of real variables*, volume 2. McGraw-Hill, 1956.

[23] R. Guski. How to forecast community annoyance in planning noisy facilities. *Noise and Health*, 6(22):59, 2004.

[24] G.J.J. Ruijgrok J.T.T. Thoen A.R. Eisses H. Eversdijk, B. M. Spee. Luid, maar duidelijk. Technical report, Commissie Deskundigen Vliegtuiggeluid, 2006.

[25] G.J.T. Heppe. *Appendices van de voorschriften voor de berekening van de geluidsbelasting in Lden en Lnight voor Schiphol*, 2012. NLR-CR-96650 L - Versie 12.2.

[26] J.D. Hunter. Matplotlib: A 2d graphics environment. *Computing in Science & Engineering*, 9(3):90–95, 2007. doi: 10.1109/MCSE.2007.55.

[27] ISO. *Acoustics - Description and measurement of environmental noise*, 1987. ISO 21996-2: 1987.

[28] ISO. *Acoustics - Attenuation of sound during propagation outdoors*, 1993. ISO 9613-1: 1993.

[29] ISO. *Unattended monitoring of aircraft sound in the vicinity of airports*, 2009. ISO 20906.

[30] C. Allmark J. Trow. The benefits of validating your aircraft noise model. 2018.

[31] J.H. Lovrinic J.D. Durrant. *Bases of Hearing Science*. Williams & Wilkins, 1995.

[32] R. Cadoux K. Jones. Metrics for aircraft noise. Technical report, CAA, 2009. ERCD REPORT 0904.

[33] K.A. Bradley K.J. Plotkin, C.M. Hobbs. Examination of the lateral attenuation of aircraft noise. Technical report, NASA, 2000.

[34] R.P.F. Koster. Using nomos measurements to assess improvements of ecac doc. 29 aircraft noise calculations. Master's thesis, Delft University of Technology, 2020.

[35] P. Lempereur L. Leylekia, M. Lebrun. An overview of aircraft noise reduction technologies. *AerospaceLab*, pages p. 1–15, 2015. 10.12762/2014.AL07-01ff. ffhal-01184664f.

[36] L.C. Sutherland L.B. Evans, H.E. Bass. Atmospheric absorption of sound: Theoretical predictions. *The Journal of the Acoustical Society of America*, 105(1):1565–1575, 1971.

[37] H. Lloyd. On a new case of interference of the rays of light. *Transactions of the Royal Irish Academy*, 17 (1):171–177, 1837.

[38] F Marshall. The accuracy of predictions from primary radar and secondary radar. *The Journal of Navigation*, 26(3):282–289, 1973.

[39] Wes McKinney et al. Data structures for statistical computing in python. In *Proceedings of the 9th Python in Science Conference*, volume 445, pages 51–56. Austin, TX, 2010.

[40] NRC. Schiphol mag groeien, maar hoe? https://www.nrc.nl/nieuws/2019/07/07/schiphol-mag-groeien-maar-hoe-a3966375, jul 2019. Accessed on 18-09-2019.

[41] T.E. Oliphant. *A guide to NumPy*, volume 1. Trelgol Publishing USA, 2006.

[42] J.B. Ollerhead. *The CAA Aircraft Noise Contour Model: ANCON Version 1*, 2003. DORA Report 9120.

[43] F. Jelinek P. Lubrani, L. Cavadini. Single european sky implementation support through validation. Technical report, Eurocontrol, 2009. D2.4.4-03.

[44] K. Pesonen. Study of the effects of aircraft noise. Technical report, Finavia corporation, 2018.

[45] C. Croux P.J. Rousseeuw. Alternatives to the median absolute deviation. *Journal of the American Statistical Association*, 88(424):1273–1283, 1993.

[46] A. Ramonjoan S. Soley R. Dalmau, X. Prats. Estimating fuel consumption from radar tracks: A validation exercise using fdr data from descent trajectories. 2018.

[47] R. Markovits-Somogyi R. Madácsi. Bank angle estimation using radar data. *Periodica Polytechnica Transportation Engineering*, 47(1):1–5, 2019.

[48] D.H.T. Bergmans M. Snellen D.G. Simons R. Merino-Martinez, S.J. Heblij. Improving aircraft noise predictions considering fan rotational speed. *Journal of Aircraft*, pages 284–294, 2019.

[49] D. Houthuijs I. van Kamp R. van Poll, O. Breugelmans. Beleving woonomgeving in nederland: Inventarisatie verstroingen 2016. Technical report, RIVM, 2018. RIVM Rapport 2018-0084.

[50] D.J.M. Houthuijs R.H. Hogenhuis S.J. Heblij J.L.A. Devilee O.R.P. Breugelmans J.A. Beintema R.C.G.M. Smetsers, P.C. Siegmund. Vliegtuiggeluid: meten, rekenen en beleven. Technical report, RIVM, 2019. RIVM Rapport 2019-0201.

[51] S.J. Heblij R.H. Hogenhuis. Trendvalidatie van doc.29 berekeningen. Technical report, NLR, 2018. NLR-CR-2017-371.

[52] D. Rhodes. *Guidance on comparing calculated aircraft noise levels with measurements*. UK Civil Aviation Authority, 2018.

[53] G. Van Rossum and F.L. Drake. *Python 3 Reference Manual*. CreateSpace, Scotts Valley, CA, 2009. ISBN 1441412697.

[54] M. Saini. Flying by the numbers: a precise approach to landing. Technical report, FAA, 2010.

[55] E.M. Salomons. *Computational Atmospheric Acoustics*. Springer, 2001.

[56] C.L. Scovel. Aviation industry performance: A review of the aviation industry, 2008–2011. 2014.

[57] Naoaki Shinohara and Ichiro Yamada. Reliability of aircraft noise evaluation by measurement for comparison with prediction. In *INTER-NOISE and NOISE-CON Congress and Conference Proceedings*, volume 249, pages 4038–4047. Institute of Noise Control Engineering, 2014.

[58] D.G. Simons. *Introduction to Aircraft Noise*. TU Delft, 2019.

[59] S.W. Smith. *The scientist and engineer's guide to digital signal processing*. California Technical Pub. San Diego, 1997.

[60] *Method for Predicting Lateral Attenuation of Airplane Noise*. Society of Automotive Engineers, 2006. SAE AIR-5662, update to SAE AIR-1751.

[61] W. Soede. Technische beschrijving vliegtuig geluidmeetsystemen: Luistervink, nomos, sensornet. Technical report, ardea, 2012.

[62] W. Soede. *Technische beschrijving vliegtuig geluidmeetsystemen: Luistervink, Nomos, Sensornet*. Ardea, 2012.

[63] Christoph Struempfel and Oliver Lehmann. Challenges and potentials of aircraft noise modeling using enhanced aircraft performance parameters and flight deck procedures. In *INTER-NOISE and NOISE-CON Congress and Conference Proceedings*, volume 255, pages 464–475. Institute of Noise Control Engineering, 2017.

[64] J. Sun. *Open Aircraft Performance Modeling: Based on an Analysis of Aircraft Surveillance Data*. PhD thesis, Delft University of Technology, 2019.

[65] De Telegraaf. Veel meer geluidshinder omwonenden schiphol. https://www.telegraaf.nl/nieuws/2734407/veel-meer-geluidshinder-omwonenden-schiphol, oct 2018. Accessed on 08-10-2019.

[66] Trouw. Met berekeningen over geluidshinder komt overheid niet langer weg. https://www.trouw.nl/nieuws/met-berekeningen-over-geluidshinder-komt-overheid-niet-langer-weg b3fcb8b3/, oct 2018. Accessed on 19-09-2019.

[67] S. White. Precision of aircraft noise measurements at the london airports. Technical report, CAA, 2005. ERCD REPORT 0506.

[68] T.J. Bruno W.M. Haynes, D.R. Lide. *CRC Handbook of Chemistry and Physics*. CRC Press, 2016.